2013

Tuning of Neuronal Excitation by a Brain Specific Microrna MIR-128: From Targets to Behavior

Chan Lek Tan

TUNING OF NEURONAL EXCITATION BY A BRAIN SPECIFIC MICRORNA MIR-128: FROM TARGETS TO BEHAVIOR

A Thesis Presented to the Faculty of
The Rockefeller University
in Partial Fulfillment of the Requirements for
the degree of Doctor of Philosophy

by
Chan Lek Tan
June 2013

TUNING OF NEURONAL EXCITATION BY A BRAIN SPECIFIC MICRORNA MIR-128: FROM TARGETS TO BEHAVIOR

Chan Lek Tan, Ph.D.
The Rockefeller University 2013

MicroRNAs constitute a vital new component of our evolving understanding of regulatory mechanisms that shape cellular gene expression. As ubiquitous regulators of protein translation, microRNAs have a unique regulatory function that is only beginning to be fully described. In addition, their role in the control of gene expression in neurons, which underpins neuronal identity and information processing, has not been fully addressed.

In this thesis, I present studies that demonstrate a potent yet previously unknown regulation of neuronal intrinsic excitability by the microRNA miR-128. I show using genetic models that endogenous miR-128 plays a powerful role in dampening the excitability of pyramidal projection neurons in the adult forebrain and demonstrate that the loss of this microRNA alone results in severe motor hyperactivity and fatal epilepsy. By employing genetic tools that permit the interrogation of miR-128-mediated repression and its downstream physiological effects in restricted neuronal populations, I show that miR-128 exerts a sensitive tuning control of target gene expression, intracellular signaling cascades activation and behavioral measures of excitability.

The work presented here will help to guide future studies of microRNA function in neurons and other cell types, and reveals a small RNA and its target network as a novel regulatory node with possible implications in animal behavior and human pathology.

To my late grandmother

李金梅

ACKNOWLEDGEMENTS

I would like to thank Paul Greengard for giving me the opportunity to join his laboratory and take on this fascinating project. His constant support and warm encouragement have been very important to me. Equally, I would like to thank Anne Schaefer, who initiated the work on microRNAs in the lab and who has been unfailingly generous and patient with me. I will miss our impassioned discussions and will be forever grateful for her guidance.

I would like to acknowledge collaborators who have contributed to various aspects of the work presented here, including Morten Venoe and Scott Dewell for their work on CLIP-seq analysis, Josh Plotkin and James Surmeier for the electrophysiological studies and Melanie von Schimmelmann for the nuclei flow cytometry studies.

I would like to thank past and present members of the Greengard Lab who have been generous with their advice and assistance. I would like to thank the administrative staff, both for helping me personally on many occasions and for running the lab seamlessly to allow myself and others to be productive in our work. I would also like to thank the research assistants Adam Intrator, Selina Locklear, Alice Min, Amanda Rubin, Philip Feinberg, Silas Mann and Annie Handler for technical assistance and contributions to the work presented here.

I would like to thank my thesis committee members, Alexander Tarakhovsky and Cori Bargmann for their insights and strong encouragement these many years. I would also like to note my appreciation for the work of members of the Dean's office for their strong support of the student body in general.

I would like to thank all my friends here at Rockefeller who truly have been my family away from home. I would especially like to thank Pinar Ayata who is like a sister to me, and my old co-conspirator David Jordan with whom I fell in love with this city and this country.

Most importantly, I am truly grateful for my partner Manu, my brother Zhanpeng and my parents Jenny and Tinghowo, whose love is the source of all my courage.

Table of Contents

List of Figures

Chapter 1: Introduction

In complex multicellular organisms, terminally differentiated somatic cells are participants in a vast division of labor. These cells perform specialized tasks that enhance the survivability and the fitness of the organism as a whole. The role of most if not all of these cells can be simplified as follows:

1. Taking a measure of their environment by probing and measuring the presence of external signals such as photons, pressure, metabolites, neurotransmitters etc.

2. Responding to the combination of these inputs by changing their own internal environment, producing a response that can be read by other cells and for some cells issuing a response that alters the great Exterior itself.

3. Employing homeostatic control to ensure their ability to respond to further inputs in a consistent manner.

For neurons of the central nervous system, the role is similar if somewhat more elaborate. While the input is composed mostly of membrane potential changes, chemical neurotransmitters and neuropeptides, the range of responses is vast. Firstly, neurons integrate multiple inputs across the dendritic network to transform input information. Secondly, neurons often engage cytoplasmic and nuclear plasticity mechanisms to change their response to future inputs. Finally, neurons require homeostatic controls that preserve not only their ability to respond to further inputs, but also their capacity to re-engage plasticity mechanisms to set down new and persistent changes.

In addition to the internal complexity of the singular neuron, the adult brain of mammals consists of a daunting diversity of functionally unique neuronal subsets. Cell types are characterized by stereotyped morphology, regional and laminar location, connectivity and neurotransmitter output and

receptivity. The reductionist approach to neuroscience, which has proven enormously useful in explaining animal behavior, requires careful accounting of neuronal diversity as well as an understanding of how information is processed in each subtype.

Both the neuronal identity and response profiles exhibited by each neuronal subtype are greatly influenced by gene expression. The combination of genes expressed, the quantity to which they are produced, the temporal pattern and spatial localization of their expression, are all salient factors. It is not surprising then that neuronal gene expression is regulated at multiple levels - epigenetic, transcriptional, post-transcriptional and translational, each conferring a unique regulatory function.

Among the post-transcriptional mechanisms discovered so far, a class of small non-coding RNAs known as microRNA (miRNAs) has drawn particular interest among neuroscientists. There exists a large number of unique miRNAs many of which are expressed in the brain and exhibit neuronal subtype specific expression patterns. This suggests a role in determining identity and/or shaping cell-type specific processes, but only a handful of neuronal miRNAs have been studied so far.

The work I present in this thesis aims to examine the functional consequences of miRNA expression in neurons. It will examine the manner in which miRNAs alter gene expression and affect physiology and information processing in specific neuronal subsets. More generally, the results presented here will improve our understanding of the multi-layered architecture of gene expression in neurons and other cells.

In this introduction, I will briefly review the original discovery of the miRNA system, outline the current understanding of miRNA biogenesis and function, discuss key miRNA regulatory motifs, and review current knowledge of miRNA function in neurons.

1.1 microRNAs: a novel small RNA family

The compendium of genetically encoded small noncoding RNAs in animals encompasses a growing list of unique classes, including piwi-interacting RNAs (piRNAs) (*1*) , pseudogene derived endogenous siRNAs (endo-siRNAs) (*2*), and microRNAs (miRNAs). Among these, miRNAs represent arguably the most ubiquitously expressed class of small RNAs, as well as the most intensely studied.

The first miRNAs *let-7* and *lin-4* were discovered in nematode worms (*C. elegans*) as a result of genetic screens for novel heterochronic genes. *let-7* and *lin-4* were found to regulate the timing of larval cell fate decisions, by repressing translation of protein-coding messenger RNAs (*3-5*), demonstrating in animals a unique form of small-RNA mediated post-transcriptional regulation.

Soon after, studies showed that miRNAs were more than simply an esoteric innovation of invertebrate evolution. The broad conservation of *let-7* throughout bilateran lineages and the detection of *let-7* and other novel miRNAs in a wide range of eukaryotic cells revealed miRNAs to be part of an ancient and ubiquitous regulatory mechanism (*6-10*). These efforts in addition to deep sequencing studies have identified hundreds of miRNAs in humans and mice, including both highly conserved miRNA families as well as species-specific members (*11-13*). The latest update in miRBase (www.mirbase.org), a comprehensive miRNA database, lists over 1200 miRNAs and over 2000 miRNAs in the mouse and human genomes respectively.

The discovery of miRNAs was contemporaneous with the seminal discovery of RNA interference (RNAi), a post-transcriptional sequence-specific mechanism of gene silencing through exogenous introduction of double stranded RNA (dsRNA) (*14*).

Starting with double stranded RNA, RNAi involves small interfering RNA (siRNA) intermediates of 22-26 nucleotide length, which mediate degradation of transcripts with complementary sequences. Sequence analysis of miRNA loci and biochemical isolation of miRNA intermediates revealed that miRNA production also involved a double stranded precursor in the form of a hairpin structure. These structural parallels between siRNA and miRNA immediately suggested the possibility of common mechanisms of biogenesis. Mechanistic links between the two were formally demonstrated by a common requirement for Dicer and Argonaute family proteins (*15-18*). Other steps required for the maturation of functional miRNA, from transcription to incorporation into effector complexes, were discovered soon after. The canonical pathway of miRNA production in mammalian cells that evolved as a result is outlined below.

1.2 Biogenesis and decay

miRNA loci are distributed in multiple locations across the genome. About half of these loci are located in intergenic regions and have unique cis-regulatory sequences such as enhancers and promoters (*19*). Other miRNAs are located in the introns of protein coding genes and are generally co-expressed with their host genes. In both cases, miRNAs can occur either singly or as one of many in a poly-cistronic cluster, with multiple hairpins located on one continuous primary RNA transcript (pri-miRNA).

Systematic studies of expression patterns of miRNAs and host genes show strong co-expression between closely spaced miRNAs and between intronic miRNAs and their host genes (*20*). This could result from their expression from a single transcript, or simply reflect the existence of common cis-regulatory regions. Like protein-coding mRNA, the vast majority of pri-miRNAs are transcribed by RNA polymerase II (Pol II) (*21*, *22*), although RNA polymerase III (Pol III) promoters have been detected in association with some miRNAs (*23*, *24*), and are likely to support higher transcription rates at these loci.

Regardless of their genomic location, further processing of miRNAs requires the formation of a hairpin structure called the precursor miRNA (pre-miRNA), which includes an imperfectly complementary double stranded stem and a terminal loop. The mature miRNAs are derived from one or both strands of the stem region. Pre-miRNAs are processed from pri-miRNA co-transcriptionally by the nuclear Microprocessor complex (*25*). This complex consists of two core-proteins: DGCR8, which binds to the hairpin stem loop and Drosha, which catalyzes the cleavage of the pre-miRNA from the rest of the

transcript (*26*, *27*). For intronic miRNAs, precursor cleavage occurs after the assembly of exon-junction complexes but before excision of introns (*28*), ensuring that accurate mRNA splicing can occur despite the presence of intronic miRNAs.

Pre-miRNAs are exported to the cytoplasm by the GTP-dependent karyopherin protein Exportin5 to be processed and incorporated into the RNA-induced silencing complex (RISC). Pre-miRNAs are processed by the RISC-loading complex (RLC), which consists of 3 core proteins - Dicer, TRBP and Argonaute (Ago) (*29*). Dicer catalyzes a second cleavage step to generate a double stranded intermediate analogous to siRNAs. This miRNA/miRNA* duplex is then loaded onto Argonaute, the core miRNA-mRNA binding subunit. Selection of the effective strand of the duplex is thought to be a stochastic process with strand use bias determined by the relative thermodynamic stability of the 5' ends (*30*, *31*). Finally, Ago catalyzes the unwinding of the duplex in an endonuclease-independent mechanism (*32-34*) to complete the miRNA maturation process.

Major deviations from the above canonical pathway (Figure 1) for miRNA production have been shown to exist in mammals, however these cases are extremely rare. Drosha-independent processing has been demonstrated for a subclass of miRNAs called mirtrons in which short intronic miRNA hairpins are excised from pri-miRNA using components of the splicing machinery (*35*, *36*). Furthermore, it was demonstrated recently that processing of the mammalian miRNA miR-451 is Dicer-independent. Instead, pre-miR-451 cleavage requires Ago2 endonuclease activity (*37-39*).

Figure 1. Canonical biogenesis of miRNA

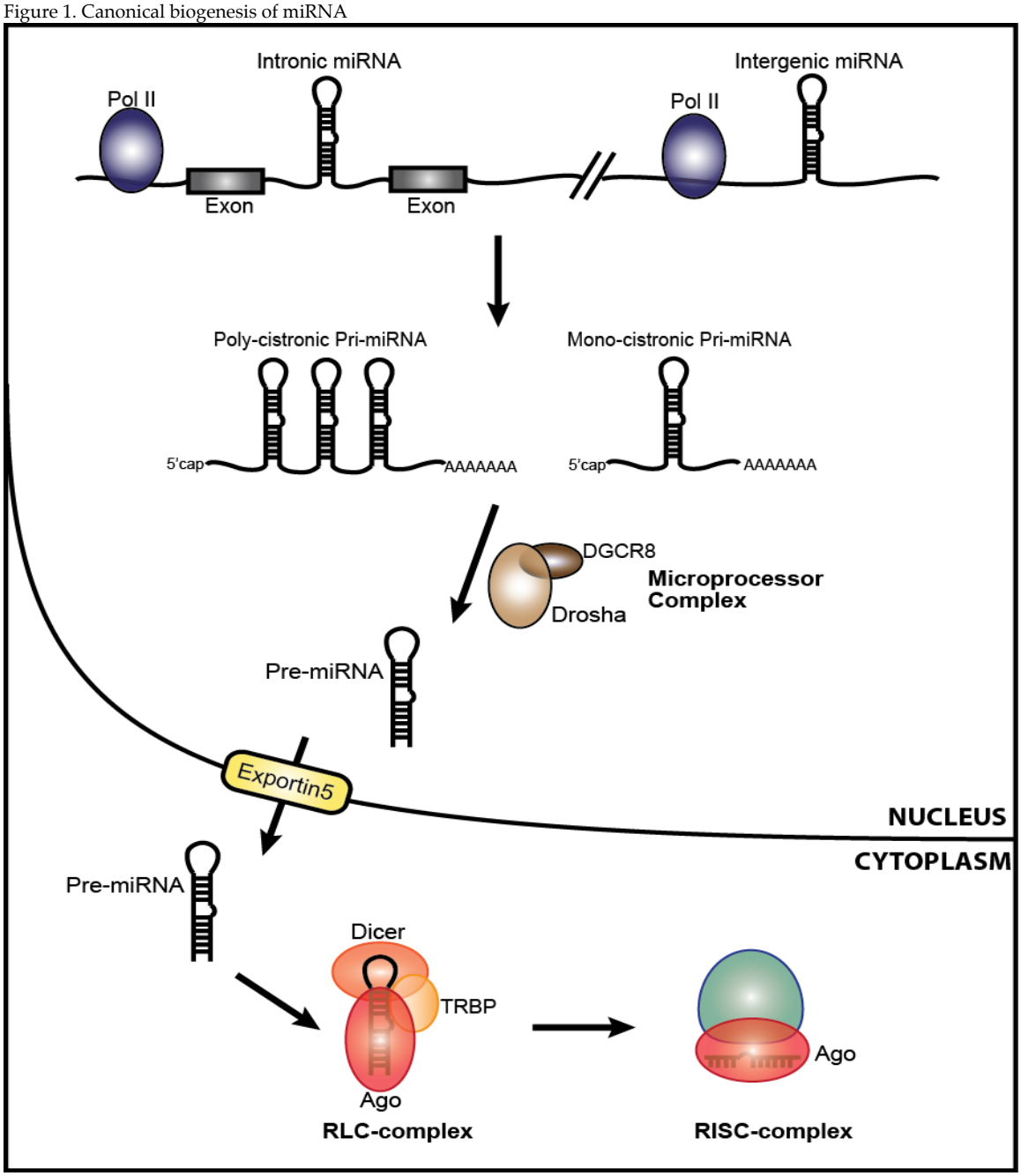

Figure 1 Canonical biogenesis of miRNA.

Pol II transcribes most intronic and intergenic miRNAs into pri-miRNA transcripts, which may contain one or multiple hairpins. Pre-miRNA hairpins are cleaved from pri-miRNAs by the Microprocessor complex, and are exported from the nucleus by Exportin5. Pre-miRNAs are further cleaved and unwound by RLC. Finally, mature single stranded miRNAs are loaded into Argonaute-containing RISC complexes.

Unlike miRNA biogenesis, relatively little is known about the regulation of miRNA degradation. Experiments that track the loss of mature miRNAs upon Dicer deletion in vivo and in cell culture suggest that miRNAs can be very long-lived. Variation in stability between miRNAs can be substantial. For example, Dicer deletion in mature Purkinje cells of the cerebellum resulted in complete absence of miR-124a at the earliest observation time point (2 weeks after deletion), but other miRNAs appear to persist for weeks (*40*). Measurements of miRNA decay rates upon Dicer deletion in mammalian fibroblast culture produced an estimated average half-life of 5 days but with substantial variation between miRNAs (*41*).

Other studies however have shown that miRNA stability is strongly dependent on cellular state, and in some cases turnover can be very rapid. miRNAs appear to have higher decay rates in cycling cells and greater stability upon mitotic arrest. Interestingly, decay in neurons appears to be activity-dependent. Glutamate-induced neuronal activation enhances miRNA decay, such that most expressed miRNAs have high turnover rates in hippocampus and cortical neurons (*42*).

1.3 miRNA target binding

The RISC complex with a single stranded 19-22 nucleotide mature miRNA is the primary effector complex in miRNA-mediated post-transcriptional repression. miRNAs serve as guide strands for RISC complexes, allowing binding to target mRNAs through partial sequence complementarity.

This partial complementarity between miRNA and target has been dissected to reveal the structural factors that contribute to functional binding. miRNA bases 2-7 from the 5' end define the minimal seed sequence, and perfect complementarity between the seed and target mRNA is the most important criteria for effective binding (*43-45*). Imperfect complementarity outside of the seed region may contribute to binding efficiency, but the effect is small and only in rare cases do such binding compensate for the lack of perfect seed complementarity. This requirement of seed binding has since been validated by structural studies (*46-49*). The major contribution of the seed sequence to target specificity has led to the classification of miRNAs into related families in which miRNAs share identical or highly similar seed sequences and are therefore likely to have highly overlapping target sets.

In addition, RISC binding is influenced by the context of the target site within the transcript. Repression is favored by the following structural factors that reduce physical occlusion of RISC-binding and improve accessibility of secondary structures: (i) Target site location in the 3'UTR as opposed to coding region or 5'UTR. (*50*, *51*) (ii) Location of seed site within the beginning and end of 3'UTR of mRNA (*52*, *53*), and (iii) Uracil and adenosine rich context of the seed (*53-55*). Lastly, most transcripts contain many potential miRNA target sites, and

often multiple target sites for one miRNA.

Binding of a single transcript by multiple RISC-complexes unsurprisingly increases the repressive effect. Biochemical analysis reveals that while most of these interactions occur in an independent and non-cooperative manner (*53*, *55*), sites spaced between 13-35 nucleotides apart result in cooperative repression (*53*, *56*, *57*).

The specific sequence requirements of seed complementarity and other sequence-based determinants of miRNA binding have encouraged a proliferation of prediction algorithms to identify targets *in-silico*. In addition to combinations of the above factors, many of these programs employ measures of site conservation to improve selectivity for biologically functional sites. Furthermore, most algorithms attempt to rank predictions based on scores generated for some of the above factors as well as others such as predicted miRNA-target pairing stability.

The resulting lists of predicted targets are largely overlapping due to the requirement of seed pairing but contain important differences related to variations in weighting factors, and the use of different transcript databases. Recent studies that rate the performances of these algorithms against experimental data largely demonstrate a significant but weak correlation even for the best performing algorithms, with false positive rates exceeding 50% (*58*). Such a result is perhaps unsurprising given that the algorithms employ only general targeting principles, most of which were derived from cell culture experiments involving highly expressed miRNAs.

Among the other factors that remain unaccounted for in most predictive algorithms, I will highlight three salient ones here. Firstly, many RNA-binding proteins regulate transcript localization and stability. How and if these proteins interact with RISC complexes is still largely unexplored. Secondly, cell-type specific expression of miRNAs and mRNAs can result in large variations in miRNA-target ratios and differing combinations of miRNAs available to target a given transcript. Finally, the mechanisms mediating miRNA-dependent repression (e.g. stability of translationally repressed transcripts) may be species and cell-type specific. As such the degree of repression experimentally observed will depend on the way in which miRNA levels were perturbed and the manner in which these observations were taken, e.g. protein versus mRNA quantification.

Given the limited utility of predicted targets in light of these factors, recent studies have tried to identify in-vivo interactions by isolating RISC complexes and their associated RNA (*59*, *60*). These early studies also had limited success due the an apparent promiscuity of miRNA-transcript interactions. Subsequent iterations have improved the specificity and reduced false positive rate.

One such example (HITS-CLIP) uses UV-crosslinking of Ago to bound RNA followed by isolation and sequencing of bound mRNA (*61*, *62*). The authors' own comparison with genome-wide protein quantification of miRNA repression suggests an improvement of false positive rate to ~30%. The technique was applied to identify miRNA targets in embryonic stem cells and in neurons (*61*, *63*). This technique however is limited by the low efficiency of UV-crosslinking and low RNA yield.

An alternative technique (PAR-CLIP) uses a photo-activatable nucleoside to facilitate the formation of mRNA-Ago covalent links. This technique also permits subsequent identification of the cross-linked nucleotide and therefore allows the exact Ago-RNA binding site on the transcript to be readily identified (*64*). The major limitation with this protocol is the requirement for synthetic nucleosides, which limits its application to cultured cells.

Finally, even the presence of Ago-miRNA-mRNA association *in-vivo* does not in itself imply target repression. At least one experimental comparison between mRNA target repression and target association using both HITS-CLIP and PAR-CLIP has been performed (*65*). The results suggest that while both CLIP techniques show good agreement, and outperformed most predictive algorithms, only 50% of predicted targets were repressed by exogenously applied miRNA.

In conclusion, substantial progress has been made in elucidating the basic determinants of miRNA-target pairing but transcript and cell specific determinants are not readily accounted for. New tools like HITS-CLIP and PAR-CLIP permit unbiased discovery of physiological miRNA-target interactions, however, only subsets of these interactions result in target repression, implying the need for independent assessments of target repression.

1.4 microRNA-mediated repression

In the vast majority of cases, miRNA-RISC binding results in downregulation of the target gene through translational repression and/or mRNA deadenylation and degradation (Figure 2). Extensive complementarity between miRNA and target RNA can result in Ago2-dependent endonucleolytic cleavage and degradation of the target as in RNAi (*66*) but this is rarely observed in animals.

Initial analysis of translation repression suggests that miRNA repression did not result in changes in polysome distribution of the target mRNA and that repression occurred at a post-initiation step, likely by stimulating ribosome drop off during polypeptide elongation (*67*, *68*). Subsequent studies however, have provided heavy evidence in favor of inhibition of translational initiation as a major mechanism of repression. Firstly, endogenous mRNA targets shift to lighter polysome fractions upon miRNA-repression (*69*, *70*). Secondly, 5' m7G cap-independent translation is not subject to miRNA repression (*71*, *72*). Furthermore, in vitro reconstituted translation experiments have also demonstrated the importance of initiation mechanisms involving the mRNA 5' m7G cap (*72-74*). Finally, structural studies show that the Mid domain of Argonaute proteins can bind directly to the 5' m7G cap (*75*).

Although miRNAs were initially thought to regulate translation with minimal effect on mRNA level, many subsequent microarray and reporter construct experiments show that target silencing is accompanied by mRNA degradation. The consensus mechanism for this involves Ago binding of GW182 and PABP which in turn recruits decapping and deadenylase enzymes to initiate

Figure 2. Modes of miRNA repression

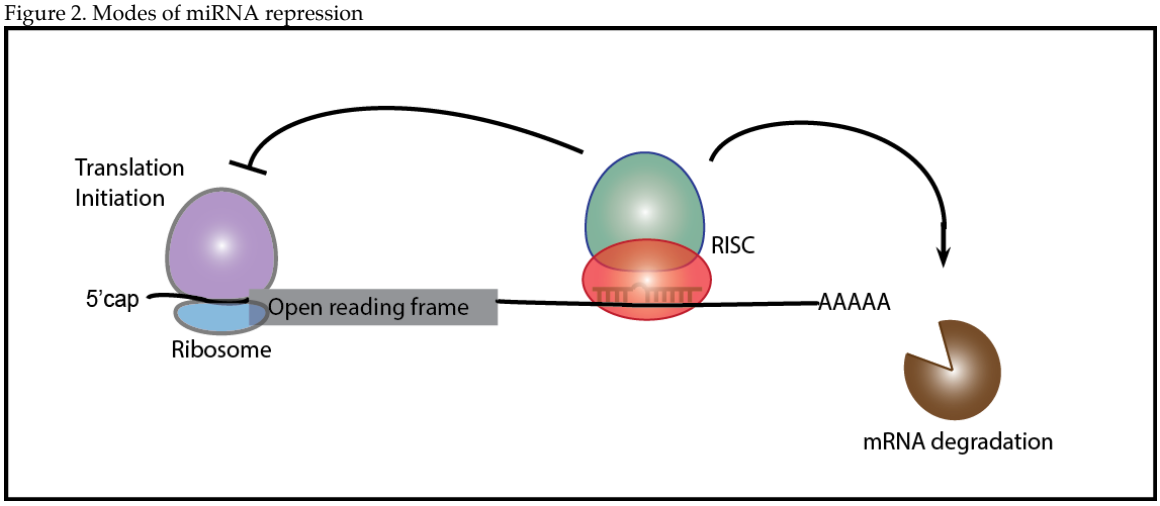

Figure 2. Modes of miRNA repression.

RISC binding to 3' untranslated region of messenger RNAs results in protein output repression by two non-mutually exclusive mechanisms. Argonaute proteins block translational initiation possibly by binding 5' cap structure and blocking recruitment of cap-dependent initiation factors. Argonaute also recruits decapping and de-adenylation enzymes via GW182 proteins to initiate mRNA degradation.

mRNA decay (*76*, *77*). It remains unresolved whether translational inhibition and mRNA degradation are mechanistically coupled or independent. Based on kinetic experiments, it appears that inhibition of initiation occurs more rapidly than mRNA decay, suggesting that the former precedes and perhaps triggers the latter. As mRNA 3'UTRs also contain other cis-regulatory sequences that may recruit other RNA-binding factors, it is also likely that the relative contribution of inhibition and decay to the overall steady state repression is transcript and context specific.

More recently, genome-wide studies have sought to address this issue by quantifying concurrent changes in protein output, mRNA-ribosome association and mRNA level upon exogenous miRNA perturbation (*58*, *78-80*). These studies indicate a strong correlation between changes in protein and mRNA levels. They also show that the repression of protein output is mildly but consistently higher than that of mRNA reductions, demonstrating that mRNA decay is a major component of repression but insufficient to account for miRNA effects alone. The result of these studies also confirms what had been observed with microarray-based quantification of target mRNAs. miRNA repression produces very mild (nearly all less than 2 fold, majority less than 1.5 fold) effects on steady state levels of both mRNA and protein.

In conclusion, miRNA repression in mammalian cells is likely to involve translational initiation inhibition followed by mRNA decay. In addition, miRNA-mediated repression is generally mild and repressive effects may not be captured by mRNA quantification alone.

1.5 Regulatory motifs and physiological roles

Despite the increasing complexity emerging around the regulation of specific miRNA production and function, the core principle of miRNA-mediated function is simple: miRNAs serve as guide strands to target multiple transcripts for repression. miRNAs bear some similarities to protein transcription factors: they can inhibit expression of hundreds of genes based on sequence determinants, and do so in combination with other miRNAs to increase specificity of regulation.

In this framework, the roles of some miRNAs are analogous to that ascribed to transcription factors, for example as binary switches during cellular differentiation. Such a classical switch interaction is exemplified by the first known miRNAs lin-4 and let-7, which are expressed to turn off specific target genes so as to alter cell fate decisions (*3*). Such a switch-like role for miRNAs has been observed during the differentiation of murine epidermal cells (*81*), smooth muscle cells (*82*) and neurons (*83*, *84*). Similarly, miR-145 promotes differentiation of human embryonic stem cells by repressing pluripotency factors (*85*). Finally, comprehensive examinations of miRNAs and conserved targets show that they are usually expressed in a mutually exclusive manner (*86*, *87*), suggesting that miRNA switches are common regulatory motifs throughout animal development.

In the above switch-like interactions, miRNAs are strongly induced during the cell fate transition and markedly repress the putative relevant targets, but miRNA expression alone is not generally sufficient to trigger the transition. In fact, premature miRNA expression often results in dysfunction of the

progenitor cell such as reduced proliferation (*81*, *84*). It is therefore possible that miRNAs more generally improve the robustness of the cell fate transition by suppressing genes that are detrimental to the transition process. In agreement with this, miR-9a is not induced during differentiation of neuronal precursors but its presence reduces phenotypic variation by helping to suppress targets below a threshold level. (*88*).

Such failsafe interactions suggest a broader utility of miRNAs as a buffer against phenotypic variation in general (*89*). Phenotypic variation might arise from intrinsic transcriptional noise. Transcription is an inherently noisy stochastic process (*90*) and phenotypically identical cells masks substantial cell-cell expression differences (*91*). Increased stochastic variability in gene expression can be detrimental, and protein networks are organized to buffer against it (*92*). In support of this theory, miR-7 is required to maintain cell fate decisions in the presence of temperature fluctuations, which increases the stochasticity of gene expression (*93*).

These switch-like and buffer-like regulations reduce target proteins below a threshold, so as to trigger or sharpen a binary process. The mild influence of miRNA on the expression of most protein targets suggests that fine-tuning of cellular processes is another important regulatory motif. In this context, the protein targets are expressed at a defined optimal range by one or more miRNAs, and deviations above and below this range are both detrimental. This form of regulation has been observed in a number of terminally differentiated cell types. For example, miR-181 regulates T-cell sensitivity, while miR-223 regulates neutrophil sensitivity. In Drosophila, miR-8 tunes the levels of atrophin to regulate neurodegeneration (*94*).

Recently, studies have begun to reconcile these different modes of interactions found in mammalian cells. When considering target changes in large cell populations, as is the case in many murine experiments, theoretical analysis suggests that buffering of small stochastic transcriptional noise can be accompanied by mild aggregate repression comparable to that associated with fine-tuning effects (*95*). This indicates that tuning interactions found in population based measurements does not exclude the possibility of buffering effects in single cells.

This notion has found experimental support recently. Using single-cell measurements, Mukherji et al. showed that while aggregate repression is modest, large variations in repressive effect occur between cells. They further demonstrate that switch-like and fine-tuning interactions may occur for the same miRNA-target pair depending on the relative abundance of miRNA and mRNA target under a given condition (*96*). It is also likely that in different cell types, miRNAs target not just different mRNAs but regulate them in different manner, limiting the generalizability of specific miRNA-target interactions drawn from studies performed in cultured cells or in one cell type.

1.6 microRNAs in neurons: expression and function

Post-transcriptional mechanisms are important in the regulation of neuronal physiology and information processing. For example, proteins like FMRP regulate the translation of specific genes while proteins such as TSC control global translational output, and deficiency of either results in severe cognitive and neurological defects. As post-transcriptional regulators, miRNAs are similarly critical to the function of neurons.

Since the maturation of nearly all mammalian miRNAs are dependent on the canonical pathway outlined before, animals deficient for one or the other of these pathway components provided some of the first demonstrations of the importance of miRNAs in mammalian neuronal physiology.

Loss of Dicer enzyme is embryonic lethal (*97*), therefore conditional deletions of Dicer have been used to study the role of miRNAs in several brain regions and neuronal populations. These mutants show that miRNAs have a important role in neuron survival. Specific loss of Dicer in a variety of neuronal populations (including cerebellar Purkinje cells, forebrain principal neurons, midbrain dopamine neurons and retinal cells) consistently led to increased apoptosis and cell death (*40*, *98-100*).

Other deficiencies that result in only partial miRNA depletion have been useful to reveal milder phenotypes. Haplo-insufficiency of the Microprocessor component and Drosha binding partner DGCR8 impairs biogenesis of a subset of miRNAs in the adult brain and resulted in behavioral and cognitive deficits reminiscent of human 22q11.2 microdeletions (*101*). Loss of Ago2 in Dopamine receptor 2 (Drd2) positive neurons in the striatum results in partial depletion in a

subset of expressed miRNAs, and reduced cocaine addiction (*102*).

More recently, several groups have focused on specific miRNAs (*103*) and I will highlight a few below. Overexpression of miR-125b induces the formation of long thin spines and reduced mEPSC amplitude, while reduced miR-125b increases the width of dendritic spines (*104*). miR-138 also negatively regulates spine size and excitatory mEPSCs (*105*). Both studies examined miRNA function in spine formation in cultured neurons.

Other studies have used knockdown of miRNAs in murine brain, allowing further characterization in their physiological context and examination of behavioral alterations. Overexpression of miR-137 in newborn cells in the adult dentate gyrus reduced dendritic complexity and spine density (*106*), while miR-134 is expressed near dendritic spines and negatively regulates spine size (*107*). Interestingly, overexpression of miR-134 in the hippocampus abrogates long-term potentiation in CA1 neurons, and impairs memory formation in the contextual fear-conditioning paradigm (*108*). That study represented a rare example in which perturbation of a single miRNA led to changes in learned behavior. Another significant example is that of miR-212, which is induced by extended cocaine self-administration in rats. Overexpression and knockdown of miR-212 in the striatum results in reduced and enhanced cocaine intake respectively (*109*).

In all the above case studies, miRNA knockdown was achieved by non-genetic means using modified RNA such as antagomirs and locked nucleic acid (LNA) as well as miRNA-sponges. In contrast, far fewer genetic mutants of specific miRNAs have been generated. A couple of unique difficulties make genetic models of miRNA function challenging. Firstly, many miRNAs exist as

multigene families, with distinct members expressed from multiple loci but sharing very similar seed sequences, resulting in functional redundancy. Secondly, many miRNAs are expressed in tightly spaced poly-cistronic transcripts, making it difficult to delete one miRNA without affecting co-expressed miRNAs at the same locus. One notable example is that of the poly-cistronic transcript which expresses both miR-132 and miR-212. Deletion of the entire locus in newborn hippocampal neurons resulted in dramatically reduced dendritic length and spine density. The authors disentangled the relative contributions of the two miRNAs by demonstrating that only miR-132 is functionally expressed in these neurons (*110*).

Studies of changes in miRNA expression in pathological tissue from human patients and disease model animals hinted at the clinical relevance of these findings. Significant changes in miRNA levels were found in tissue samples from patients of neurodegenerative diseases such as Huntington's disease and Alzheimer's disease (*111-113*). Other changes have been noted in post-mortem tissue from sufferers of schizophrenia and schizoaffective disorder (*114*, *115*). In spite of this, few specific roles have been attributed to miRNAs in the modulation of either neurodegenerative or psychiatric disorders.

The above studies nearly always ascribe miRNA-dependent phenotypes to single targets, often selected on the basis of predicted seed interactions and shown to be plausible targets using reporter constructs in culture. The contribution of single miRNA-target pairings to the observed effects is often not directly addressed and when it is, has somewhat limited explanatory power. Target discovery tools detailed in the previous sections have not been utilized in the study of neuronal miRNAs. In summary, evidence of the various roles of

miRNA in post-developmental neuronal function has accumulated in recent years but there exist significant gaps in our current understanding.

In the following chapters, I will present the results of our study. First, we demonstrate that changes in miR-128 levels in the principal projection neurons of the forebrain sensitively tune motor activity and seizure susceptibility. Second, we show that miR-128 is uniquely important in striatonigral projection neurons. Third, we have found that miR-128 represses a specific subset of target genes in this neuronal population. Lastly, we show that miR-128 regulates ERK signaling and suppresses electrical excitability as well as transcriptional response.

Chapter 2 miR-128: Expression and function in forebrain principal projection neurons

2.1 Spatial enrichment of a neuronal miRNA

A large body of work over the last decade has examined the expression levels of a large and growing list of mammalian miRNAs in a nearly exhaustive list of organs and tissues obtained at various developmental stages and disease states.

A notable point that arises from these studies is the very high level of tissue and developmental stage specificity to miRNA expression. Many well-established central nervous system (CNS)-specific miRNAs such as miR124a are highly expressed at the earliest stages of neuronal differentiation and are likely to have a most substantial role in developmental processes (*116*, *117*). However, these expression studies also consistently identify a handful of well expressed miRNAs with specific expression in the mature CNS, suggesting an involvement in the processes of neuronal information processing that underlie learning and behavior. Among these, one specific miRNA, miR-128, exhibits an intriguing set of characteristics.

Northern blot quantification of miRNAs from a panel of human and mouse organs reveal a number of miRNAs that are brain specific in both species including miR-128, miR9, miR132, miR137, miR139 (*118*). Microarray quantification of miRNA in the developing and adult brain shows that a number of miRNAs including miR-128, miR132 and miR29 among others are strongly upregulated during development to reach peak expression levels in adult. (*119*). Expression profiles based on cloning frequency reveal that miR-128 and miR143 are enriched in the adult cortex, striatum and hippocampus compared to the embryonic brain and various neuroblastoma and glioblastoma cells (*120*).

Our own quantification of miR-128 levels using semi-quantitative RT-PCR shows that miR-128 is expressed in the CNS at higher levels than any other organ examined (Figure 3a). miR-128 expression begins just before birth and accelerates rapidly after birth into adulthood after which it remains at peak levels (Figure 3b).

Although hundreds of *bona fide* miRNAs have been identified from mammalian tissue, a majority is expressed at very low levels and only a few dozen are consistently expressed at high levels in one or more tissues. Differences in expression levels often span a few orders of magnitude. Using absolute quantitation with RT-PCR and synthetic miRNA mimics, we found that the expression of miR-128 in the adult brain is very high (~10^4 per cell) (Figure 3e), comparable to the expression of ubiquitous miRNAs such as let-7 (*121*).

miR-128 appears to be a vertebrate innovation, as it has been identified in the lamprey genome but has not been identified in any invertebrate genome so far. In most vertebrates, miR-128 is expressed from hairpins encoded at two distinct loci: *miR-128-1* and *miR-128-2*, which are located in the longest introns of two related protein coding genes (R3Hdm1 and Arpp21 respectively). Both proteins share a common putative RNA-binding R3H domain.

Sequence divergence of the hairpins is nearly identical to sequence divergence of the protein coding host genes, suggesting that the association between miR-128 and members of the R3H domain protein family formed before duplication of the ancestral loci.

Interestingly, studies examining the distribution of miRNA expression in the adult and developing zebrafish CNS show that the highest expression was detected in adult forebrain structures including the telencephalon (*122*, *123*). In-

situ hybridization studies using LNA probes against mature miR-128 show that expression is higher in forebrain structures such as olfactory tubercle, cortex, striatum and the hippocampus (Figure 3c,d). The high and restricted miR-128 expression pattern, as well as the conservation of this pattern across the vertebrate lineage, strongly suggests an involvement in post-developmental CNS function.

Recently developed techniques extend these expression studies by profiling miRNAs expressed in genetically-defined neuronal populations. One such study showed that, within the cortex, excitatory Calcium-calmodulin kinase 2a (Camk2a)-positive neurons expressed much higher levels of miR-128 than inhibitory GAD-positive neurons, indicating a greater spatial specificity than previously appreciated. Among miRNAs expressed in Camk2a-positive neurons, miR-128 is one of the most highly expressed (*124*).

While this and other previous studies have quantified the relative expression of miRNAs among related cell or tissue types, it remains unclear what the significance of these differences in expression levels might be, especially in relation to the number and distribution of targets and in relation to the strength and kinetics of repression. One alternative to expression profiling to gauge the relative functional importance of miRNAs is to examine in-vivo targeting of messenger transcripts, for example quantifying the density of targets of a given miRNA among the set of all Ago-RISC bound transcripts.

Figure 3. Postnatal forebrain enrichment of miR-128.

a, Expression levels of mature miR-128 were quantified by qRT-PCR from organs of adult mice and expressed relative to the mean levels in liver. (n=2).

b, miR-128 and neuronal miRNA miR-124a in adult and embryonic brain (E12) were quantified as in **a** and expressed as fold increase over expression levels in the embryonic brain (n=3).

c, Expression of miR-128 in adult brain shown by *in-situ* hybridization on sagittal brain slice using antisense LNA-probe to mature miR-128.

d, miR-128 levels in selected brain regions were quantified by qRT-PCR and expression levels are expressed relative to mean hippocampus expression. (n=3).

e, Absolute quantification of miR-128. Titration standard (left) showing qRT-PCR cycle number for varying concentrations of synthetic mature miR-128 (left). Estimated per-cell copy number of miR-128 in adult striatal samples (n=16) (right) assuming an average of 15 pg total RNA per cell. Bold line indicates sample mean.

Error bars show s.e.m.

Figure 3. Postnatal forebrain enrichment of miR-128.

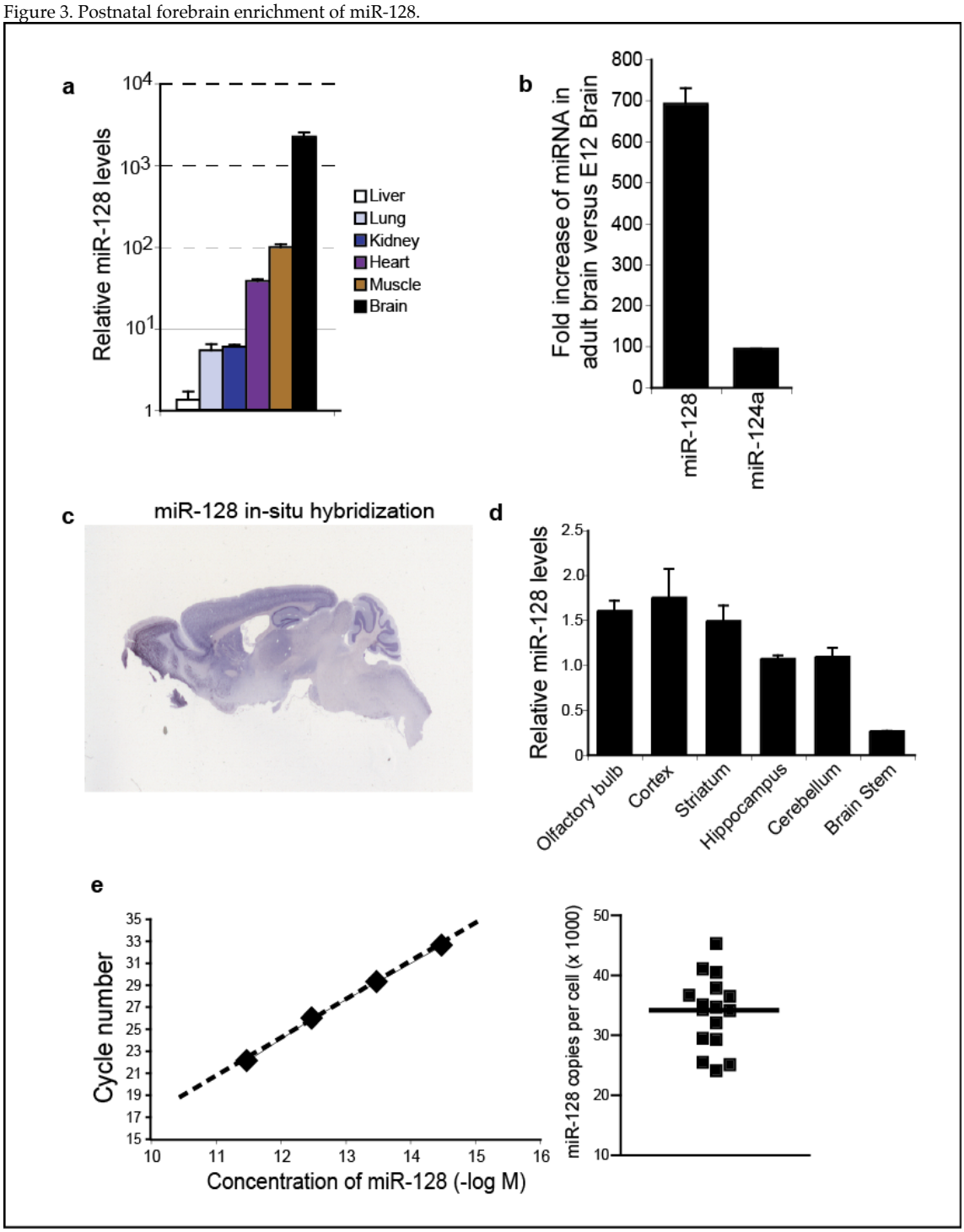

2.2 CLIP-Seq isolation of miRNA targets in projection neurons

To do this we made use of data generated by visiting student Morten Venoe here in the lab, who identified Argonaute binding sites on expressed transcripts in mature projection neurons. Briefly, we generated mice that permit conditional Cre-dependent expression of Argonaute2 (Ago2) protein tagged with a Flag epitope. Transgenic mice were crossed to mice expressing the Cre recombinase in Camk2a-positive neurons, generating doubly transgenic animals in which tagged Ago2 was expressed only postnatally in projection neurons of the cortex, hippocampus and striatum. Ago-bound and protected RNA sequences were isolated using an adapted protocol similar to one published previously (*63*): starting with dissected and homogenized half forebrain samples, RNA transcripts were UV-crosslinked to bound protein, unbound RNA was digested, and tagged Ago2 protein was immuno-precipitated using antibody against the Flag epitope. Adaptors were ligated to both ends of the RNA fragments in the immuno-precipitated fraction and RNA was de-crosslinked from protein by protease digestion. RNA fragments were then sequenced, processed for quality and trimming of adapter sequences, and aligned to the mouse genome (mm9) (Figure 4a).

The dataset of sequenced fragments forms clusters of overlapping RNA fragment reads that correspond to putative sites of miRNA-RISC binding (Figure 4b). As the miRNAs that mediate the binding to each cluster cannot be definitively determined from the data, we made use of the fact that most miRNA targeting is determined by the minimal seed site hexamer (*125*). The candidate miRNA(s) potentially mediating Ago-RISC targeting to each cluster can be

Figure 4. Ago2 associated mRNAs in Camk2a-positive projection neurons.

a, CLIP-seq bound sites are enriched in 3'UTRs of mRNAs. The distribution of the mouse (mm9) genome (left) and CLIP-seq read clusters (right).

b, Example CLIP-seq cluster of sequenced reads on the 3'UTR of Slc39a13 gene, with a miR-128 6mer target site indicated below.

c, Scatter plot showing statistical enrichment of all 4096 possible 6mers in CLIP-seq clusters located within Refseq annotated 3'UTRs. x-axis shows z-score which is the number of standard deviations the observed frequency of a hexamer exceeds the normalized frequency of occurrences in the corresponding RefSeq region. y-axis shows -log(p-value) from chi-squared test. Hexamers enriched above Refseq background are shown as grey dots; 6mer complementary to the miR-128 seed is highlighted in red. Green line represents Bonferroni-corrected critical p-value: $0.05/(4^6) = 1.22 \times 10^{-5}$.

d, Distribution of cluster read-count among miR-128 CLIP-seq targets, defined as genes with miR-128 target 6mer-containing CLIP-seq clusters within their 3'UTRs. Genes are ranked by total associated read-counts from left to right and read-counts for each gene are shown.

e-f, Genes with above-average CLIP-seq cluster read-counts are associated with neurological disorders and neurotransmission. Functional annotations significantly associated with miR-128 CLIP-seq targets shown in **d** were obtained by IPA Ingenuity analysis and the median and average per-gene read counts for each annotation are shown in scatter plot (**e**). Annotations associated with high read counts are highlighted, all other annotations are shown in grey circles. Specific highlighted annotations are shown with associated gene count, p-value, and median and average read-counts (**f**).

Figures **a-c** courtesy of Morten Venoe.

Figure 4. Ago2-associated mRNAs in Camk2a-positive projection neurons

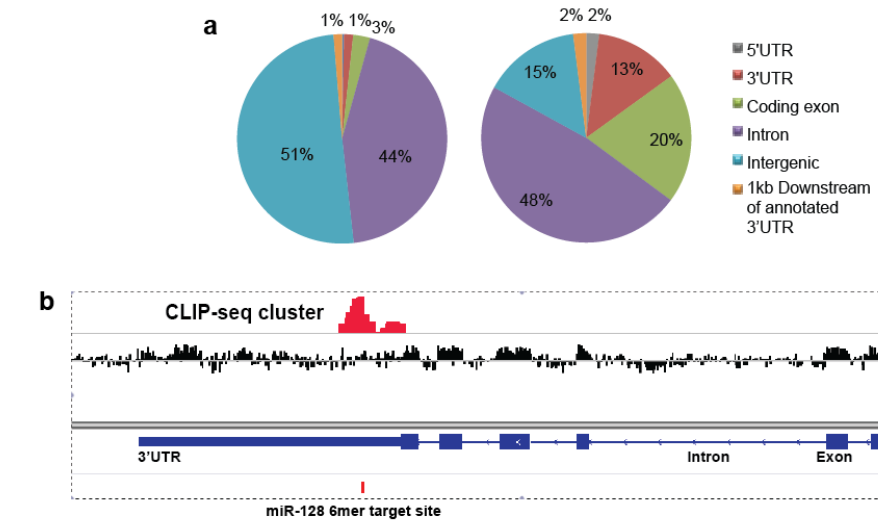

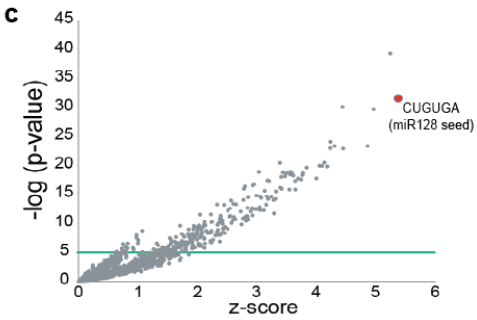

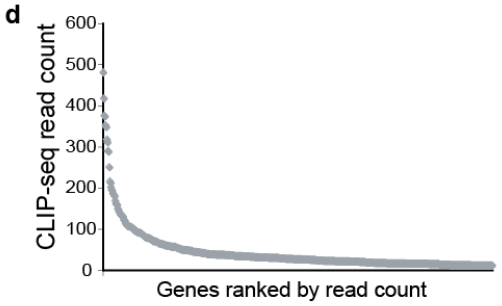

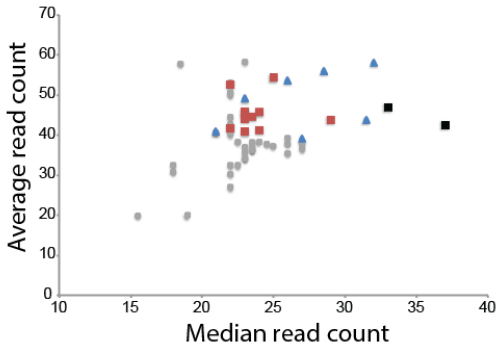

f

Functions	Gene count	p-value	Median	Average
Disease and Disorder				
movement disorder	77	6.29E-09	23	41
ataxia	23	1.74E-08	22	42
seizures	27	1.82E-06	24	41
neurological signs	49	5.99E-06	23	46
disorder of basal ganglia	55	6.06E-06	24	46
dyskinesia	48	7.55E-06	23	44
Huntington's disease	46	9.76E-06	23	45
mental retardation	13	1.95E-05	25	54
neuromuscular disease	58	2.94E-05	23.5	45
growth failure	40	2.31E-04	29	44
neurodegeneration	16	3.63E-04	22	53
Neuronal signaling and transmission				
excitatory postsynaptic potential	16	2.42E-07	23	49
neurotransmission	32	1.88E-06	28.5	56
synaptic transmission	27	6.29E-06	26	54
long-term potentiation of synapse	15	2.90E-05	27	39
long-term potentiation	18	2.84E-04	31.5	44
transport of vesicles	11	4.12E-04	32	58
action potential of neurons	11	5.72E-04	21	41
Biochemical Function				
phosphorylation of L-amino acid	17	0.000055	37	43
phosphorylation of protein	43	0.000413	33	47

identified by the presence of hexamers complementary to the miRNA seed site within each cluster. Consequently, the potential in-vivo targets of each miRNA can be determined.

Analysis of the combined sequence space given by all read clusters was performed to determine if any particular hexamer sequence was enriched in Ago-bound sites over the corresponding genomic region (3'UTR) as a whole. The hexamer corresponding to the binding complement of the miR-128 seed was the most enriched hexamer sequence (Figure 4c). Targets of miR-128 are therefore among the most over-represented miRNA targets among all neuronal Ago-bound transcripts.

The targets of miR-128 include 707 unique target genes (Figure 4d), whose roles encompass a substantial range of neuronal processes based on literature-curated functional annotation-IPA (Ingenuity® Systems, www.ingenuity.com). To parse the relative importance of these functional annotations, we examined the read count density of each target. Targets with higher read count density are deemed to be more likely to be functionally relevant. The median read count of each cluster is 26, with a surprisingly wide range of up to hundreds of reads. Since each functional annotation is based on a defined subset of target genes, each of which can be assigned a read count, we calculated the average and mean read counts associated with each annotation. We have plotted the average and median gene read counts on a scatter plot, with each point representing a single annotation (Figure 4e,f).

This analysis of miR-128 targets suggests that miR-128 is likely to have important roles in neuronal plasticity and in disorders such as seizures and motor disorders. We address this hypothesis in the following chapter.

2.3 miR-128 expression in projection neurons suppresses spontaneous seizures and locomotor activity

To assess the effect of miR-128 levels on neuronal physiology and the cell specific role of miR-128, we generated mouse models that permit the conditional deletion of the miR-128 loci as well as the conditional overexpression of miR-128.

For the deletion models, we generated mice carrying floxed alleles of each of the two miR-128 loci (Figure 5). These alleles contain *loxP* sequences that flank the miRNA hairpins, enclosing the 1-kilobase region centered on the 2 hairpins. The presence of *loxP* sequences permits excision of intervening sequences by Cre recombinases which are expressed in a cell-type specific manner, thus allowing for the genetic deletion of miR-128 hairpins in restricted cell populations. The presence of modified alleles in our mice models was confirmed by Southern blot analysis against genomic DNA with an external probe, as well as by PCR amplification and sequencing of modified regions. Regular genotyping was performed with PCR reactions that permit rapid identification of wild type, floxed and null (excised) alleles.

Crossing targeted floxed mice to transgenic mice ubiquitously expressing Cre-recombinase generated germline deletions of both loci. Examination of null mutants revealed a heavy bias in loci contribution to mature miR-128 levels in the brain. Deletion of miR-128-2 reduced brain miR-128 levels by 80% while deletion of miR-128-1 produced reductions of only 20% (Figure 6a-c). In addition, the heterozygous condition resulted in approximately half the depletion compared the null condition. These data suggest that no significant transcriptional/processing compensation occurs in the absence of one miR-128

Figure 5. Deletion targeting strategy.

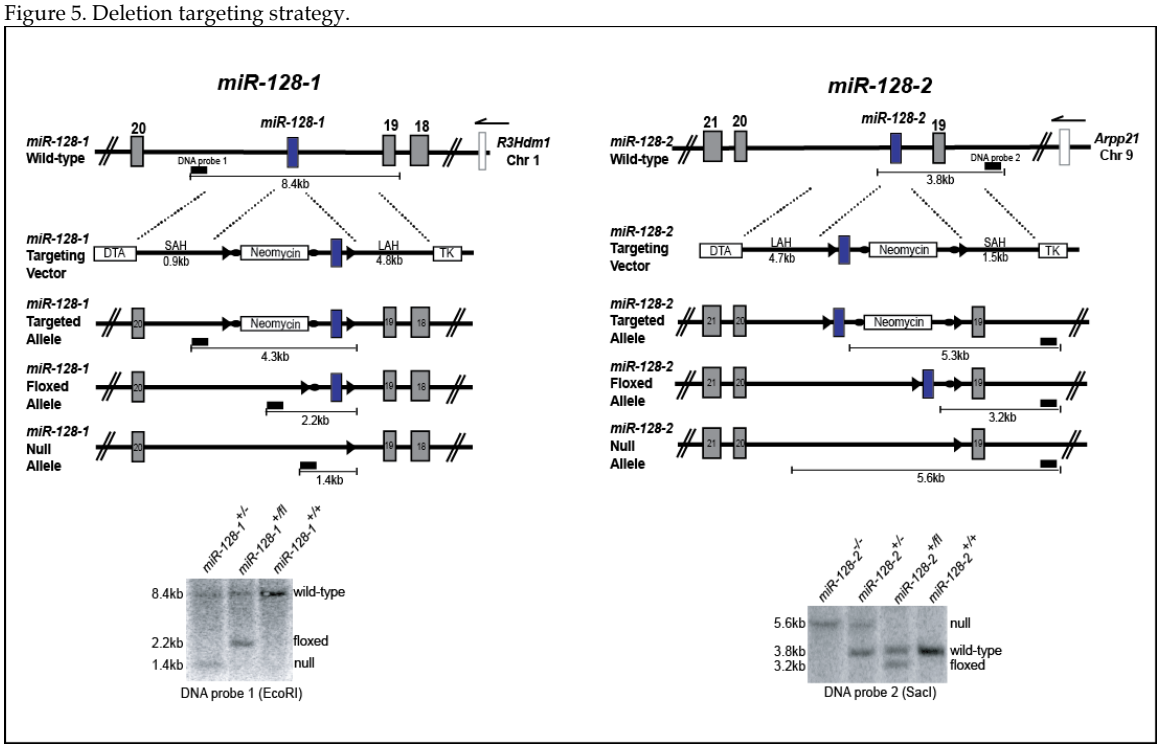

Figure 5. Deletion targeting strategy.

Targeting strategy for *miR-128-1* (left) and *miR-128-2* (right) loci. 1 kb region containing the miRNA hairpin was flanked with *loxP* sequences to generate *miR-128-1*$^{fl/fl}$ and *miR-128-2*$^{fl/fl}$ mice. miRNA hairpin (blue rectangles); exons (grey rectangles); *loxP* sites (black triangles); DTA - diphtheria toxin gene; TK - thymidine kinase gene; LAH/SAH - long/short arms of homology. Neomycin resistance gene flanked by *frt* sequences (black circles) was removed from targeted locus in vivo using Flp recombinase transgenic mice. Modified alleles were identified by probing EcoRI or SacI digested genomic DNA with DNA probes 1 and 2, respectively (black rectangles).

Figure 6. miR-128 levels are reduced by *miR-128-1* and *miR-128-2* deletion.

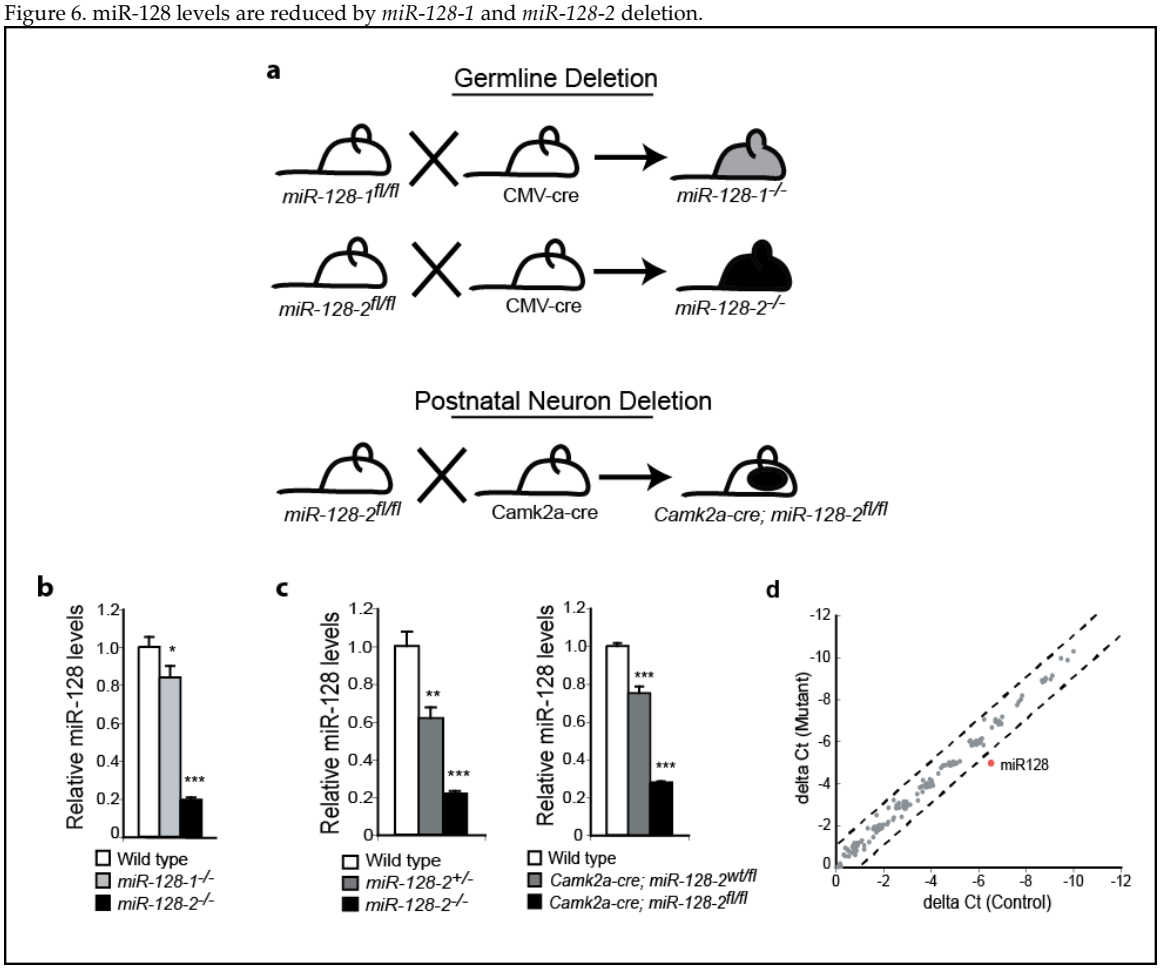

Figure 6. miR-128 levels are reduced by *miR-128-1* and *miR-128-2* deletions.

a, Mating scheme for generation of germline and postnatal deletions.

b, *miR-128-2* is the dominant locus. miR-128 levels in the brains of *miR-128-1*$^{-/-}$ and *miR-128-2* mice were assayed by qRT-PCR and expressed relative to mean wildtype levels. n=3-5.

c, Germline and neuronal deletion of *miR-128-2* result in similar reductions of miR-128 levels, n=4-5.

d, , Levels of other miRNAs were unaffected in the absence of *miR-128-2.* miRNA levels from Camk2a mutants and controls (n=2) were quantified by Taqman Low Density qRT-PCR arrays. Scatter plot shows normalized expression levels given by delta Ct (raw cycle count - global average cycle count) in mutant and control samples. Dotted lines indicate 2 fold increase or decrease relative to control. Red dot corresponds to mature miR128.

Error bars show s.e.m.* p<0.05; ** p<0.01; *** p<0.001, Welch's t-test.

allele. Due to the dominant contribution of *miR-128-2*, all deletion mutants mentioned subsequently in this thesis will refer to this locus alone unless otherwise stated.

For the conditional overexpression models, we used homologous recombination to insert a transgene segment into an intron of the ROSA26 gene, which is ubiquitously expressed (Figure 7a). The transgene consists of a strong CAG promoter (a combination of cytomegalovirus early enhancer element and chicken beta-actin promoter), a transcriptional STOP cassette flanked by loxP sequences, and a 1 kilobase genomic sequence that includes the miR-128-2 hairpin. In the absence of Cre recombinase expression, the STOP cassette terminates transcription upstream of the miR-128-2 hairpin. In the presence of Cre recombinase, the STOP cassette is excised and strong transcription of miR-128-2 hairpin occurs. Gene targeting was confirmed by Southern blot analysis using an external probe and PCR amplification and sequencing. Modified locus was followed by PCR-based genotyping. Cre-dependent expression of miR-128 was confirmed in both embryonic stem cells and in the adult brain. The level of overexpression in the brain was mild, possibly due to the high endogenous levels already present (Figure 7b,c).

Examination of these miR-128 mutants demonstrates that miR-128 regulates seizure susceptibility and motor functions. While miR-128-2 null mutants were fertile and viable, they had severely restricted lifespans, with a median of about 55 days (Figure 8a). We suspected that mutants had succumbed to seizures as home cage deaths were sudden and spontaneous and exhibited postural signs of seizures such as extended posture. Continuous video recording of mutants in the home cage captured intermittent bouts of severe spontaneous

Figure 7. Targeting strategy for transgenic expression.

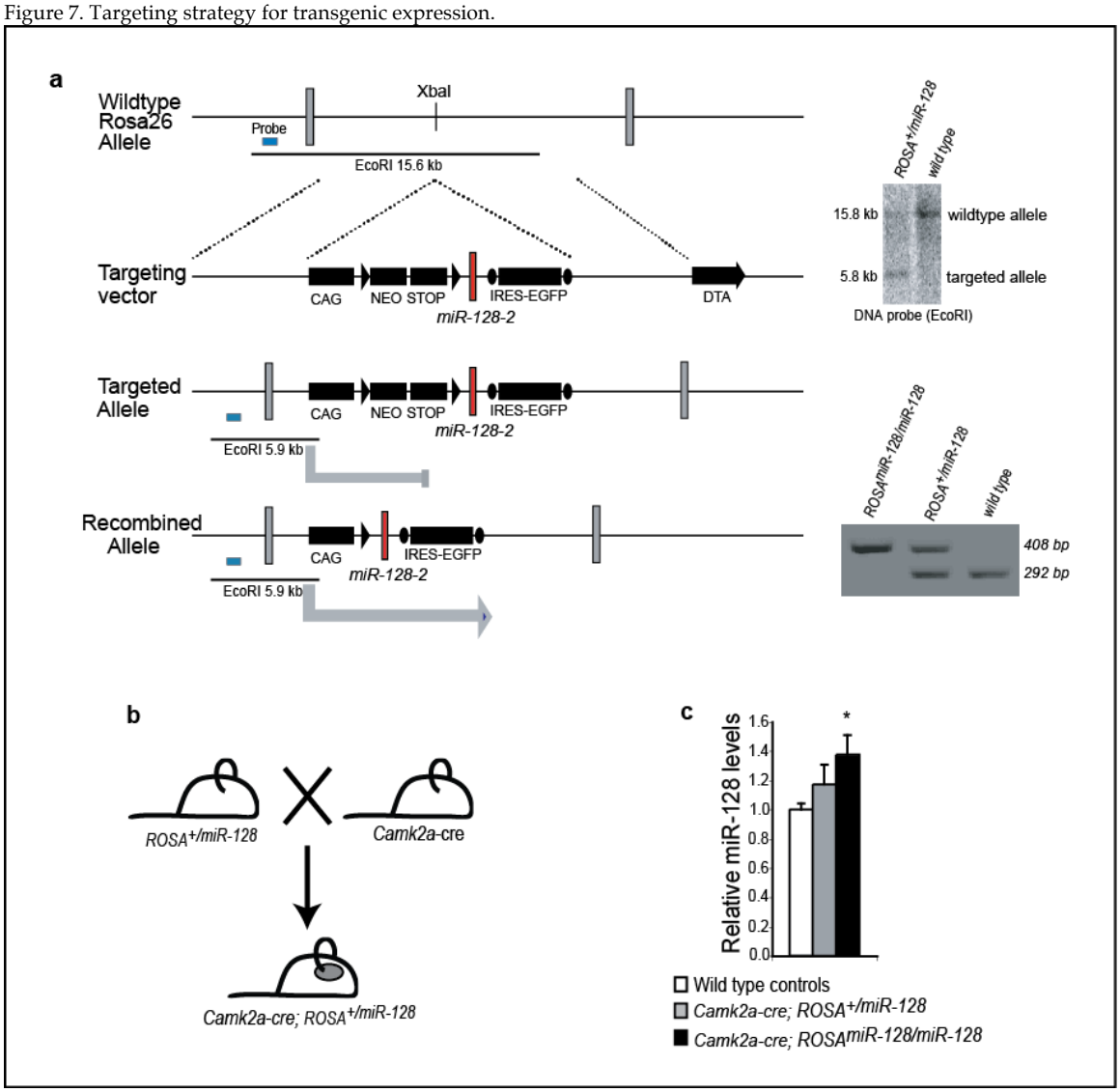

Figure 7. Targeting strategy of transgenic expression.

a, Left: Targeting strategy for conditional overexpression of miR-128 using knock-in transgenic strategy at the ROSA26 locus. A 1-kb region that includes the *miR-128-2* hairpin (red rectangle) was cloned downstream of a strong CAG promoter and a floxed-STOP-Neomycin cassette. Modified allele was identified by Southern blot (top right), or PCR genotyping (bottom right).

b, Mating scheme for postnatal neuron-specific overexpression of miR-128.

c, miR-128 levels in striata of double transgenic (*Camk2a-cre; ROSA*$^{miR\text{-}128/miR\text{-}128}$), single transgenic (*Camk2a-cre; ROSA*$^{+/miR\text{-}128}$), or wild type mice (n=3 each) were measured by qRT-PCR. Error bars show s.e.m. * $p<0.05$ Welch's t-test

tonic-clonic seizures (Figure 9a). Strong seizure episodes preceded deaths of recorded mutants. Consequently, we were able to rescue survival by continuous administration of the anti-convulsant valproate, demonstrating that fatalities resulted from a severe epileptic condition (Figure 9b).

Furthermore, miR-128-2 null animals were significantly more hyperactive than wild type animals in the open-field chamber (Figure 8b,c). For open-field chamber quantification, horizontal distance traveled was measured over an hour for animals exposed to a novel chamber. Mutants treated with valproate also remained hyperactive, suggesting that hyperactivity was not dependent on the development of prior seizures (data not shown). In agreement with the low expression at the miR-128-1 locus, deletion of this locus produced no significant hyperactivity and no increases in mortality (data not shown).

Using cell-type specific isolation and quantification of Ago-associated miRNAs, a previous study had shown that miR-128 was highly enriched in Camk-positive excitatory neurons compared to GAD-positive inhibitory neurons (*124*). Given that result, in combination with our observation that miRNA targets in Camk2a neurons were highly enriched for miR-128 targets, we hypothesized that deletion of miR-128 in this neuronal population alone might recapitulate most if not all of the observed mutant phenotypes.

Projection neuron-specific deletion of miR-128-2 was generated by crossing floxed mice with mice expressing Cre recombinase in Camk2a neurons (Figure 6a). Cre expression was present in principal neurons of the cortex and hippocampus as well as medium spiny neurons of the striatum. Cre expression starts in the first week after birth and reaches maximum at P15, allowing temporal restriction to to post-migratory mature neurons (*126*).

Figure 8. Germline and neuron-specific deletion of *miR-128-2*.

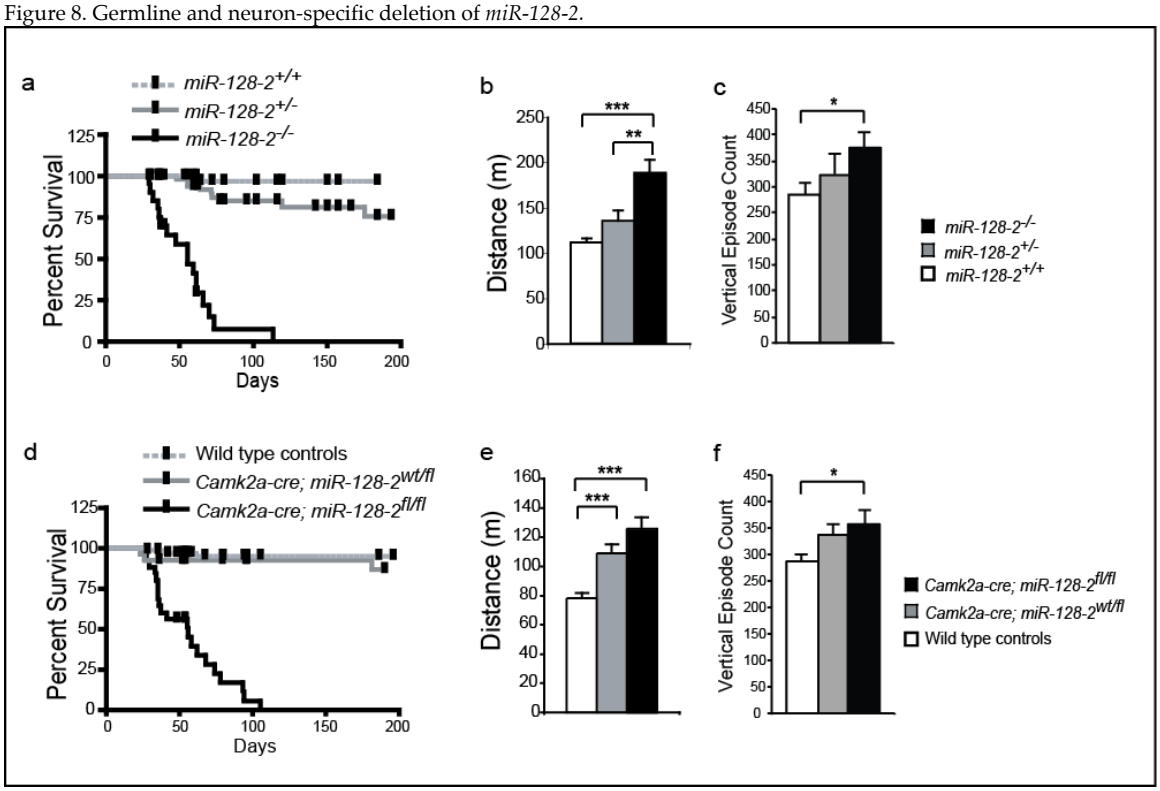

Figure 8. Germline and neuron-specific deletion of *miR-128-2*.

a and d, Premature mortality. Kaplan-Meier plot showing percentage of surviving animals as a function of days after birth in **a,** germline deletions: *miR-128-2*$^{-/-}$ (n=20, median 55 days), *miR-128-2*$^{+/-}$ (n=49), *miR-128-2*$^{+/+}$ (n=46). p<0.0001, log-rank test, and in **d,** postnatal neuron deletions: *Camk2a-cre; miR-128-2*$^{fl/fl}$ (n=25, median 56 days), *Camk2a-cre; miR-128-2*$^{wt/fl}$ (n=26), wild type controls (n=68). p<0.0001, log-rank test.

b, c, e and f, Increased motor activity. **b and e,** Total horizontal distance travelled in open field chamber over 60 minutes. **c and f,** Total vertical episodes (rearing) in open field chamber over 60 minutes. **b and c,** *miR-128-2*$^{-/-}$ (n=12), *miR-128-2*$^{+/-}$ (n=14) and wild-type littermates (n=23). **e and f,** *Camk2a-cre; miR-128-2*$^{fl/fl}$ (n=8), *Camk2a-cre; miR-128-2*$^{wt/fl}$ (n=21) and wild-type littermates (n=41).

Error bars show s.e.m.

* p<0.05; ** p<0.01; *** p<0.001, one-way ANOVA followed by Tukey's post test.

Figure 9. Premature mortality is caused by an epileptic condition.

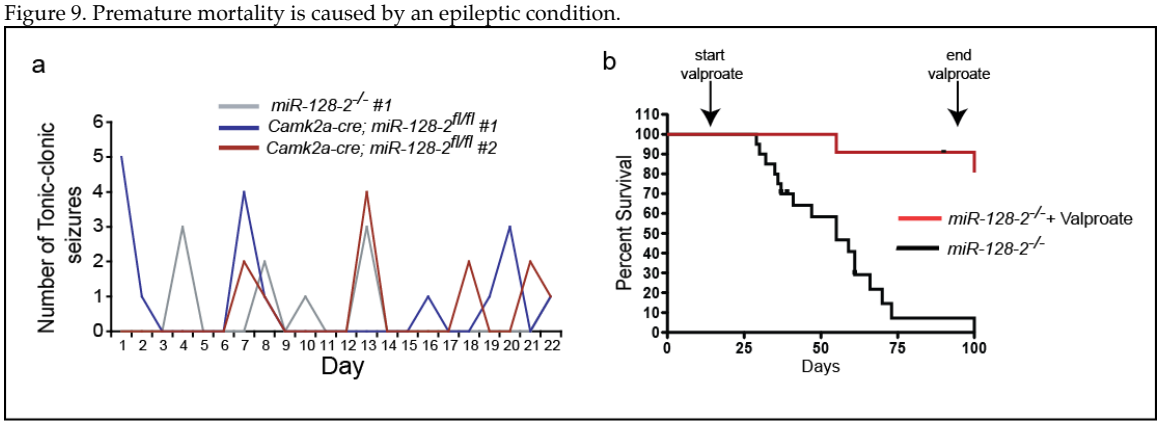

Figure 9. Premature is caused by an epileptic condition.

a, Depletion of *miR-128-2* results in severe, spontaneous seizures. Daily frequency of tonic-clonic seizures of a *miR-128-2*$^{-/-}$ (average 0.45 seizures per day) and two *Camk2a-cre; miR-128-2*$^{fl/fl}$ mutants (average 0.77 and 0.54 seizures per day) during the 22-day period preceding a recorded fatal seizure.

b, Mortality is rescued by administration of anti-convulsant valproate. Kaplan-Meier plot showing *miR-128-2*$^{-/-}$ mice (n=11) treated with sodium valproate from weaning to 90 days of age (red line), compared to untreated mutants (black) Percentage survival of *miR-128-2*$^{-/-}$ mutants at age 90 days: valproate treated=90% ; untreated=8%. $p<0.001$ log-rank test.

Projection neuron specific deletion of miR-128-2 (*Camk2a-cre; miR-128-2*$^{fl/fl}$) produced a reduction of mature miR-128 levels in the adult brain identical to that observed in miR-128-2 null mutants (Figure 6c,d). This suggests that previous estimates of Camk2a-neuron miR-128 enrichment are likely to be an underestimate. This is perhaps unsurprising given the likelihood of cross-contamination during the isolation process. Importantly, *Camk2a-cre; miR-128-2*$^{fl/fl}$ mutants had identical reductions in lifespan and increases in basal locomotor activity as null mutants (Figure 8d-f). These results suggest two important conclusions: (i) the biological function of miR-128 relates to function of post-developmental mature neurons and (ii) miR-128 is uniquely important to processes that occur in this neuronal subset.

To rule out the possibility that the effects demonstrated by the genetic deletion of miR-128-2 might be caused by unintended perturbations of the host gene (Arpp21) or neighboring genes, we crossed *Camk2a-cre; miR-128-2*$^{fl/fl}$ mutants to transgenic animals that overexpress miR-128 so that miR-128-2 deletion and expression from the ROSA locus both occurred in Camk2a-neurons. This genetic rescue experiment showed that miR-128 alone was sufficient to normalize survival rates and locomotor activity (Figure 10).

The relation between the concentration of miRNA in a cell and the resultant effects on physiology are thought to depend on the expression profile of its targets. In its role as a buffer against transcriptional noise, miRNAs suppresses the translation of rare aberrant transcripts, in which case the cell might be insensitive to relatively large changes in miRNA concentration above a certain concentration at which all relevant target transcripts are bound. In its role as a fine-tuner of transcript expression, moderate changes in miRNA concentration might lead to similar changes in target transcript availability and expression, and in turn that of cellular properties.

Figure 10. Transgenic miR-128 expression rescues epilepsy and hyperactivity

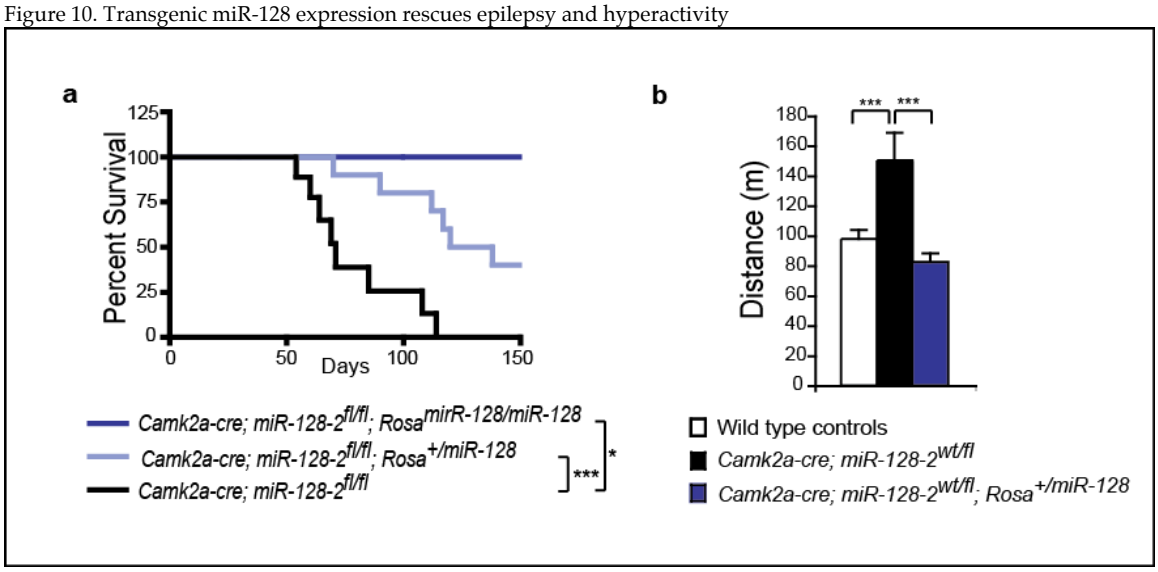

Figure 10. Transgenic miR-128 expression rescues epilepsy and hyperactivity .

a, Expression of miR-128 from transgenic allele rescues epileptic mortality in Camk2a deletion mutants. Kaplan-Meier survival plot for homozygous Camk2a deletion mutants carrying no transgenic alleles (black, n=9, median lifespan 71 days), or one transgenic allele (light blue, n=11, median lifespan 129 days) or two transgenic alleles (dark blue, n=4, median >200 days).

* $p<0.05$; *** $p<0.001$, log rank tests.

b, Expression of miR-128 from conditional transgenic allele normalizes hyperlocomotion in *Camk2a-cre; miR-128-2*$^{wt/fl}$ heterozygous mutants. Total horizontal distance traveled over 60 minutes in an open-field chamber by heterozygous deletion mutants carrying either no transgenic allele (black, n=12), or one transgenic allele (blue, n=15) and wild type controls (white, n=25).

Error bars show s.e.m. *** $p<0.001$, one-way ANOVA followed by Tukey's post test.

Basal locomotor activity was strongly dependent on the dosage of miR-128. Heterozygous and homozygous deletion of miR-128-2 resulted in increasing levels of hyperactivity in the open field. Conversely, heterozygous and homozygous transgenic over-expression of miR-128-2 resulted in increasing levels of hypo-activity compared to wild type controls (Figure 11b,c).

To further determine the dosage dependence of seizure susceptibility, we examined the survival of mice with neuronal deletion of combinations of miR-128-1 and miR-128-2. Different combinations of loci deletions correspond to different levels of approximate miR-128 availability. The survival statistics clearly show that decreasing levels of miR-128 are correlated with increased mortality rates (Figure 12).

Finally, increased miR-128 endogenous levels suppressed the progression of seizures induced by chemical convulsants. Seizures developed upon imbalances in the ratio of excitatory to inhibitory tone. Increased excitatory tone can be achieved using agonists of glutamatergic receptors e.g. kainic acid. Correspondingly, suppression of inhibition can be achieved using GABA receptor antagonists e.g. picrotoxin. The proportion of miR-128 overexpressing mice that develop tonic-clonic seizures upon systemic administration of either kainic acid or picrotoxin was lower than that of controls (Figure 11a). In summary, loss and gain of miR-128 in Camk2a projection neurons of the adult forebrain increases and suppresses seizure susceptibility and motor activity respectively.

Figure 11. Transgenic expression suppresses seizures and locomotion.

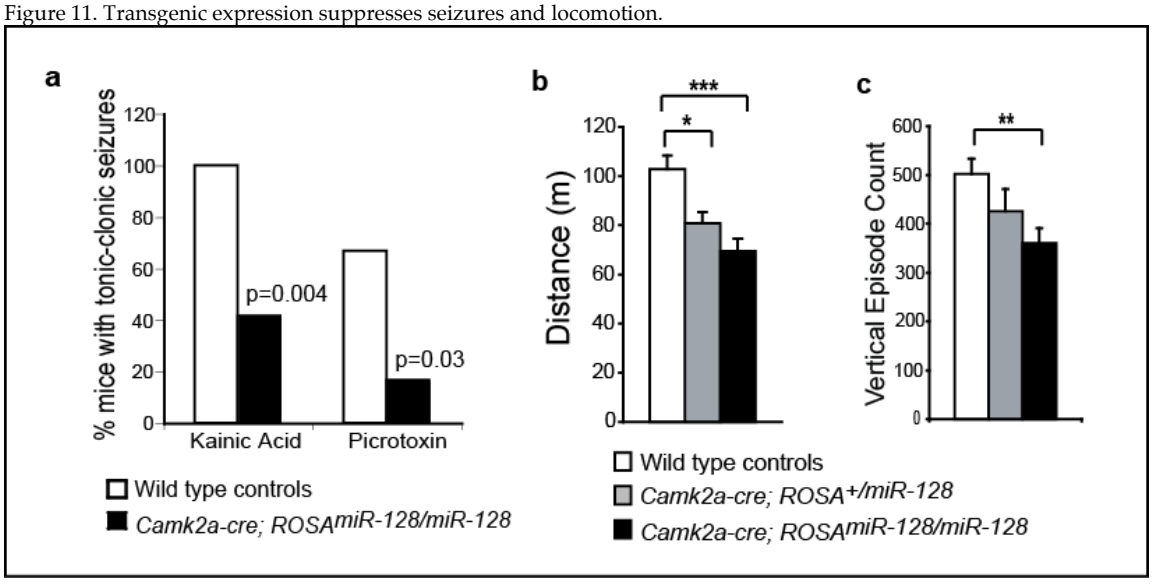

Figure 11. Transgenic expression suppresses seizures and locomotion.

a, Expression of miR-128 from transgenic allele suppresses chemical induction of tonic-clonic seizures. Percentage of mice exhibiting tonic-clonic seizures upon systemic injection of kainic acid or picrotoxin (n=12 per group). p-values calculated by Fisher's exact test.

b and c, Reduced motor activity upon miR-128 overexpression. **b,** Total horizontal distance traveled and **c,** total rearing activity in an open-field over 60 minutes by double transgenic (black, n=21), single transgenic (gray, n=21) and control mice (white, n=33).

Error bars show s.e.m. * $p<0.05$; ** $p<0.01$; *** $p<0.001$, one-way ANOVA followed by Tukey's post test.

Figure 12. Epileptic mortality is miR-128 dosage dependent.

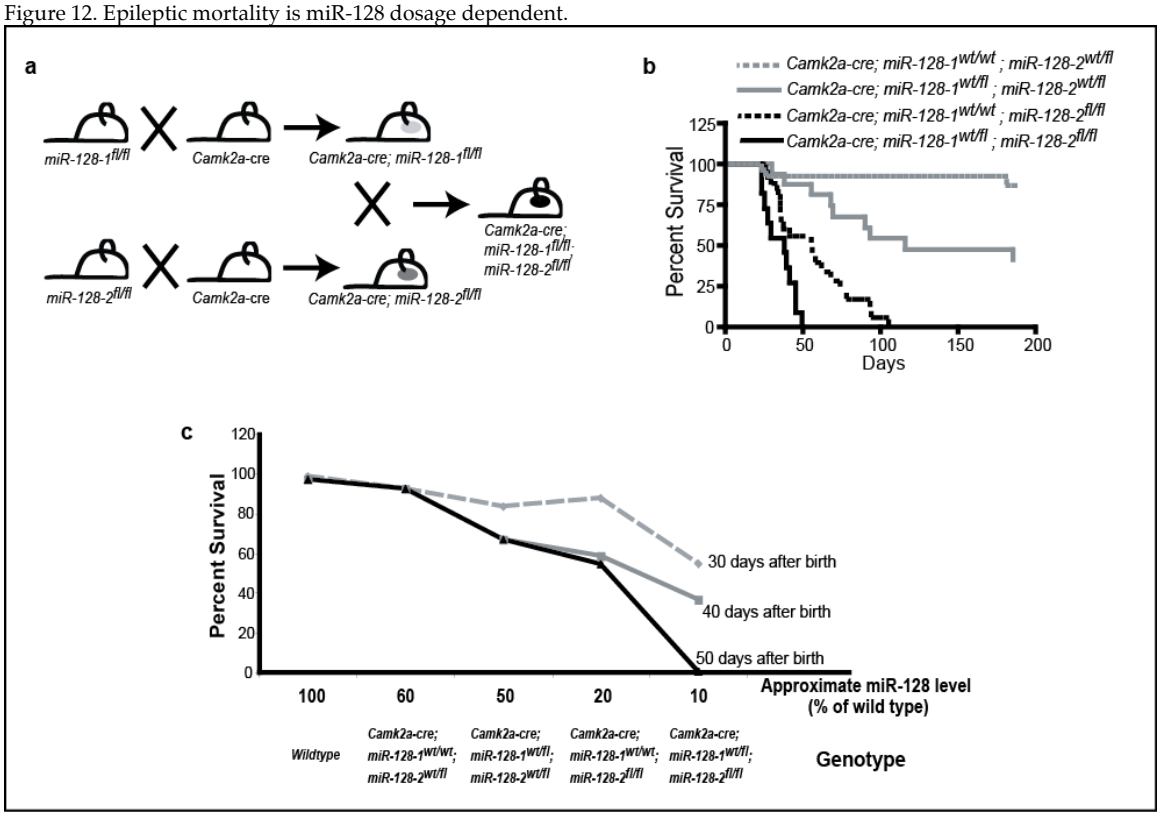

Figure 12. Epileptic mortality is miR-128 dosage dependent.

a, Mating scheme for generation of postnatal neuron-specific double knock-out of *miR-128-1* and *miR-128-2*.

b, Kaplan-Meier plot, percentage of surviving animals as function of days after birth is shown for listed mutants carrying combinations of *miR-128-1* and *miR-128-2* alleles (sample number, median lifespan): *Camk2a-cre; miR-128-1*$^{wt/wt}$*; miR-128-2*$^{wt/fl}$ (n=26, >360 days), *Camk2a-cre; miR-128-1*$^{wt/fl}$*; miR-128-2*$^{wt/fl}$ (n=16, 116 days), *Camk2a-cre; miR-128-1*$^{wt/wt}$*; miR-128-2*$^{fl/fl}$ (n=25, 56 days), *Camk2a-cre; miR-128-1*$^{wt/fl}$*; miR-128-2*$^{fl/fl}$ (n=11, 38 days). All pairwise log-rank test $p<0.005$.

c, Line graphs summarize percentage animals surviving at 30, 40 or 50 days after birth for each genotype. Approximate miR-128 levels for each genotype are indicated.

2.4 miR-128 expression in the striatum suppresses hyperlocomotion

Distance travelled during ambulatory activity is one example of a broad set of normal motor activities, and serves as a reliable and consistent measure of motor output as a whole. In the last few decades, large strides have been made toward understanding the distinct neuronal subsets and networks that control motor coordination, action selection or the magnitude of motor outputs. Some of these studies have been undertaken to try to understand the range of motor dysfunctions that afflict human patients such as Huntington's disease or Parkinson's disease.

The striatum is the major input structure of the basal ganglia system and has an important role in the control of motor output. Loss of dopaminergic tone within this structure is the primary cause of akinesia in sufferers of Parkinson's disease.

To examine the relative contributions of striatal expression of miR-128 to the regulation of basal activity, we generated mice with region-specific deletions of miR-128-2. Adeno-associated virus expressing Cre-recombinase was injected into the striatum of miR-128-2 floxed or wild type mice. Peak expression of Cre recombinase occurs at around 20 days after injection. This experiment demonstrates that miR-128-2 deletion in the striatum was sufficient to produce increased baseline activity (Figure 13).

Figure 13. Striatal deletion is sufficient to induce hyperactivity.

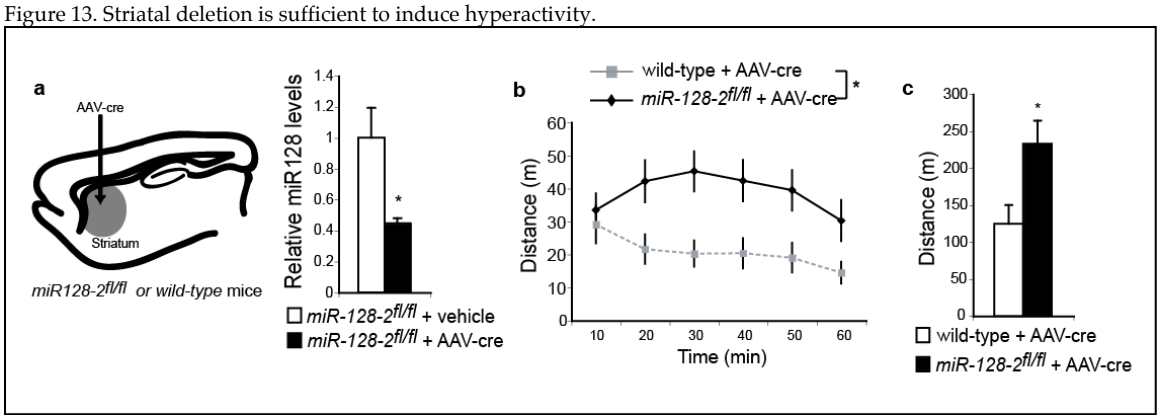

Figure 13. Striatal deletion is sufficient to induce hyperactivity.

a, Schematic of striatal deletion of *miR-128-2* by bilateral stereotactic injection of adeno-associated virus expressing Cre-recombinase (AAV-cre) into striatum of either *miR-128-2*$^{fl/fl}$ or wild-type mice (left). miR-128 levels in striatum of *miR-128-2*$^{fl/fl}$ mice injected with either AAV-Cre or vehicle were quantified by qRT-PCR (n=3). * $p<0.05$, Welch's t-test.

b-c, Striatal deletion of *miR128-2* was sufficient to induce basal hyperlocomotion.

b, Horizontal distance travelled in an open-field chamber in 10 minute intervals. *miR128-2*$^{fl/fl}$ (n=14) or controls (n=8) stereotactically injected with AAV-Cre. * $p<0.05$, 2-way repeated-measures analysis of variance (genotype).

c, Total horizontal distance traveled in an open-field chamber over 60 minutes.

* $p<0.05$, Welch's t-test. All error bars indicate S.E.M.

2.5 Summary

Our work confirms the post-developmental restriction and forebrain enrichment of miR-128. Our data also complements previous finding that miR-128 is enriched in Camk2a-positive projection neurons by showing a strong enrichment of miR-128 targets among the pool of Ago2 bound transcripts in Camk2a-positive neurons of the adult forebrain. This CLIP-seq dataset allows us to narrow down the list of possible physiological targets of miR-128 and these targets suggest a role for miR-128 in the modulation of seizure and locomotion. We addressed this hypothesis by deleting miR-128 both ubiquitously and specifically in Camk2a-positive forebrain projection neurons. Depletion of miR-128 in either case produced nearly identical, dose-dependent increases in epileptic mortality and basal locomotor activity. These phenotypes are consistent with a sensitive regulation of neuronal excitability by miR-128 in projection neurons across the forebrain. In addition we show that miR-128 loss in the striatum was sufficient to induce hyperactivity. In the next chapter we examine miR-128 function in the striatum in detail.

Chapter 3: miR-128 in medium spiny neurons of the striatum

3.1 D1-MSNs and D2-MSNs: distinct projection neurons in the striatum

Camk2a-positive neurons in the striatum include two similarly sized populations of DARPP-32-positive projection neurons called medium spiny neurons (MSNs), which together account for over 90% of neurons in this structure. Morphologically identical and anatomically intermingled, these neurons also receive similar inputs from extra-striatal regions including dopaminergic input from the midbrain and glutamatergic input from the cerebral cortex and thalamus. However, these two populations project to completely distinct output structures of the basal ganglia and participate in two largely parallel circuits reviewed in (*127*). Furthermore, these two populations are further differentiated by the unique expression of key proteins. Striatonigral projecting MSNs (D1-MSNs) preferentially express Dopamine type 1 receptors (Drd1), substance P and dynorphin. Striatopallidal projecting MSNs (D2-MSNs) preferentially express Dopamine type 2 receptors (Drd2), Adenosine type 2 receptors (A2A) and enkephalin.

D1 and D2- MSNs exhibit a wide array of functional differences. They display distinct dendritic excitability (*128*), engage distinct signaling outcomes in response to dopamine (*129*, *130*), employ distinct dopamine-dependent plasticity mechanisms (*131*), and mediate distinct behavioral and learning outcomes upon pharmacological and optogenetic stimulation (*132-134*). Furthermore, recent expression studies identified hundreds of genes differentially expressed in the two subtypes, expanding our understanding of known differences in signal transduction and integration and revealing novel ones (*135*).

D1- and D2-MSNs of the striatum constitute a unique and fascinating system to study divergent signaling architectures in similar neuronal populations. Little is known about miRNA expression and function in MSNs, but miR-128 is highly expressed in the striatum and we have shown that striatal depletion alone can induce locomotor hyperactivity reminiscent of MSN hyperstimulation. Furthermore, differences in signaling responses D1- and D2-MSNs suggest different requirements of miR-128 activity. This is the hypothesis we address in this chapter.

3.2 Relative miR-128 expression in MSN populations

We first determined whether miR-128 is differentially expressed between these two MSN populations. To this end, we generated mice expressing epitope tagged-Ago2 in either D1 or D2 MSNs by breeding mice carrying the conditional tagged-Ago2 allele with the respective Cre-driver lines. Tagged Ago2 was immunoprecipitated from adult striatum tissue and total bound RNA was isolated and the levels of most major murine miRNA families were quantified using qRT-PCR on low-density arrays (Figure 14a). To correct for background contamination by non-specific pull-down of miRNA, mice not expressing Cre were used as controls, and processed in parallel.

Among all tested miRNAs, 184 were recovered at levels above non-specific background. To compare expression levels between the two cell types, it was necessary to normalize for the total isolated miRNA content of each population. This was done in two ways: (1) using cycle count for miR-124, a highly expressed neuronal miRNA induced early in neuronal differentiation and (2) using the global mean cycle count for all miRNAs expressed above background. Only miRNAs showing significant differences using both methods were considered to be differentially expressed between D1 and D2-MSNs (Figure 14b). The analysis shows that 21 miRNAs were more highly expressed in D1 MSNs, including miR-128, and that 12 miRNAs were more highly expressed in D2 MSNs. Real time PCR quantification was repeated and we confirmed that miR-128 was expressed about two fold higher in D1 MSNs than D2 MSNs, suggesting D1-MSNs make a greater contribution to the dysfunctions of miR-128 mutants (Figure 14c).

Figure 14. Differential expression of miR-128 in D1 and D2 MSNs.

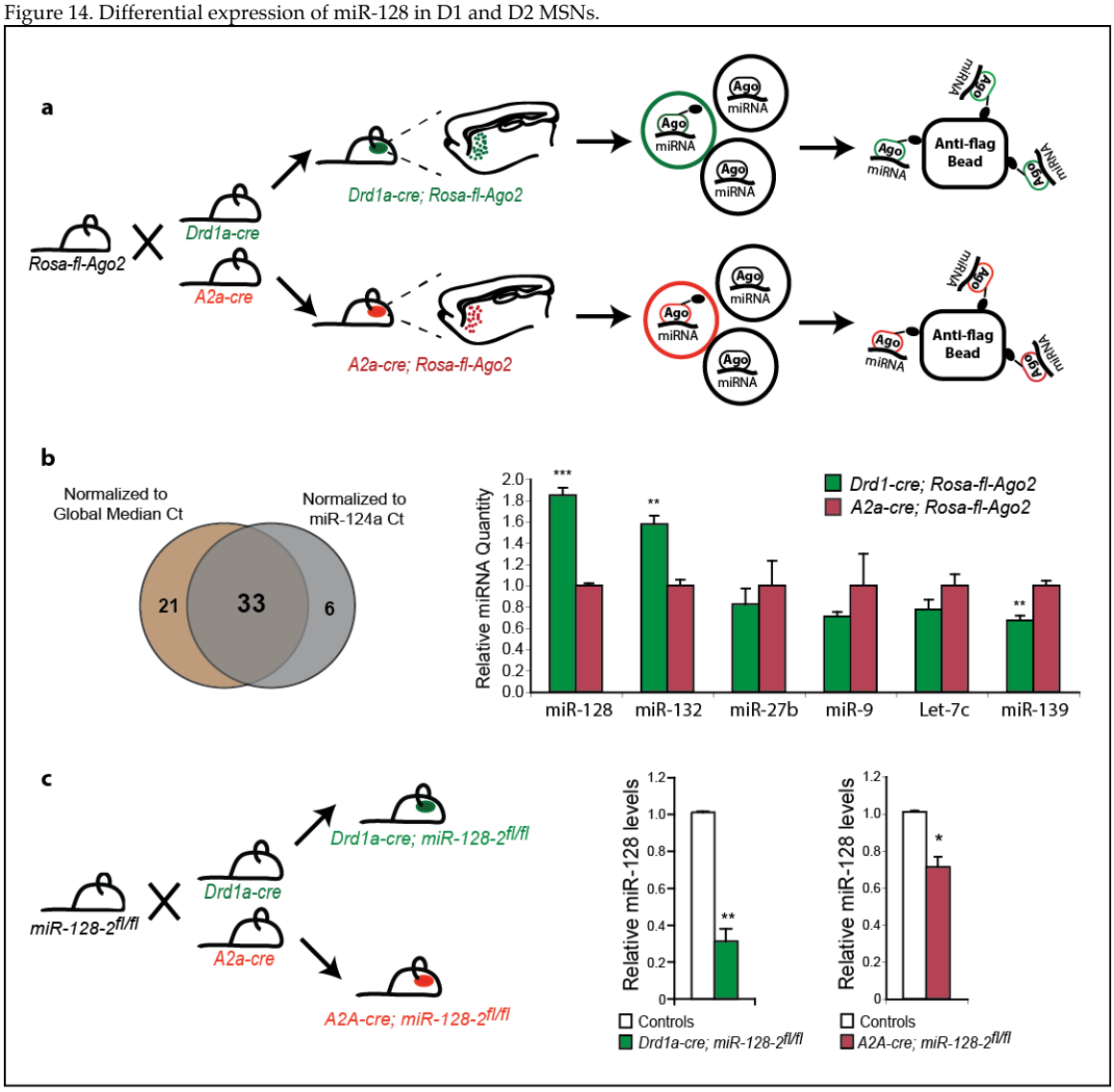

Figure 14. Differential expression of miR-128 in D1 and D2-MSNs.

a, Schematic summarizes generation of mice expressing flag-tagged Ago2 in either D1- (green) or D2- (red) MSNs and cell-type specific isolation of Ago2-associated miRNAs.

b, Left: miRNAs were quantified by qRT-PCR and normalized using cycle count (Ct) of either the population median or miR-124a. Only the 33 miRNAs with significant ($p<0.05$) differential expression in both cases were considered. Right: Relative miRNA expression of selected miRNAs.

c, Left: Mating scheme to delete *miR-128-2* in D1 or D2-MSNs in the striatum. Right: miR-128 levels in adult striatum upon deletion in D1- or D2- MSNs.

All error bars indicate S.E.M. *** $p<0.001$ ** $p<0.01$, * $p<0.05$, Welch's t-test.

3.3 miR-128 has a unique role in D1-MSNs

To test whether D1-MSNs provide a greater contribution to the observed hyperlocomotion and seizures, we generated mice with deletion of *miR-128-2* in either D1- or D2-MSNs (hereafter *Drd1a-cre; miR-128-2*$^{fl/fl}$ and *A2a-cre; miR-128-2*$^{fl/fl}$ respectively). To help quantify the non-striatal contribution to hyperactivity, we also generated mutants in which miR-128-2 was deleted in all neuronal populations of the hippocampus and cortex (*Emx-cre; miR-128-2*$^{fl/fl}$). These subtype-specific deletions exhibited interesting differences of phenotype.

Reductions in pan-striatal miR-128 levels upon deletion in D1-MSNs were greater than that upon deletion in D2-MSNs, supporting our previous observation that miR-128 was comparatively enriched in D1-MSNs (Figure 14c). In the open-field assay, *Drd1a-cre; miR-128-2*$^{fl/fl}$ mutants displayed a strong hyperactivity compared to controls similar to that observed with *Camk2a-cre; miR-128-2*$^{fl/fl}$ mutants (Figure 15a-c). Like *Camk2a-cre; miR-128-2*$^{fl/fl}$ mutants, the increased locomotor activity of *Drd1a-cre; miR-128-2*$^{fl/fl}$ mutants was not accompanied by increased thigmotaxis (the tendency of mice to conduct most of their exploratory behavior at the periphery of the chamber due to the presence of tactile responses to chamber walls). Other measures of behavioral anxiety using elevated plus maze and light-dark chamber also confirmed that hyperlocomotion was not accompanied by increased anxiety (data not shown). In contrast, *A2a-cre; miR-128-2*$^{fl/fl}$ mutants showed no difference in locomotor activity compared to wild-type littermates (Figure 15d-f).

Figure 15. miR-128 deletion in D1 but not D2 MSNs results in hyperactivity.

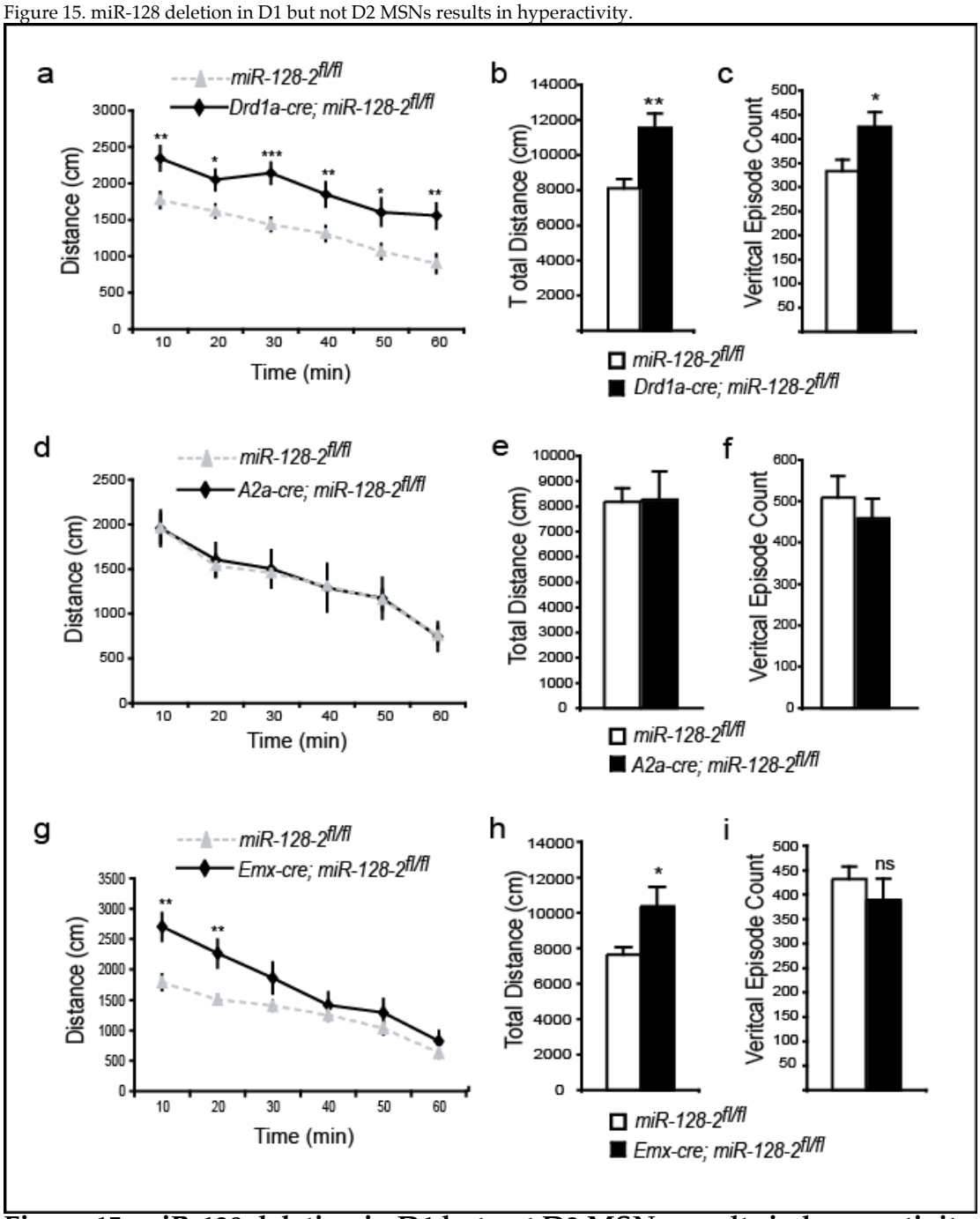

Figure 15. miR-128 deletion in D1 but not D2 MSNs results in hyperactivity.

Open field activity of *Drd1a-cre; miR-128-2*$^{fl/fl}$ mutants (**a-c**), *A2a-cre; miR-128-2*$^{fl/fl}$ mutants (**d-f**), and *Emx-cre; miR-128-2*$^{fl/fl}$ mutants (**g-i**).

a, d, g, Horizontal activity in 10 min intervals. **b, e, h,** Total horizontal activity over 60 mins. **c, f, i,** Total rearing activity over 60 mins.

All error bars indicate S.E.M. *** p<0.001 ** p<0.01, * p<0.05, Welch's t-test.

Emx-cre; miR-128-2$^{fl/fl}$ mutants displayed a milder locomotor phenotype that was also qualitatively different from that of *Drd1a-cre; miR-128-2*$^{fl/fl}$ mutants (Figure 15g-i). These mutants showed the greatest activity difference occurs in the initial period of exposure to the open field chamber and this activity difference progressively narrowed over time. Two-factor (time and genotype) analysis of variance (ANOVA) showed a clear dependence on both and a significant interaction between the two factors. In contrast, *Drd1a-cre; miR-128-2*$^{fl/fl}$ mutants showed identical activity increase over controls throughout the 60 minutes in the open field chamber. Two-way ANOVA showed a lack of dependence on time interval and no interaction between time interval and genotype. This suggests that while miR-128 deletion in D1-MSNs produces constant elevated activity, deletion in the cortex and hippocampus results in higher novelty-induced locomotion, which diminishes over time. The severe phenotype seen in *Camk2a-cre; miR-128-2*$^{fl/fl}$ mutants is likely to result from a combination of these two aspects.

Finally, *Drd1a-cre; miR-128-2*$^{fl/fl}$ mutants displayed spontaneous home cage seizures resulting in increased mortality although not as severe as that observed in *Camk2a-cre; miR-128-2*$^{fl/fl}$ mutants, with a median lifespan of 142 days (Figure 16a) In contrast, *A2a-cre; miR-128-2*$^{fl/fl}$ mutants showed no increase in mortality over littermates and all mutants survived over a year (Figure 16b).

The rate of epileptic mortality was even greater in *Emx-cre; miR-128-2*$^{fl/fl}$ mutants, with a lower median lifespan of 105 days, consistent with a known role of the hippocampus in promoting seizure generalizations (Figure 16c). Interestingly, using the inverse of the median lifespan to approximate the rate of death of each mutant line (rate = 1/(median lifespan)), a simple addition of the death rates of *Emx-cre; miR-128-2*$^{fl/fl}$ and *Drd1a-cre; miR-128-2*$^{fl/fl}$ mutants very closely approximates the death rate of *Camk2a-cre; miR-128-2*$^{fl/fl}$ mutants.

Figure 16. miR-128 deletion in D1 but not D2 MSNs results in fatal epilepsy.

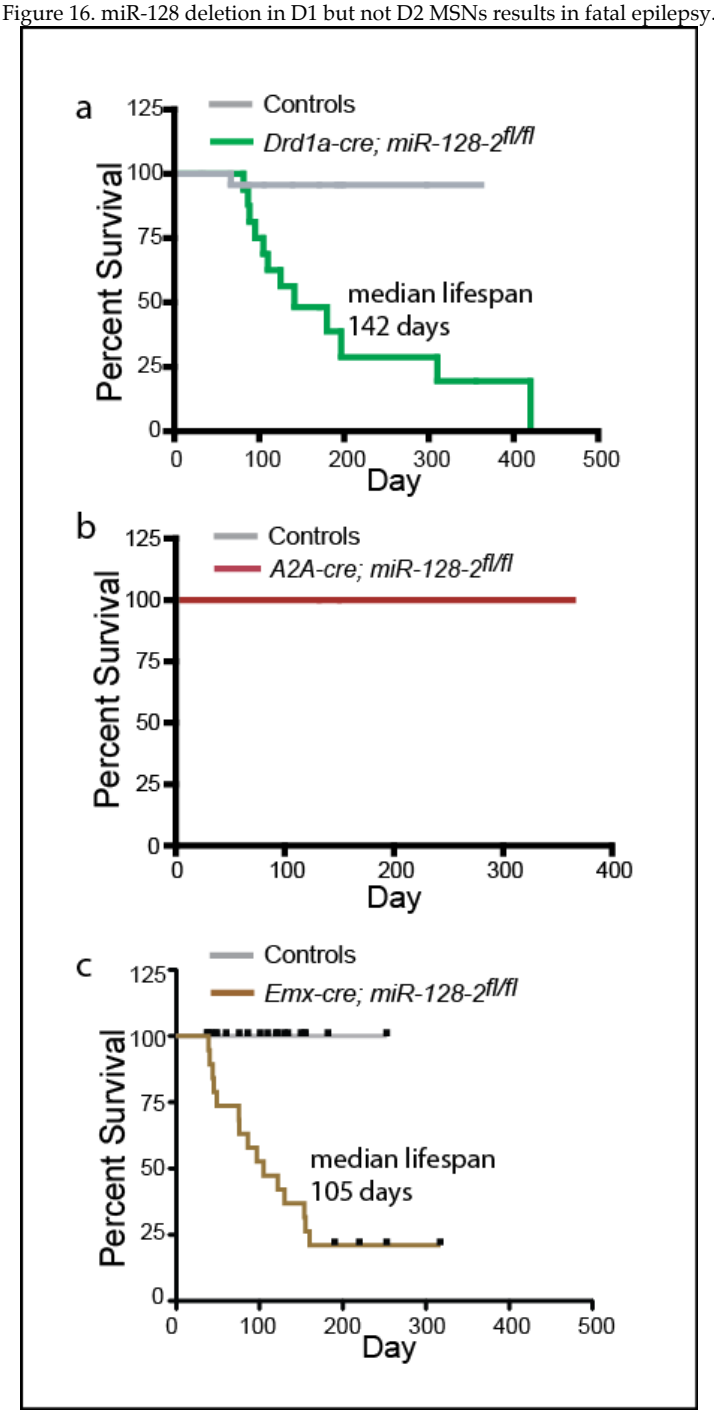

Figure 16. miR-128 deletion in D1 but not D2 MSNs results in fatal epilepsy. Kaplan-Meier survival plots for: **a,** *Drd1a-cre; miR-128-2*$^{fl/fl}$ mutants (green, n=16) and controls (grey, n=39); **b,** *A2a-cre; miR-128-2*$^{fl/fl}$ mutants (red, n=8) and controls (grey, n=8) and **c,** *Emx-cre; miR-128-2*$^{fl/fl}$ mutants (brown, n=19) and controls (grey, n=54). **a, c,** $p<0.001$ log rank tests. All *A2a-cre; miR-128-2*$^{fl/fl}$ mutants survived for a year until they were sacrificed.

3.4 Summary

Behavioral changes resulting from deletion of miR-128 in D1-MSNs but not D2-MSNs was sufficient to recapitulate the phenotypes observed in *Camk2a-cre; miR-128-2*$^{fl/fl}$ mutants, suggesting a unique role of miR-128 in regulating the properties of D1-MSNs. The cortical-hippocampal contribution to seizure susceptibility is larger but we show that loss of miR-128 in D1-MSNs is necessary and sufficient for a novelty-independent baseline increase in motor activity and fatal epilepsy.

Chapter 4: miR-128 targets and MAPK pathway

4.1 Ribosomal profiling in D1-MSNs reveals regulated targets

The primary effect of miRNA expression is the translational suppression and/or degradation of specific target mRNA transcripts. Most, if not all, of the biological consequences of miRNA expression stems from this repression of target transcripts. To understand how miR-128 depletion results in the behavioral and cellular dysfunction demonstrated so far, we need to identify physiological targets of miR-128.

We have shown that D1-MSNs contain most of the striatum-expressed miR-128 and that D1 specific deletion of miR-128 results in hyperactivity and seizure. To determine target genes dysregulated in D1-MSNs in the absence of miR-128, we made use of a ribosomal profiling strategy-TRAP (*135*) that allows the comprehensive quantification of mRNA levels in a specific population of cells. By crossing our *Drd1a-cre; miR-128-2*$^{fl/fl}$ mutants with transgenic mice expressing tagged ribosomal subunits in D1-MSNs, we generated animals in which D1 neurons are miR-128 deficient and express tagged ribosomes. Briefly, *Drd1a-cre; miR-128-2*$^{fl/fl}$ mutants carrying tagged ribosomes in D1-MSNs were used for polysome immunoprecipitation and polysome-associated transcripts were analyzed by microarray. Control mice carrying tagged ribosomes but negative for Cre recombinase were used for comparison. Two independent experiments were performed involving 8 controls and 9 mutants. Using a non-conservative analysis, over 2000 probes showed significantly different expression levels in the absence of miR-128 ($p<0.05$, two-way ANOVA for genotype) (Figure 17a).

As typical expression changes of target genes in response to miRNAs are very small (<1.5 fold), and could involve an unknown number of primary targets, we chose a non-conservative significance cutoff and no minimum cutoff for fold change. While this means that most of the primary targets of miR-128 are likely to be included in this list, it would also include secondary expression changes and a significant number of false positives. To test if the expression changes detected include changes in primary target genes, we looked at differences in mean derepression levels of various sub-populations:

Firstly, genes with one or more miR-128 6-mer seed sites within their annotated full-length Refseq transcripts had much greater levels of derepression compared with genes that contained no sites. Furthermore, Ago-associated genes containing miR-128 seeds within isolated clusters (CLIP-seq) showed even higher levels of derepression (Figure 17b).

Secondly, among CLIP-seq positive genes, those in which miR-128 seed-containing clusters occurred in the 3'UTR were more derepressed than those in which such clusters occurred in the coding region (Figure 17b). This is in line with some previous findings that most functional interactions between miRNA and its target occur in the 3'UTR (*50*, *51*)

Figure 17. Ribosomal expression profiling in D1-MSNs.

a, Schematic summarizes D1-MSN specific ribosomal profiling. Mice with D1-MSN specific deletion of *miR128-2* and transgenic expression of tagged ribosomal subunit. Total striatum was dissected from mutant (*Drd1a-cre; miR128-2*$^{fl/fl}$*; Drd1a-eGFP-L10a*) and control (*miR128-2*$^{fl/fl}$*; Drd1a-eGFP-L10a*) littermates. Polysome associated mRNA transcripts were isolated and profiled from 2 independent experiments by microarray (7-8 mice per group total). Green ribosomes: eGFP-tagged ribosome; black ribosomes: untagged ribosomes.

b-c, Ago-bound CLIP-seq miR-128 targets are preferentially upregulated.

b, Mean log fold changes of all differentially expressed genes (All); genes with either 0 or ≥1 miR-128 6mer target site in its full annotated sequence (No 6mer and Refseq 6mer); and genes with 6mer-containing CLIP-seq cluster anywhere, in 3'UTR only, or in coding regions only (CLIP-seq 6mer, CLIP-seq 6mer 3'UTR, CLIP-seq 6mer ORF). Number of probes indicated in brackets.

c, Mean log fold changes of all differentially expressed genes (All), CLIP-seq targets of miR-128 and that of other miRNAs. CLIP-seq targets are genes with a CLIP-seq cluster in the 3'UTR that contains 6mer target site(s) for a given miRNA.

d, Venn diagram illustrates definition of primary target genes as miR128 CLIP-seq targets that are differentially expressed in the absence of miR128 as shown by ribosomal profiling.

** $p<0.01$, *** $p<0.001$, one-way ANOVA followed by Dunnett's post test against group of all differentially expressed genes (All). All error bars indicate s.e.m.

Figure 17. Ribosomal expression profiling in D1-MSNs.

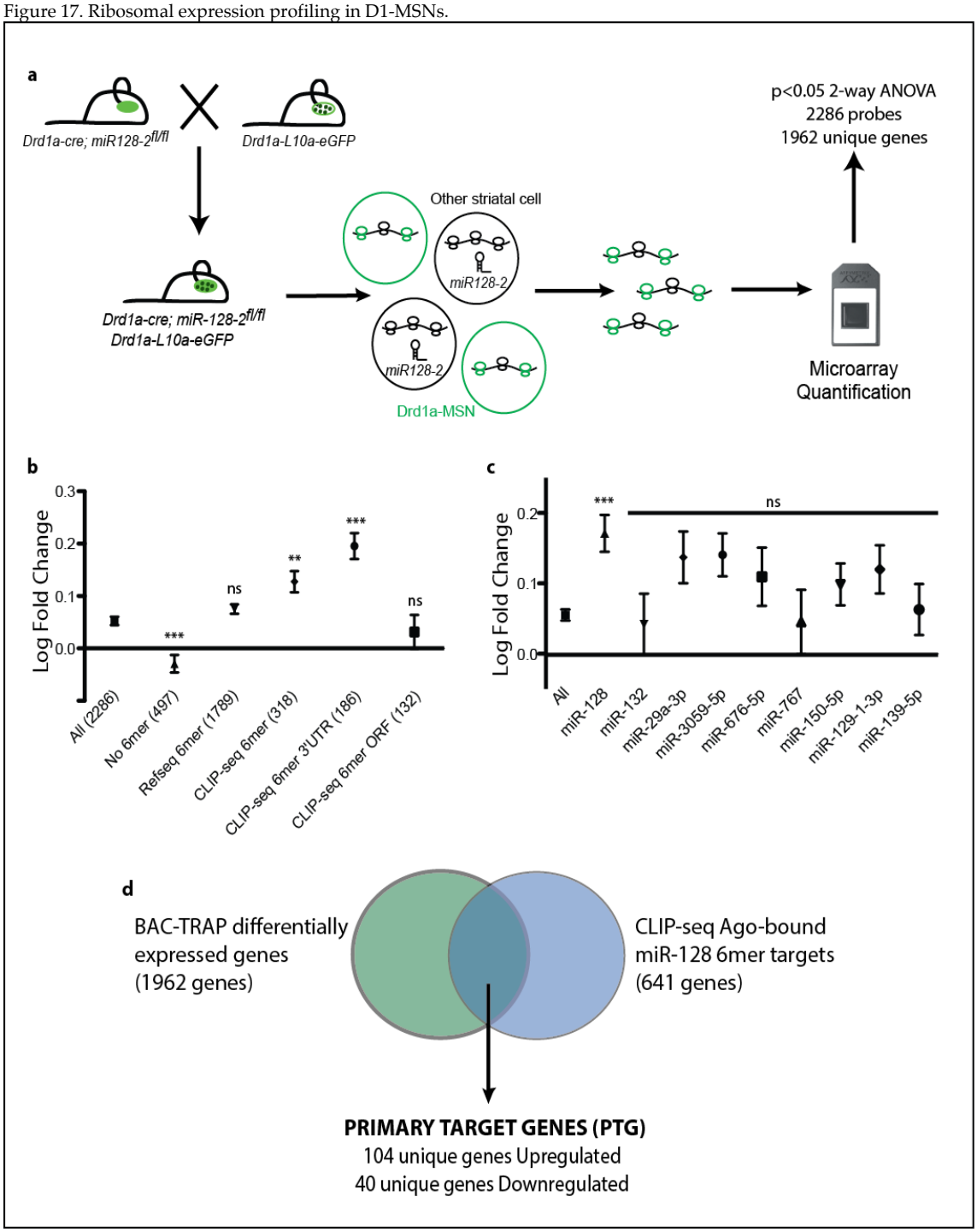

4.2 Primary target genes

Based on the above results, we restricted the list of primary targets genes (PTGs) to those which fulfilled the following conditions:

1. Association with Ago2 in neurons as shown by the presence of 3'UTR CLIP-seq cluster(s) containing at least one miR-128 6mer seed.
2. Significant expression change in the absence of miR-128 as assayed by ribosomal profiling in D1-MSNs.

In further validation of our stringent criteria, we compared the mean de-repression of miR-128 primary targets with that of other miRNAs using the same criteria (presence of miRNA seed site within Ago CLIP-seq cluster in the 3'UTR) and with the entire population of altered genes as a whole. Primary miR-128 targets (and not that of other miRNAs expressed in Camk2a neurons) were significantly more de-repressed than the set of all altered genes (Figure 17c). This confirms the utility of using CLIP-seq data to isolate actual targets from the large population of genes with altered expression.

Applying the above criteria narrowed our search to 104 upregulated PTGs (131 probes). For comparison purposes, there are significantly fewer downregulated genes (40 unique genes, 47 probes) fulfilling our criteria (Figure 17d). As miRNAs are solely thought to repress targets, the presence of this smaller but significant group of downregulated PTGs was taken to indicate the false positive rate of our analysis. For now, both groups are included in our analysis although we will address this issue below.

To confirm that most if not all of upregulated primary targets were bona fide miR-128 targets, full-length 3'UTRs of 10 randomly selected targets were cloned downstream of a firefly luciferase gene and expressed in cultured Neuro2A cells. Responsiveness to exogenous miR-128 mimics co-transfected with the reporter plasmid could be assayed by luciferase activity. All tested targets showed significant repression by miR-128 mimic compared to scramble control mimic, while none of the negative controls showed significant responses (Figure 18b).

The level of derepression was mild, ranging for 1.2-fold to just over 2-fold increase in the absence of miR-128 (Figure 18a). This is in line with most previous studies examining the level of repression by miRNAs (*58*). Quantification of selected proteins by Western blot analysis indicated that repression of protein levels was only slightly higher than that observed with ribosomal profiling (Figure 18c).

The use of ribosomal profiling confers many advantages over expression studies using total RNA samples extracted from dissected tissue. Firstly, genetic targeting allows cell-specific isolation of transcripts. Therefore, expression changes are not diluted by the presence of transcripts from non-miR-128 expressing cells (glia, interneurons), or cells in which miR-128 expression is lower and might lead to smaller repression rates (D2-MSNs). This is especially significant if targets are also relatively depleted within the target cell type. Secondly, miRNAs affect the recruitment and translation of transcripts by ribosomes, with mRNA degradation occurring subsequently in most but not all cases. Ribosomal profiling thus provides a more accurate picture of expression changes compared to mRNA quantification alone.

Figure 18. Primary target genes.

a, Heat map of upregulated primary target genes showing fold changes in ribosomal association in D1-MSNs. Genes are listed in descending order of average fold change over control samples. Columns show each of two experimental repeats.

b, In-vitro confirmation of primary targets. Luciferase reporters carrying full 3'UTR sequences of a subset of primary target genes were tested for responsivity to either scrambled control or miR-128 mimics in Neuro2A culture. Mean normalized luciferase activity for each reporter is expressed relative to that in the presence of control mimic. RCS and BDNF constructs are included as negative controls. All tested primary target reporters showed significant responses to miR128 mimics. * $p<0.05$; ** $p<0.01$; *** $p<0.001$, Welch's t-test.

c, Mean protein level changes in the striatum were quantified for 3 primary targets D4ertd22e (left), Pea15a (middle) and Tarpp/Arpp21 (right). Bar graphs show mean expression levels quantified from dissected striata (n=4 each) by Western blot, normalized to actin loading controls and expressed relative to mean control expression. Representative blots for each target are shown above respective bar graph. * $p<0.05$; ** $p<0.01$, Welch's t-test.

All error bars indicate S.E.M.

Figure 18. Primary target genes.

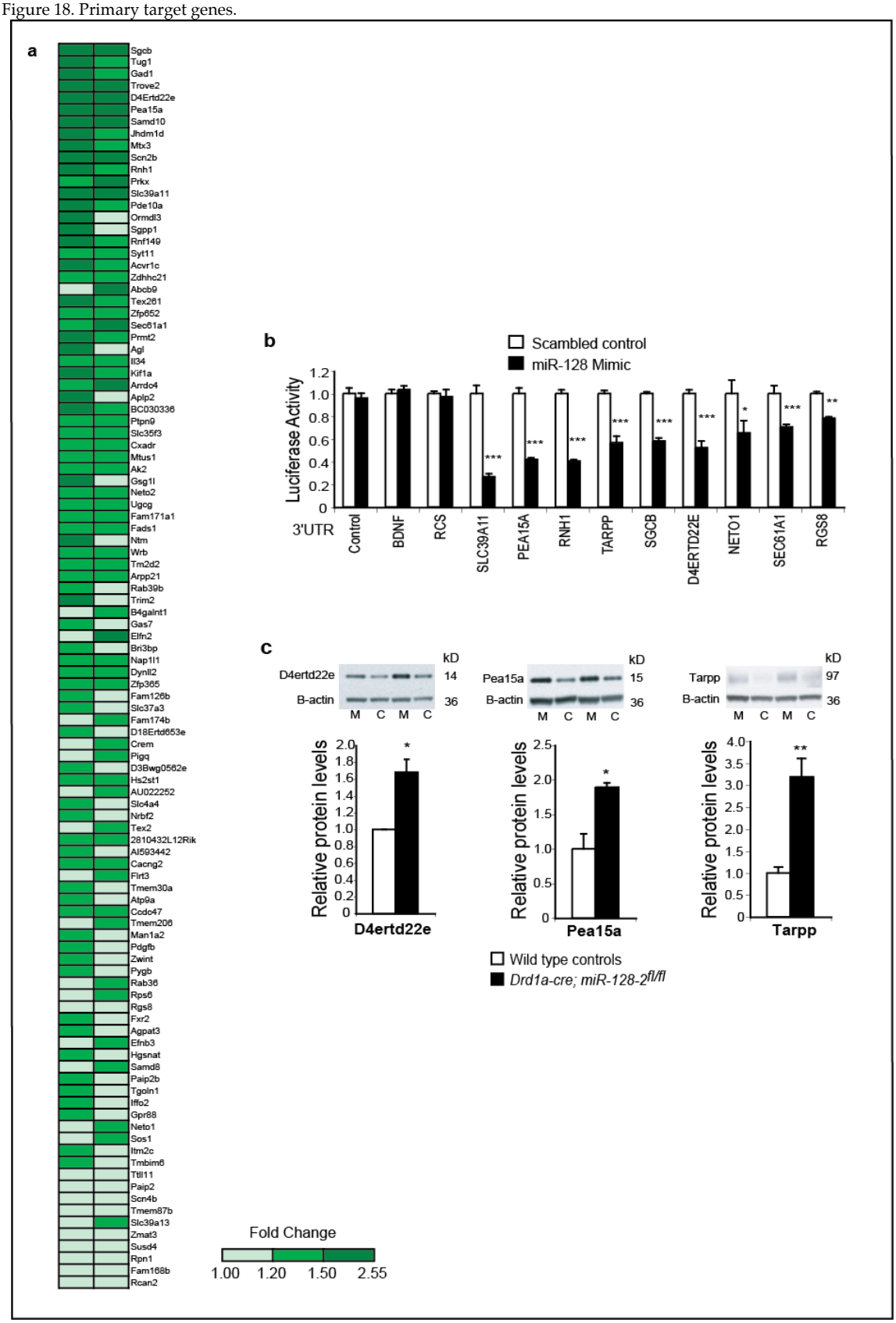

To illustrate the advantages of this method, we made use of the *Camk2a-cre; miR-128-2*$^{fl/fl}$ mutants described in Chapter 2. Total RNA was extracted from dissected striata of both mutants and their respective controls and mRNA expression quantified by microarray. We compared mean fold changes of the 178 miR-128 PTGs obtained from D1-MSN ribosomal profiling experiments to those obtained from analyzing total striatal RNA from *Camk2a-cre; miR-128-2*$^{fl/fl}$ mutants. Previous work using ribosomal profiling to quantify target expression changes have shown that for the majority of targets, changes in ribosome association is accompanied by reductions in target mRNA (*79*).

The observed fold changes were significantly higher using ribosomal profiling as expected for the reasons listed above. In spite of this, we were able to detect mild derepression of nearly all the upregulated PTGs, and a very significant derepression of the population as a whole, suggesting that we could use microarray assays of total RNA to examine other properties of the PTGs.

We have shown earlier that miR-128 exerts a bidirectional control of both locomotor activity as well as seizure susceptibility. It is therefore likely that the primary targets of miR-128 should exhibit similar bidirectional dynamics. To test this, we made use of the *Camk2a-cre; miR-128-2*$^{fl/fl}$ deletion mutants and *Camk2a-cre; ROSA*$^{miR\text{-}128/miR\text{-}128}$ overexpression mutants described in Chapter 2. Total RNA was extracted from the striata of both mutants and their respective controls and quantified by microarray. Up-regulated PTGs showed highly significant bidirectionality - up-regulated in deletion and repressed in overexpressing mutants ($p<10^{9}$). In contrast the 47 downregulated primary targets did not show bidirectionality ($p>0.05$), confirming our previous view that these genes were not primary targets (Figure 19a,b).

To test if PTGs were similarly targeted in other brain regions, we dissected cortical, hippocampal and striatal samples from *Camk2a-cre; miR-128-2*$^{fl/fl}$ mutants and analyzed total RNA as above. Each PTG was marked as either up-regulated or down-regulated for each brain region. For example, a particular subset of the upregulated PTGs would be seen upregulated in the cortex, while a different subset might be upregulated in the hippocampus. 25 genes were not upregulated in any region, consistent with the lower resolution using total RNA. Of the remaining genes, we found a very significant overlap of upregulated genes across all 3 regions, suggesting a broad conservation of miR-128-target pairings in multiple cell types (Figure 19c,d).

Figure 19. Upregulated PTGs are bidirectionally regulated and shared across brain regions.

Upregulated (**a,c**) and downregulated PTGs (**b,d**) are assessed for co-regulation across brain regions (**a,b**) and for bidirectionality (**c,d**).

a, b, mRNA from hippocampus, striatum and cortex of *Camk2a-cre; miR-128-2*$^{fl/fl}$ mutants were quantified by microarray. **a,** Upregulated PTGs were assessed if they were upregulated over control samples in each region and numbers were represented in Venn diagram. $p<0.001$ for all 3-way and 2-way interactions, log-linear analysis. **b,** Downregulated PTGs were assessed if they were downregulated over control samples in each region and similar represented. $p>0.05$ for all interactions, log-linear analysis.

c, d, mRNA from striatum of deletion mutants (grey, *Camk2a-cre; miR-128-2*$^{fl/fl}$) and transgenic overexpression mutants (blue, *Camk2a-cre; ROSA*$^{miR\text{-}128/miR\text{-}128}$) were quantified by microarray. Mean log fold changes of upregulated PTGs (**c**) and downregulated PTGs (**d**) are shown. p-values calculated by paired t-test.

All error bars indicate S.E.M.

Figure 19. Upregulated PTGs are bidirectionally regulated and shared across brain regions.

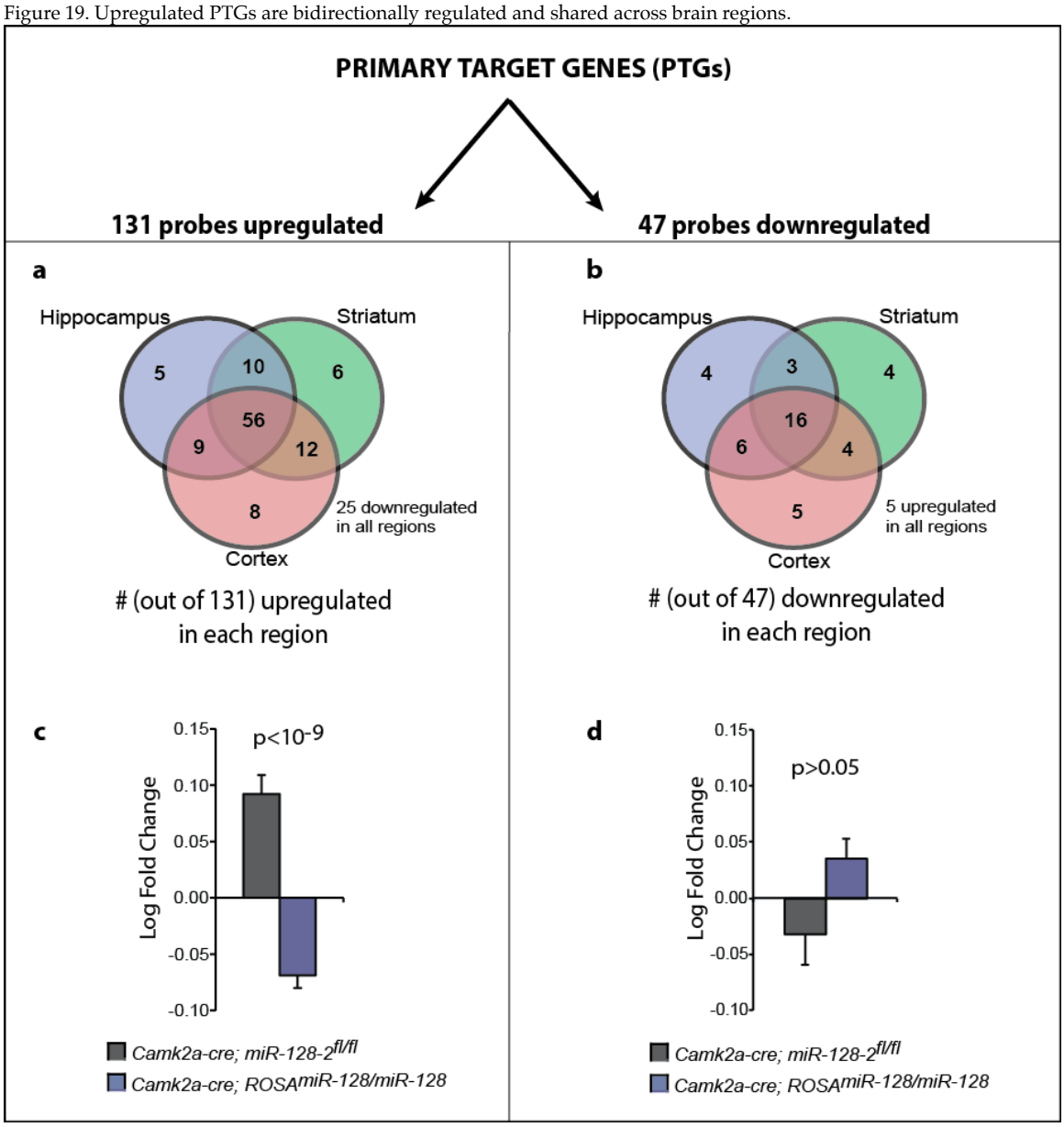

4.3 Convergent modulation of ERK pathway by miR-128 targets

The relation between miRNA targets and the apparent biological function of a miRNA is necessarily a complex one. Many studies have focused on the role of single or few targets often selected from predicted target lists based on the presence of miRNA seed sites. While such strategies are useful in explaining narrowly defined effects of miRNA perturbation, they can only partially account for broader phenotypic outcomes. A fuller accounting for miRNA effects might require examining the consequences of repression of all real target genes, but it is often difficult to see how large groups of genes might interact.

To assess if these genes converge upon common biochemical networks or pathways, we used literature curated analysis programs to look for enrichment of known pathways and networks among these genes. Ingenuity network analysis predicts gene networks from a given set of genes using known and predicted biochemical interactions, enabling diverse genes to "merge" around a few common interactions. Such an analysis produced a top ranked network in which many of the miR-128 targets we identified converge on MAP kinase-ERK1/2 proteins (Figure 20). The MAP kinase-ERK pathway was also among the two pathways showing significant enrichment with our primary target gene list using KEGG pathway annotations (Figure 20). These findings were surprising as many of these interactions were predicted or poorly studied. Closer examination of links between targets and the ERK signaling pathway might reveal further possible interactions.

Figure 20. Primary targets are enriched for genes that modulate the ERK signaling pathway.

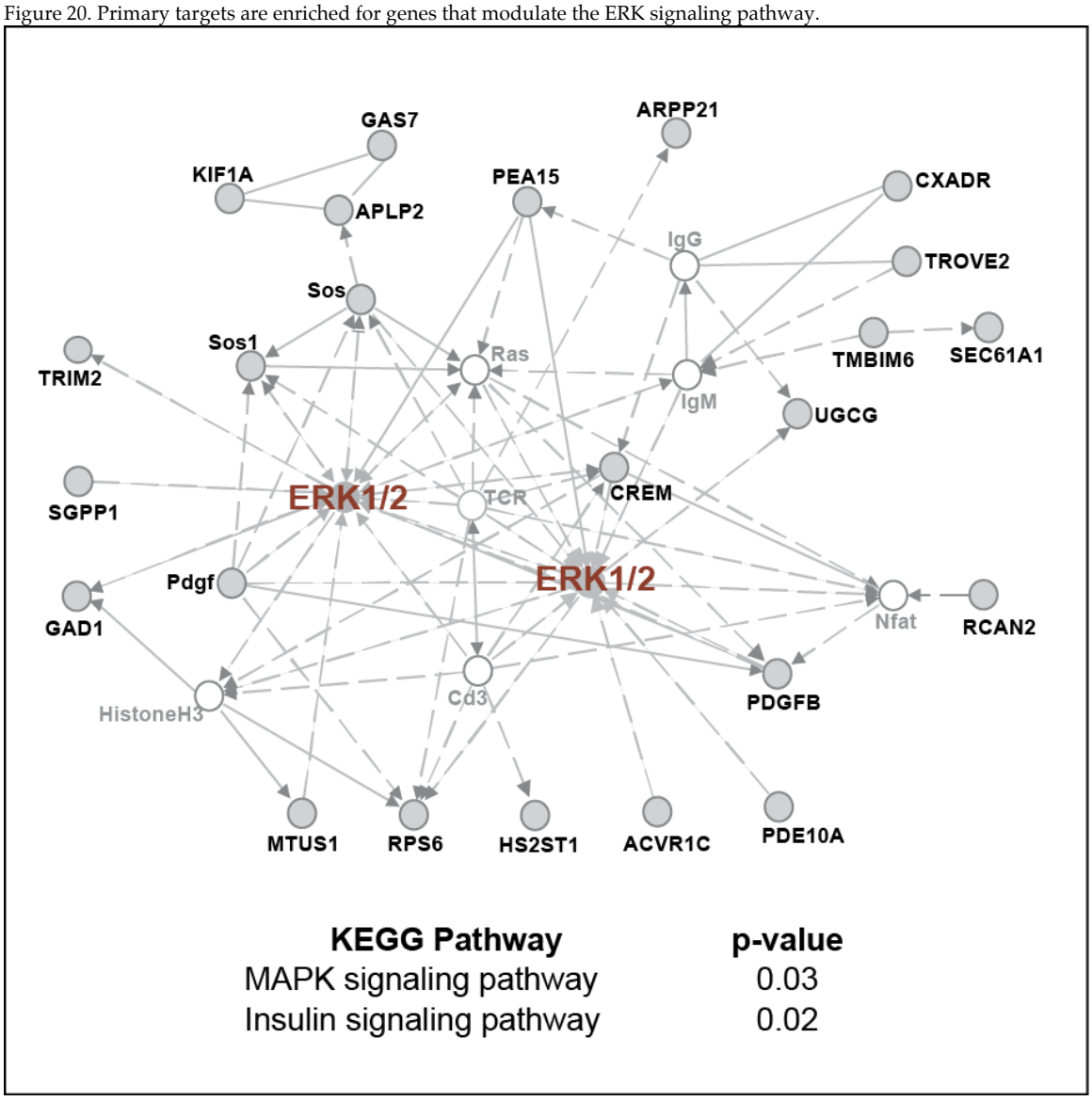

Figure 20. Primary targets are enriched for genes that modulate the ERK signaling pathway.

Above: Top ranked network cluster from Ingenuity Network analysis of all upregulated PTGs. Below: KEGG pathway analysis of upregulated PTGs showing significantly enriched pathways.

To test if phosphorylation levels of ERK or other signaling pathways were altered in the absence of miR-128, we measured levels of total and phosphorylated signaling intermediates and kinases using enzyme-linked immunosorbent assay (ELISA). Among these, only levels of phosphorylated ERK were significantly elevated in *Drd1a-cre; miR128-2*$^{fl/fl}$ mutant striata (Figure 21a). Relating absorbance readings to serial dilutions of control samples suggested that mutant samples contained approximately 1.6-fold higher concentration of phospho-ERK than controls (Figure 21b). No other assayed phospho-proteins (including, JNK/SAPK and AKT kinase) were altered, demonstrating a specific effect on ERK pathway activation.

Western blot quantification using similarly processed samples demonstrated a 1.6-fold increase in phosphorylation levels of ERK2/P42 (Figure 21c), with no increase in ERK1/P44 phosphorylation (data not shown). We found no change in the baseline phosphorylation levels of DARPP-32 Thr34 suggesting that that is no increase in levels of dopamine or dopamine receptors or no enhanced dopamine receptor activation (data not shown). Similar quantification of phospho-ERK from striata of neuronal deletion and overexpression miR-128 mutants showed that this phenomena was also bidirectionally regulated by miR-128, consistent with the bidirectionality seen both in the phenotypes of these mutants and in the expression of primary targets genes (Figure 21d,e).

Figure 21. ERK signaling is enhanced in the absence of miR-128.

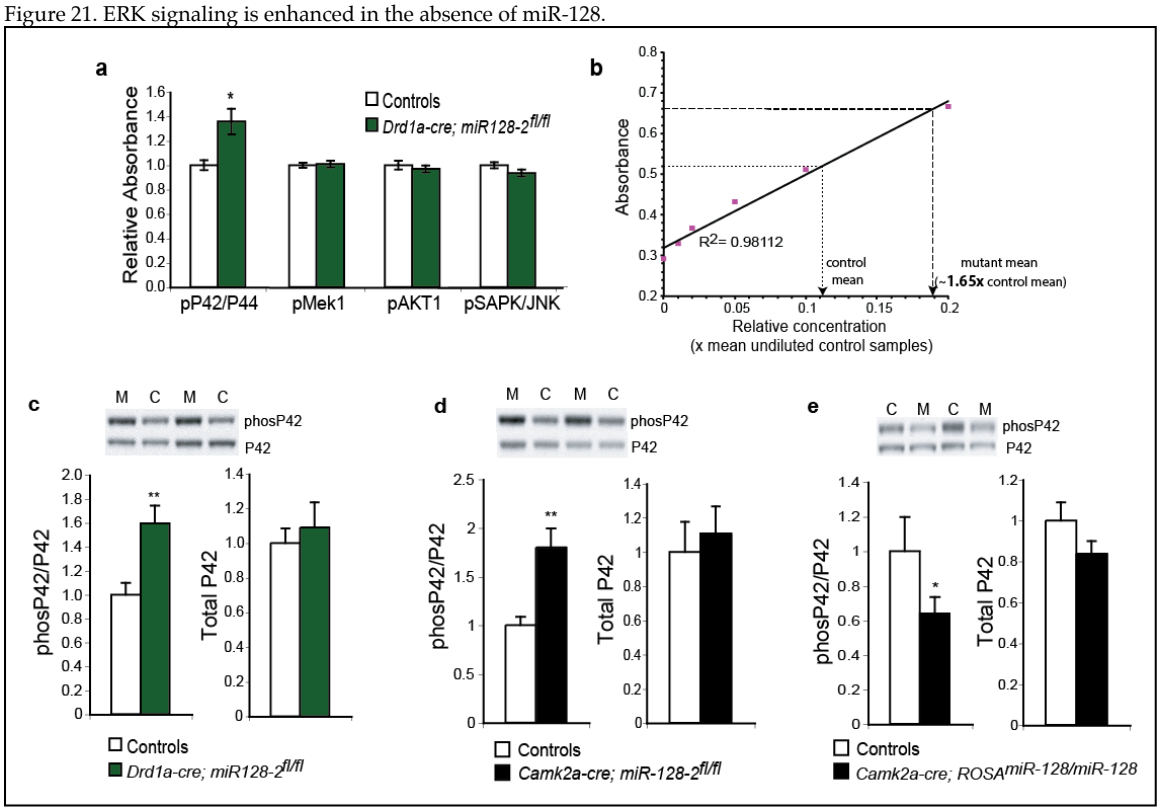

Figure 21. ERK signaling enhanced in the absence of miR128.

a, Increased activation of ERK but not other kinases in *Drd1a-cre; miR-128-2*$^{fl/fl}$ mutants (n=4). Levels of phosphorylated species of kinases indicated were quantified from striatal samples by ELISA.

b, ELISA titration curve using combined control samples show that mutant phosphoErk levels are increased 1.65 fold over control. * p<0.05, Welch's t-test.

c-e, Levels of P42 and phosphorylated P42 were quantified by western blot from striatal samples, phosP42 levels were normalized to total P42 levels, P42 levels were normalized to β-actin loading controls, and all values expressed relative to control mean. Increased P42 phosphorylation in *Drd1a-cre; miR-128-2*$^{fl/fl}$ mutants (**c**), and *Camk2a-cre; miR-128-2*$^{fl/fl}$ mutants (**d**). Decreased P42 phophorylation in *Camk2a-cre; ROSA*$^{miR-128/miR-128}$ transgenics overexpressing miR-128 (**e**). Represenative blots are shown. (n=4 each). * p<0.05. ** p<0.01, Welch's t-test.

All error bars indicate S.E.M.

4.4 Summary

The demonstration of the strong functional significance of miR-128 in D1-MSNs (previous chapter) presents a relatively homogeneous neuronal population in which to isolate miR-128 targets. We have made use of different approaches to identify the physiologically relevant targets of miR-128 in vivo that exhibit the following properties: (i) 3'UTR association with Ago2 in neurons; (ii) presence of miR-128 seed within region of Ago2 association; (iii) significant derepression in the absence of miR-128; (iv) bidirectionality of regulation by miR-128; (v) regulation by miR-128 in multiple regions of the forebrain. The list of primary target genes we identified suggested a role for miR-128 in the regulation of ERK-mediated pathways. In agreement with this, we showed that uniquely among kinase-mediated signaling pathways, activation of the ERK2 was sensitively controlled by miR-128. Control of ERK2 by miR-128 is consistent with the effect of miR-128 on behavioral excitation. We will examine the possible physiological effects of ERK regulation and its contribution to hyperlocomotion in the next chapter.

Chapter 5: Control of ERK activation by miR-128 in D1-MSNs

5.1 ERK signaling in D1-MSNs

Extracellular signal-regulated kinases 1 and 2 (ERK1/2) are members of a broader family of serine/threonine kinases known as the mitogen-activated protein kinases (MAPK), and arguably the best characterized (reviewed in (*136*)). Like all MAP kinases, ERK1/2 are activated by a series of upstream kinases that transduce and amplify an initial extracellular or intracellular event. Upstream kinases have high substrate specificity, phosphorylating only a restricted subset of MAP kinases. In the case of ERK1/2, MAP/ERK kinases 1/2 (Mek1/2) are the unique upstream activating kinases.

ERK1 (P44) and ERK2 (P42) are nearly identical (85% sequence similarity) and universally expressed. However, some important functional differences exist. While ERK1-deficient mice display only subtle phenotypic effects (*137*), ERK2 deficiency is embryonic lethal (*138*). In the adult brain, basal phosphorylation and glutamate induced phosphorylation of ERK2 is much stronger than ERK1 (*139*). Furthermore, ERK1 deletion does not appear to affect learning ability (*140*), but mild reductions in ERK2 levels impairs long term memory (*141*).

Previous studies showed that the elevation in basal activation of ERK2 upon miR-128 depletion is consistent with the epilepsy and hyperlocomotion phenotypes we observed. Postnatal expression of a constitutively active MEK1 in projection neurons resulted in higher phospho-ERK levels and caused spontaneous and severe seizures (*142*). In addition, mice with constitutive ERK1 deletion show enhanced ERK2 signaling in the striatum and cortex, and increased basal horizontal and vertical activity in the open field (*139*).

The drugs of abuse cocaine and amphetamine strongly induce ERK2 phosphorylation in the striatum. Induction of ERK2 phosphorylation occurs almost exclusively in D1-MSNs and requires activation of both Dopamine D1 receptors and NMDA glutamate receptors (*130*, *143*). Therefore, ERK2 phosphorylation mediates detection of coincident dopamine and glutamate inputs within D1-MSNs.

A number of studies contributed to our current understanding of coincident detection (*132*, *143-145*). D1 activation results in phosphorylation of Thr34 on DARPP-32 by PKA, which in turn inhibits protein phosphatase 1 (PP1). PP1 inhibits STEP, which dephosphorylates ERK (*143*). D1 receptor activation therefore promotes ERK activation by suppressing dephosphorylation. Glutamate activation of ERK is less well understood but it is thought to require calcium entry via NMDA receptors and Ras-GRF1 (*144*, *145*).

ERK2 activation initiates a cascade of phosphorylation events in the cytoplasm and nucleus to promote synaptic plasticity and transcriptional adaptations that accompany cocaine stimulation. Pre-treatment with MEK1 inhibitor SL327 at high dose inhibits the locomotor response to acute cocaine (*146*). In addition, paired pre-treatment with SL327 prior to cocaine administration abolishes locomotor sensitization (*147*). These results suggest a role for ERK in the regulation of basal excitability as well as the persistent changes that result from it.

Both high-frequency afferent stimulation and cocaine administration induce ERK-dependent long-term potentiation (LTP) in D1-MSNs (*148*). The specific mechanisms that transduce ERK activation into dendritic and synaptic potentiation in MSNs are still unclear but are thought to be similar to those that

occur in hippocampal neurons. ERK phosphorylation inactivates Kv4.2 potassium channels (*149*), which regulate MSN dendritic, and spine excitability (*128*). ERK activity also promotes AMPA receptor insertion at synapses (*150*, *151*), and increases dendritic branching and spine density in MSNs (*152*). The significance of these mechanisms was demonstrated in a recent study in which optogenetic depotentiation of cocaine-potentiated synapses in D1-MSNs was sufficient to reverse the expression of locomotor sensitization (*148*).

In the D1-MSN nucleus, cocaine-induced ERK activity promotes phosphorylation of MSK1. MSK1 activation in turn activates CREB phosphorylation at Ser133 and Histone H3 phosphorylation at Ser10, to induce immediate early genes (*130*, *153*). This ERK-dependent transcriptional response is an important component of long-term behavioral adaptations, as MSK1 deficient animals display reduced locomotor sensitization upon repeated cocaine administration (*153*).

Aside from these plasticity mechanisms, the regulation of ERK pathway in D1-MSNs is also an important component in the pathology of Parkinson's disease (PD). In Parkinson's disease, death of midbrain dopamine neurons results in loss of dopaminergic tone in the striatum, silencing of D1-MSNs and progressive akinesia (*154*). The study of Parkinson's disease has been greatly aided by the use of animal models of Parkinsonian-like dopamine depletion. One widely used murine model involves the stereotactic injection of the dopamine derivative 6-hydroxydopamine (6-OHDA) into the striatum, where it is taken up at dopamine releasing terminals by the dopamine re-uptake mechanism. Uptake into cells results in apoptotic death and destruction of nigrostriatal input (*155*).

One well-known epiphenomenon of dopamine depletion is dopamine supersensitivity (*156*), which takes the form of exaggerated behavioral and signaling responses to dopamine agonists such as L-dopa. Dopamine supersensitivity occurs in response to D1 agonists but not D2 agonists, and results in supersensitive activation of ERK and its downstream targets in D1-MSNs (*157*). The induction of ERK activation by D1 receptor agonists is very mild in normal mice. The requirement for contemporaneous dopamine and glutamate inputs to induce ERK phosphorylation might explain this restricted response. In the dopamine-depleted striatum however, most D1-MSNs become phospho-ERK positive upon stimulation by similar doses of agonist (*158*).

L-dopa induced dyskinesia (LID) is a common and early-noted side effect of treating PD with L-dopa (*159*), which involves a range of abnormal involuntary movements which include orofacial and limb dyskinesias. LID has been successfully modeled in rat and mouse by chronic L-dopa administration in 6-OHDA lesioned animals. D1-MSN supersensitivity shares many mechanistic similarities with LID. Both acute and chronic administrations of L-dopa in lesioned animals induce abnormal activation of the ERK pathway in D1-MSNs (*158*, *160*). Furthermore, pharmacological inhibition of ERK during chronic L-dopa treatment reduces LID (*158*).

The ERK pathway mediates several physiological and pathological processes in D1-MSNs. miR-128 regulates steady state ERK activation in D1-MSNs. In this chapter, we will explore the biological effects of this regulation.

5.2 miR-128 suppresses basal electrophysiological excitability of D1-MSNs

MAPK activation can result in changes in intrinsic excitability. ERK phosphorylation inactivates dendritic potassium channel Kv4.2, changes AMPA cycling kinetics to favor increased AMPA receptor insertion and promotes spine formation. To examine electrophysiological changes in D1-MSNs in the absence of miR-128, we collaborated with Dr. Josh Plotkin at Northwestern University. In order to interrogate D1-MSNs specifically we made use of *Drd1a-cre*; *miR128-2*$^{fl/fl}$ mutant mice expressing eGFP-tagged L10a ribosomal subunit in D1 MSNs (D1-eGFP-L10a). The eGFP-tagged ribosomes produce a robust green fluorescent signal in the nucleolus, allowing for easy identification by fluorescence microscopy. Mutant D1-MSNs showed greater dendritic excitability, potentiated synaptic AMPA response and increased density of distal spines, consistent with the cocaine-induced ERK-dependent effects previously described (Figure 22).

Dendritic membrane excitability is measured by the decrease in back-propagating action potential (bAP) amplitude in distal dendrites compared to proximal dendrites upon current injection at the soma. Dendritic membrane excitability is believed to be regulated by Kv4.2 voltage-activated K^+ channels in cortical, hippocampal and striatal neurons. It is also known that Kv4.2 channels are inactivated by ERK phosphorylation. Furthermore, Mek inhibition of basal phospho-ERK also reduces basal phosphorylation of Kv4.2 and decreases distal dendrite bAP amplitude. Therefore, our finding of heightened distal dendritic membrane excitability is fully consistent with the increased basal phospho-ERK levels.

Figure 22. miR-128 suppresses intrinsic excitability of D1-MSNs.

a, Dendritic excitability is enhanced in D1-MSNs in *Drd1a-cre; miR128-2$^{fl/fl}$; Drd1a-eGFP-L10a* mutants. Single action potentials were generated in the soma by injecting positive current through the electrode. The evoked calcium transients were measured in proximal (~50 μm from soma) and distal (~100-120 μm from soma) dendritic shafts by performing synchronized line scans. The attenuation of the bAP signal along the dendrite was calculated by dividing the distal calcium signal by the maximum proximal calcium signal per cell. Attenuation was significantly enhanced in mutant dendritic shafts. n=4 cells, 11-21 shafts per group.

b, Synaptic excitability is enhanced. Miniature excitatory post-synaptic currents (mEPSCs) were recorded by whole-cell patch recording on control and mutant D1-MSNs.

c, Spine density is increased. Left: Maximum intensity projection (MIP) images of distal (~100 μm from soma) dendrites in control and mutant D1-MSNs. Right: Box plots showing population spine densities. n=10-11 cells per group.

d-e, Somatic excitability is unaltered. **d,** Example responses of a wild type (top) and mutant (bottom) D1-MSN to somatic current injections. Voltage traces are in response to -100, -50, +100, +190 and +250 pA. **e,** Frequency-current (F-I) plot showing average firing frequencies to somatic current injection. No difference was observed between WT (N=6) and KO (N=7) dSPNs (Mann-Whitney nonparametric test, $p>0.05$).

* $p<0.05$, *** $p<0.001$, Mann-Whitney nonparametric test.

Data and figures courtesy of Josh Plotkin.

Figure 22. miR-128 suppresses intrinsic excitability of D1-MSNs

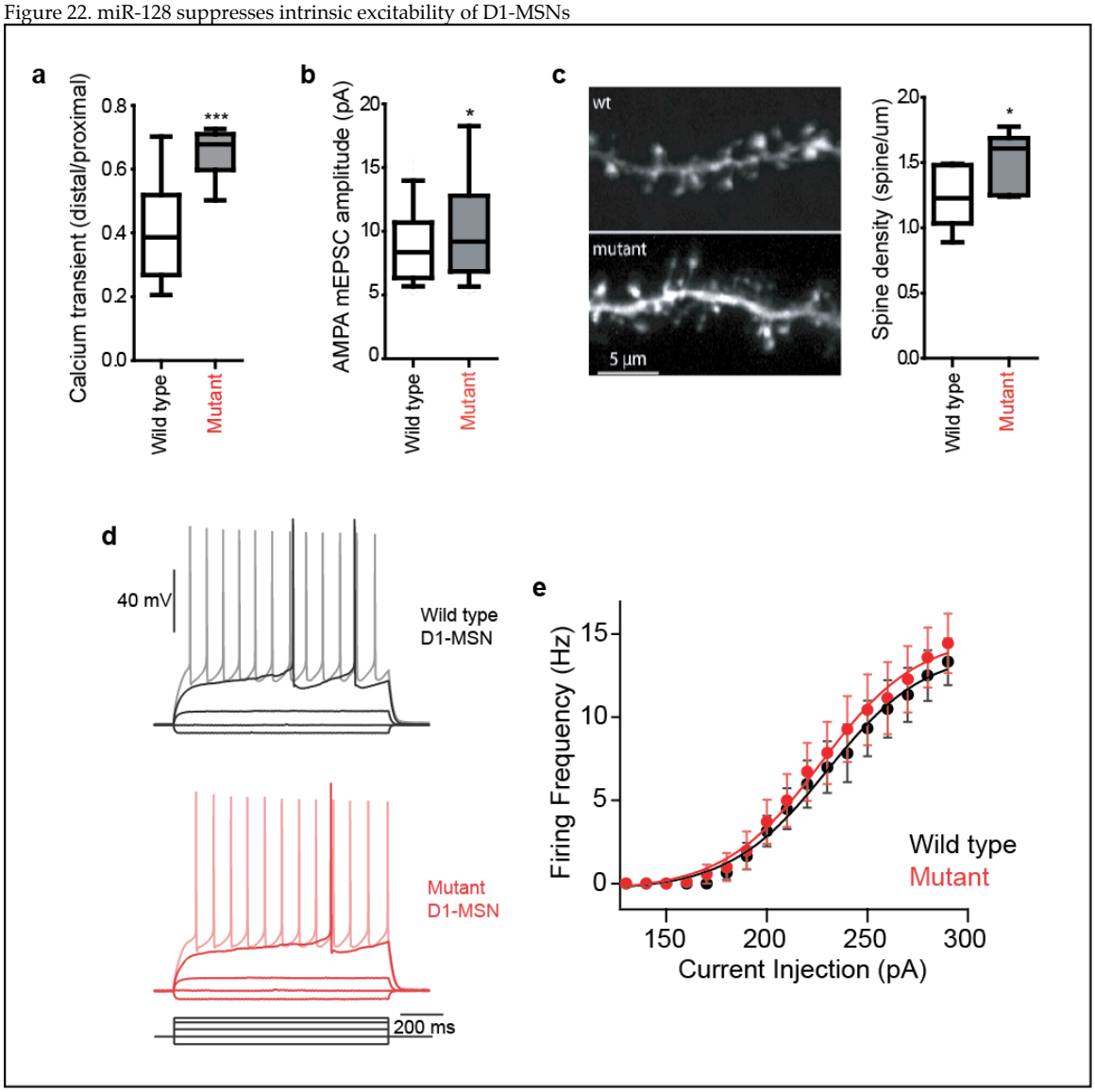

5.3 ERK inhibition reverses hyperlocomotion in *Drd1a-cre; miR128-2$^{fl/fl}$* mutants

Cocaine-induced synaptic potentiation in D1-MSN is one major cause of locomotor sensitization. Similarly, the increased excitation profile of the miR-128 depleted D1-MSN might be a likely cause of basal hyperlocomotion of *Drd1a-cre; miR128-2$^{fl/fl}$* mutants. In this model, mutant D1-MSNs have greater firing propensity in response to unchanged endogenous input. If chronic ERK2 activation is a cause of higher excitability of D1-MSNs, then ERK inhibition might be sufficient to normalize basal hyperlocomotion.

Systemic administration of SL327 (a blood-brain barrier crossing derivative of U0126, a MEK1 inhibitor) resulted in inhibition of locomotion in the open field chamber. We examined the distance traveled in the open field by mutants and control mice after injection of increasing doses SL327 and found that mutants responded more strongly to SL327 inhibition. At a dose of 12.5mg/kg, SL327 inhibited activity of mutants with no significant effect on controls. To confirm this finding, the experiment was repeated with a second cohort of mice. In this experiment, mutants and controls were injected with either vehicle (DMSO/Saline) or a 12.5mg/kg dose of SL327. The results clearly show that at this low dose, mutant and control locomotion was equalized with no change in the activity of control mice (Figure 23b). The experiment was repeated and phospho-ERK levels were quantified 30 minutes post-injection, showing that baseline ERK activation was also normalized at this dose (Figure 23a).

As SL327 injection resulted in broad inhibition of MEK1, we further tested the causative role of ERK in mutant hyperlocomotion using genetic means by making use of a previously generated transgenic mouse line with Cre dependent expression of dominant negative MEK1 (dnMEK). The dominant negative MEK1 protein contains a lysine to methionine substitution within the ATP binding site, eliminating its kinase activity but preserving the ability to bind ERK1/2.

The protein is expressed downstream of a chicken beta-actin promoter region and a floxed STOP-cassette, which permits recombinase control of expression. We crossed dnMEK transgenic animals with *Drd1a-cre; miR128-2*$^{fl/fl}$ mutants to generate mice in which heterozygous miR-128-2 deletion and dnMEK expression occur in D1-MSNs. Total activity in the open field was lower in mutants expressing dnMEK, and did not significantly differ from that of wild type control mice (Figure 23c).

In conclusion, using pharmacological and genetic means of MEK1 inhibition, we have tested and shown that increased ERK activation had a causative role for the hyperactivity observed in the mutant animals in which miR-128 was depleted in D1-MSNs.

Figure 23. miR-128 modulates motor activity via ERK activation in D1-MSNs.

a, Increased Erk2 phosphorylation is normalized by low dose Mek inhibitor. *Drd1a-cre; miR-128-2*$^{fl/fl}$ or controls were injected with either vehicle or 12.5mg/kg SL327 (n=5) and striata were dissected 30 min later. Right: Phosphorylated P42 levels were quantified by Western blot, normalized to total P42 levels and expressed relative to mean control levels. Left: Representative blot is shown. * $p<0.05$, ** $p<0.01$, 2-way ANOVA followed by Bonferroni post test.

b, Basal hyperlocomotion is normalized by pharmacological Erk inhibition. Left: Horizontal distance travelled in an open-field chamber in 10 minute intervals. *Drd1a-cre; miR128-2*$^{fl/fl}$ mutants and littermate controls were injected with either vehicle or 12.5mg/kg SL327 prior to measurement. (n=16 each group). ** $p<0.01$, two-way repeated measures ANOVA (treatment). Right: Total horizontal distance travelled in an open-field chamber over 60 minutes. *** $p<0.001$, 2-way ANOVA followed by Bonferroni post test.

c, Genetic suppression of Erk2 phosphorylation using conditional transgenic dominant negative MEK1 (dnMEK1) rescues basal hyperactivity in *Drd1a-cre; miR128-2*$^{wt/fl}$ heterozygous mutants. Left: Horizontal distance travelled in an open-field chamber in 10 minute intervals. *Drd1a-cre; miR128-2*$^{wt/fl}$ heterozygous deletion mutants carrying one transgenic dnMEK1 allele (*Drd1a-cre; miR-128-2*$^{wt/fl}$*; dnMEK1+*, n=11), mutants carrying no transgenic alleles (*Drd1a-cre; miR-128-2*$^{wt/fl}$, n=13) and and wild type controls (n=23) were compared. * $p<0.05$ ** $p<0.01$, 2-way repeated measures ANOVA. Right: Total horizontal distance travelled in an open-field chamber over 60 minutes. * $p<0.05$ ** $p<0.01$, one-way ANOVA followed by Tukey's post test.

All error bars indicate S.E.M.

Figure 23. miR-128 modulates motor activity via ERK activation in D1-MSNs.

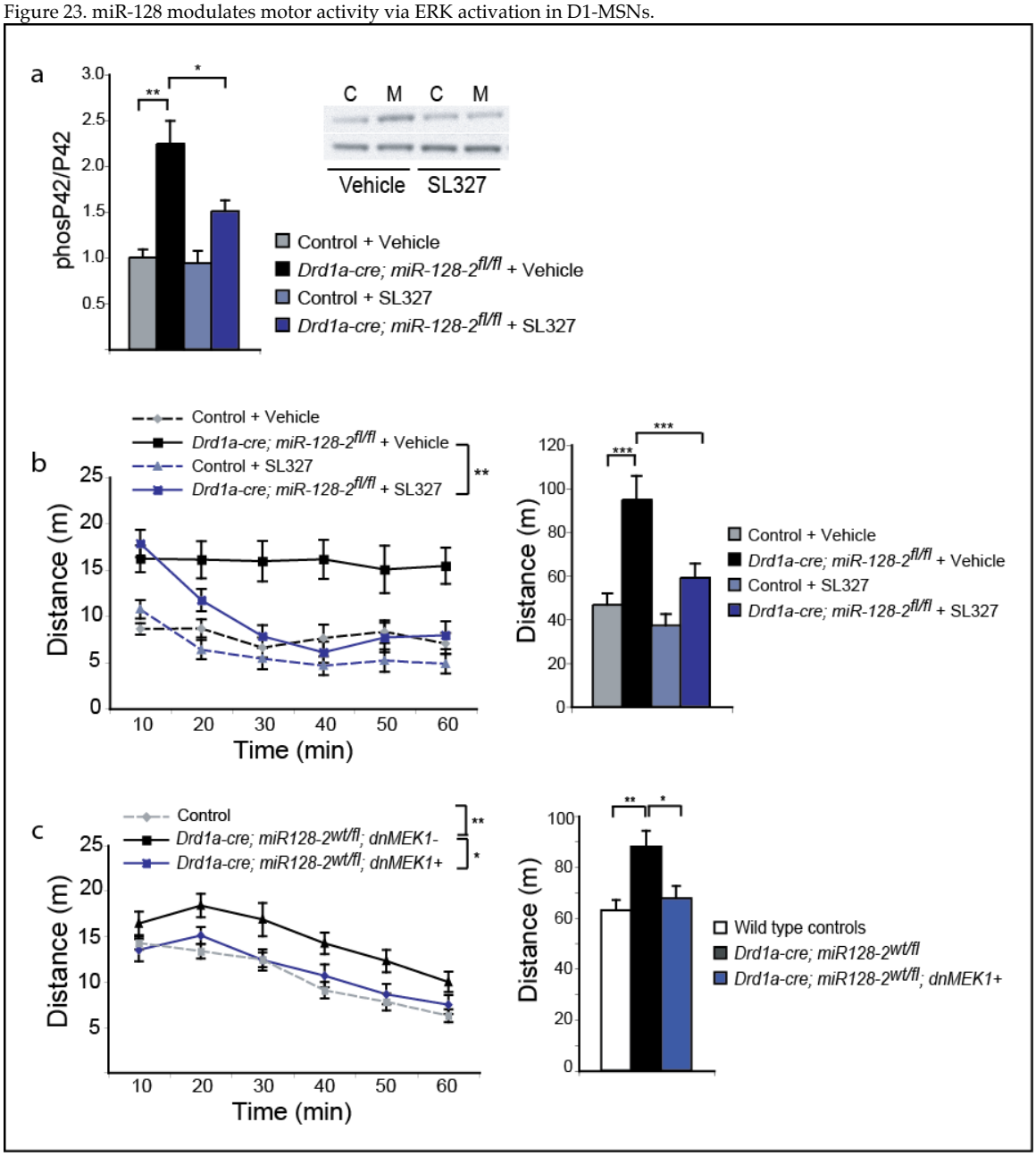

5.4 miR-128 suppresses supersensitive dopamine response

Firing of D1 MSNs induced either by pharmacological activation of D1 receptors or by direct optogenetic stimulation induces locomotor activity (*134*). It is therefore likely that the hyperlocomotion observed in *Drd1a-cre; miR-128-2*$^{fl/fl}$ mutants reflects a higher population firing rate of D1-MSNs. To test if this baseline difference was accentuated, preserved or occluded in the presence of further stimulation, we tested the locomotor activity of *Drd1a-cre; miR-128-2*$^{fl/fl}$ mutants in the presence of a D1 receptor specific agonist. Low dose of agonist induced locomotor activity in wild type mice, with the peak occurring about 30 minutes post injection. Interestingly, *Drd1a-cre; miR-128-2*$^{fl/fl}$ mutants showed an even greater locomotor response with a similar duration to peak activity and slower return to baseline (Figure 24a).

The pharmacological activation of D1-MSNs by cocaine leads to ERK signaling activation, phosphorylation of Histone H3 at Serine S10 (H3S10) and upregulation of immediate early genes (IEGs) (*146*, *153*). Similarly, D1-MSNs of the dopamine-depleted striatum are characterized by a supersensitive ERK response, H3S10 phosphorylation, and transcriptional activation in response to L-DOPA.

Besides basal ERK2 elevation, D1 agonist stimulation induced further increases in ERK2 phosphorylation in *Drd1a-cre; miR-128-2*$^{fl/fl}$ mutants at a dose that induced almost no increase in ERK2 phosphorylation in control mice (Figure 24b). This result suggests that mutant D1-MSNs are supersensitive in a manner reminiscent of those in dopamine-depleted striata.

Figure 24. miR-128 suppresses supersensitive dopamine response.

a, Locomotor response to dopamine agonist is heightened by the loss of miR-128. Horizontal distance travelled in an open-field chamber shown 5 minute intervals. Saline and D1-agonist SKF81297 were injected intraperitoneally 10 and 20 minute after introduction to the chamber. *Drd1a-cre; miR128-2*$^{fl/fl}$ (n=25) and controls (n=30). * p<0.05; ** p<0.01; *** p<0.001, Welch's t-test.

b, *Drd1a-cre; miR-128-2*$^{fl/fl}$ mutants show supersensitivity of Erk2 phosphorylation in response to dopamine agonist. Mutants and controls were injected with either saline or D1-agonist SKF81297 (n=5 each) and phosphorylation levels of P42 were quantified by western blot, normalized to total P42 levels and expressed relative to mean control levels. Representative blot is shown. * p<0.05, two-way ANOVA Tukey's post test.

c-d, Neuronal activation by dopamine agonist is increased by loss of miR128. Mutant (*Drd1a-cre; miR128-2*$^{fl/fl}$*; Drd1a-eGFP-L10a*) and control mice (*miR128-2*$^{fl/fl}$*; Drd1a-eGFP-L10a*) are injected with either saline or agonist and sacrificed 30 minutes later and total striatum is dissected for flow cytometry. **c,** Representative nuclei counts showing eGFP-positive D1-MSN nuclei and activation as assayed by phosphorylated Histone H3S10. **d,** Number of activated D1 MSN nuclei was counted and expressed as percentage of total D1 MSN nuclei. Each symbol represents sample for one mouse. * p<0.05, 2-way Anova followed by Tukey's post-test.

e-f, Transcriptional activation by dopamine agonist is increased. Mutant (*Drd1a-cre; miR128-2*$^{fl/fl}$*; Drd1a-eGFP-L10a*) and control mice (*miR128-2*$^{fl/fl}$*; Drd1a-eGFP-L10a*) were injected with either saline or agonist and sacrificed 30 minutes later and polysome-associated transcripts were quantified by either microarray or qRT-PCR. **e,** Hierarchical clustering was performed on probes corresponding to immediate-early genes (IEG). Only agonist-injected samples cluster according to genotype. **f,** Selected immediate early genes and Darpp32 were quantified by qRT-PCR from polysome associated transcripts and expressed relative to control saline samples. ** p<0.01, *** p<0.001, 2-way ANOVA followed by Tukey's post-test. All error bars indicate S.E.M.

Figure 24. miR-128 suppresses supersensitive dopamine response.

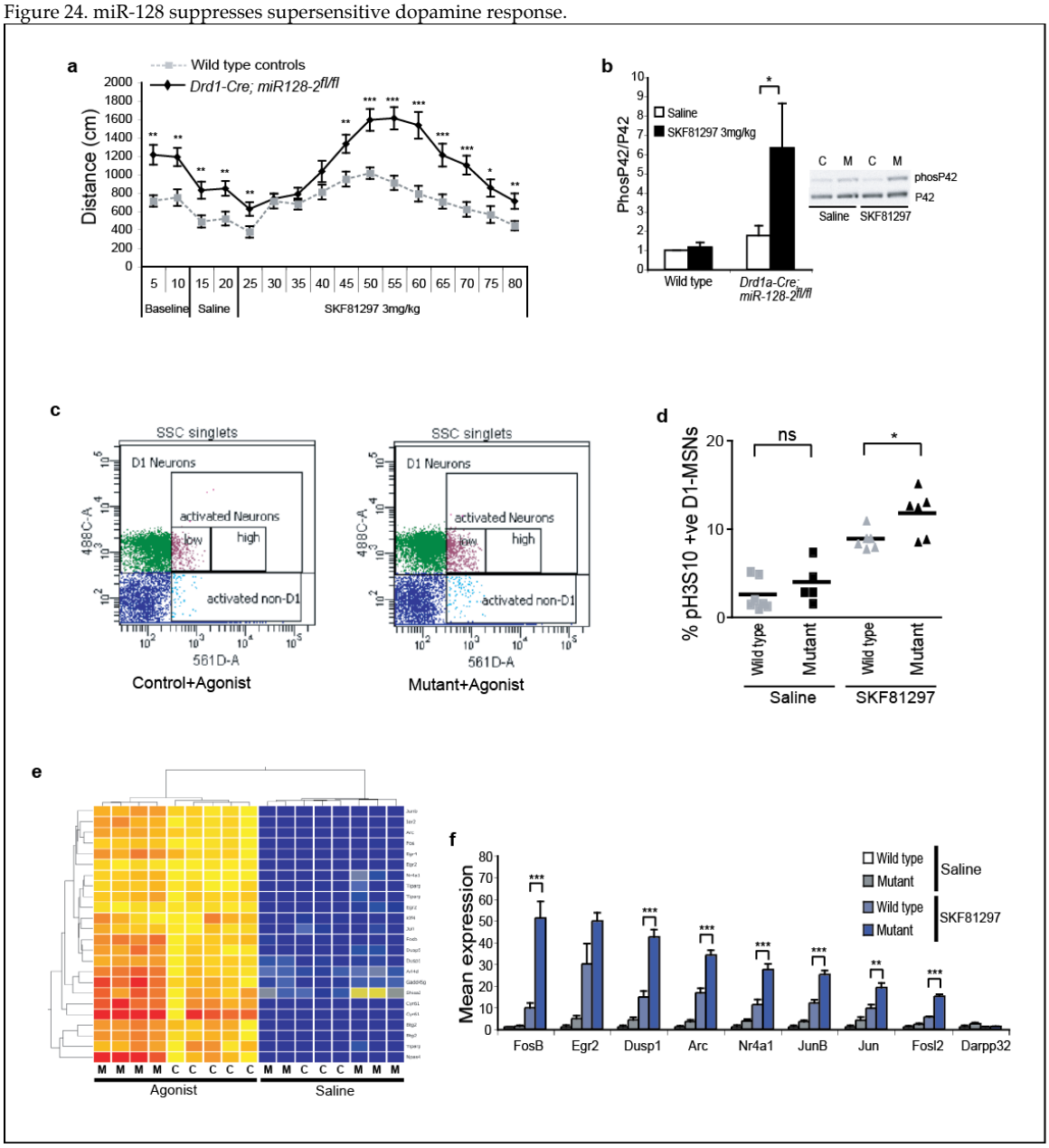

To extend this observation, we tested if locomotor and ERK supersensitivity is accompanied by potentiated histone phosphorylation and transcriptional response. Using *Drd1a-cre; miR-128-2*$^{fl/fl}$ mutants and control mice expressing tagged ribosomes in D1-MSNs - *Drd1a-cre; miR128-2*$^{fl/fl}$*; Drd1a-eGFP-L10a*, we were able to assay the extent of these responses in a cell-specific manner.

To quantify H3S10 phosphorylation, we enlisted the help of Dr. Melanie von Schimmelmann. EGFP-positive nucleoli in the nuclei of D1-MSNs allow quantification of histone activation in the D1-MSN population. *Drd1a-cre; miR128-2*$^{fl/fl}$*; Drd1a-eGFP-L10a* mutants and controls were injected with either saline vehicle or D1 agonist SKF81297. Animals were sacrificed 30 minutes later and striata dissected and nuclei were isolated. Nuclei were then incubated with antibodies against phosphorylated H3S10 and processed for flow cytometry. Agonist induction resulted in a higher percentage of phospho-H3S10 positive D1-MSNs (Figure 24c,d).

To quantify transcriptional activation, *Drd1a-cre; miR128-2*$^{fl/fl}$*; Drd1a-eGFP-L10a* mutants and littermate controls were injected with either saline vehicle or D1 agonist SKF81297. Animals were sacrificed 30 minutes later and striata rapidly dissected and processed for polysome immunoprecipitation and RNA isolation followed by microarray analysis. IEGs were defined as genes upregulated in control mice by at least 5 fold in response to agonist (19 unique genes). Cluster analysis of IEG expression levels show that mutant samples segregated from control samples upon agonist injection (Figure 24e). Based on two-way ANOVA analysis, aggregate IEG expression levels were higher in mutants than controls upon induction, confirming greater transcriptional

activation. Selected IEGs were quantified further by qRT-PCR and these showed significantly higher agonist-induction in mutants (Figure 24f).

We have shown earlier that miR-128 overexpression suppresses endogenous ERK activation. We therefore tested if excess miR-128 suppresses the development of behavioral supersensitivity. Firstly, transgenic mice overexpressing miR-128 showed a reduced locomotor response to acute D1-agonist administration, with similar induction kinetics (Figure 25a).

We further tested if miR-128 could suppress supersensitive responses in the hemiparkinsonian mice model. To do this, we made use of an assay of rotational behavior in unilateral 6-OHDA lesioned mice. In this model, both the extent of denervation and D1-MSN supersensitivity can be assayed by quantifying rotational behavior. Systemic administration of cocaine results in ipsilateral rotations toward the side of the lesion due to the imbalance of dopamine releasing terminals, while systemic administration of either L-dopa or D1 receptor agonist, result in contralateral rotations due to supersensitive responses in the lesioned striatum (*156*) (Figure 25b).

We performed unilateral lesions of transgenic mice in which 6-OHDA was stereotactically injected into the left striatum and vehicle was injected into the right striatum. After a 3-week recovery period, rotational responses were quantified. Mice did not result in net rotations in either direction at baseline. Cocaine injection led to similar net ipsilateral rotations in control and transgenic mice. In contrast, upon D1 agonist injection, transgenic mice showed lower net contralateral rotation compared to controls indicating reduced D1-MSN supersensitivity (Figure 25c).

Figure 25. Transgenic miR-128 expression suppresses excitability.

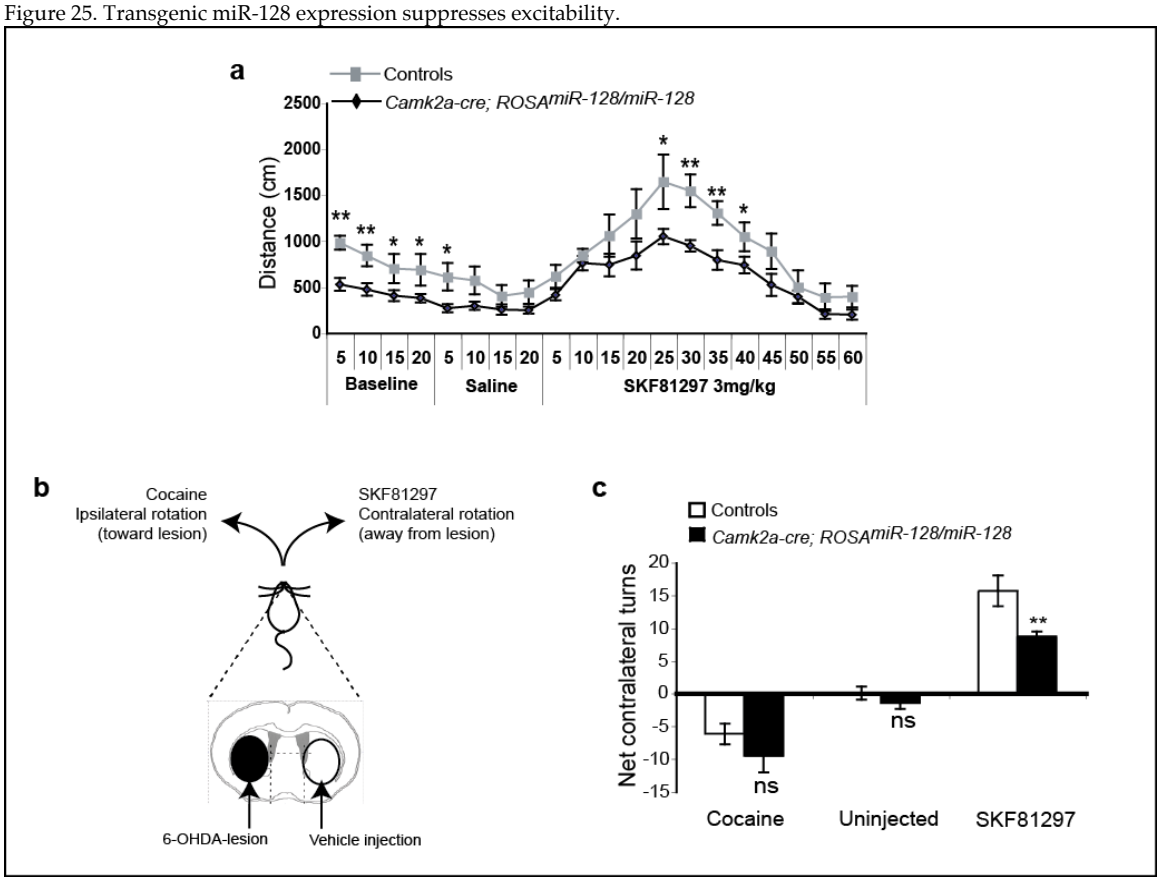

Figure 25. Transgenic miR-128 expression suppresses excitability.

a, Locomotor response to dopamine agonist is dampened by increased miR-128. Horizontal distance travelled in an open-field chamber shown 5 minute intervals. Saline and D1-agonist SKF81297 were injected intraperitoneally 20 and 40 minute after introduction to the chamber. *Camk2a-cre; ROSA*$^{miR\text{-}128/miR\text{-}128}$ and controls (n=11 each). * $p<0.05$, ** $p<0.01$, Welch's t-test.

b-c, Unilateral 6-OHDA lesions were performed on *Camk2a-cre; ROSA*$^{miR\text{-}128/miR\text{-}128}$ and control mice, by stereotactic injection into the left striatum. Vehicle injections were performed on the right striatum. Rotational responses to cocaine and D1 agonist SKF81297 were measured after a 3 week recovery period.

b, Cocaine injection induces ipsilateral rotations due to presence of functional dopamine terminals in the unlesioned striatum. SKF81297 induces contralateral lesions due to increased dopamine response of D1-MSNs in the lesioned striatum. **c,** Overexpression of miR-128 suppresses contralateral rotation in response to D1 agonist. (n=10 per genotype) ** $p<0.01$ Welch's t-test. All error bars indicate S.E.M.

5.5 miR-128 depletion impairs learning and memory

ERK-dependent changes are crucial to synaptic and transcriptional mechanisms of plasticity and the loss of ERK signaling impairs animal performance in memory tasks and the ability to acquire new associations.

In cocaine-conditioned place preference (CPP), cocaine administration is paired with a specific context during training phase. At the test phase, test subjects are allowed to roam freely between cocaine and saline-paired chambers. Successful conditioning results in substantially more time spent in the cocaine-paired chamber due to the rewarding effects of cocaine (Figure 26a). Inhibition of ERK activation during conditioning abolished place preference (*146*), while in models with enhanced ERK2 signaling, mice showed increased cocaine sensitization and increased CPP responses (*161*). Therefore, we tested if *Drd1a-cre; miR128-2*$^{fl/fl}$ mutants have higher CPP responses too. We found that these mutants show a significantly reduced CPP response compared to controls, as shown by the lower duration spent in exploration of the cocaine-paired chamber (Figure 26b).

To examine this effect further, we examined the performance of miR-128 depleted mutant mice in a separate behavioral task. In the novel object recognition task, experimenters make use of the robust, innate rewarding effects of novelty to produce a heightened exploratory response. This behavior is analogous to the novelty-induced hyperactivity upon inital exposure to the open-field chamber. In this paradigm, mice are trained by exposure to two identical objects in a chamber to which the mice have been previously acclimated. At 1 hour and 24 hours after training, test phases are conducted in which one of the

objects is replaced by a novel object prior to the introduction of the test subject into the chamber. Mice spend more time in exploration directed toward the novel object compared to the training object, indicating retention of memory of the trained object (Figure 26c). ERK suppression by hippocampal injection of MEK1 inhibitor during the training phase spares short-term memory (10min post-training) performance but severely impairs long-term memory (24 hours post-training) (*162*).

As the majority of homozygous *Camk2a-cre; miR-128-2*$^{fl/fl}$ mutants suffer from frequent seizures and die before 2 months of age, we performed this test on heterozygous *Camk2a-cre; miR-128-2*$^{wt/fl}$ mutants. Both mutant and control mice spent equal time exploring both objects during the training phase and significantly increased novel-object exploration during the 1 hour test phase. Interestingly, mutant mice showed severe impairments during the 24 hour test phase (Figure 26d).

Since ERK inhibition impairs acquisition and retention of learned associations, we expected that increased ERK sensitivity of miR-128 mutants would exhibit improved performance in learning and memory tasks. The reasons for this discrepancy will be discussed in the final chapter.

Figure 26. miR-128 depletion results in learning and memory deficits.

a, Schematic shows cocaine place preference in a 3-chamber test set-up. During test phases, mice are placed in center chamber and allowed to freely explore all 3 chambers for 5 minutes. During conditioning, mice are injected with either saline or cocaine (15 mg/kg) and placed in the correspondingly paired chamber for 15 minutes. The other pairing is performed 4 hours later. This conditioning protocol is repeated daily for 3 days. Free exploration test is performed on the 4th day.

b, *Drd1a-cre; miR128-2*$^{fl/fl}$ mutants are less efficiently conditioned by cocaine. Ratio of duration spent in cocaine-paired chamber to duration spent in saline-paired chamber is shown.

(n=12 per group). ** $p<0.01$, 2-way ANOVA followed by Bonferroni post test.

c, Novel object recognition task. During training phase, mice are allowed to freely explore a chamber with 2 identical objects. Mice are tested for recognition memory at 1 hour and 24 hours after training phase, with replacement of one of the training objects in each case.

d, *Camk2a-cre; miR-128-2*$^{wt/fl}$ heterozygous mutants are impaired for long-term memory object recognition memory. Line graphs show time spent exploring the novel object as proportion of total time spent exploring both objects. (n=15 per group) ** $p<0.01$, 2-way ANOVA followed by Bonferroni post test.

All error bars indicate S.E.M.

Figure 26. miR-128 depletion results in learning and memory deficits.

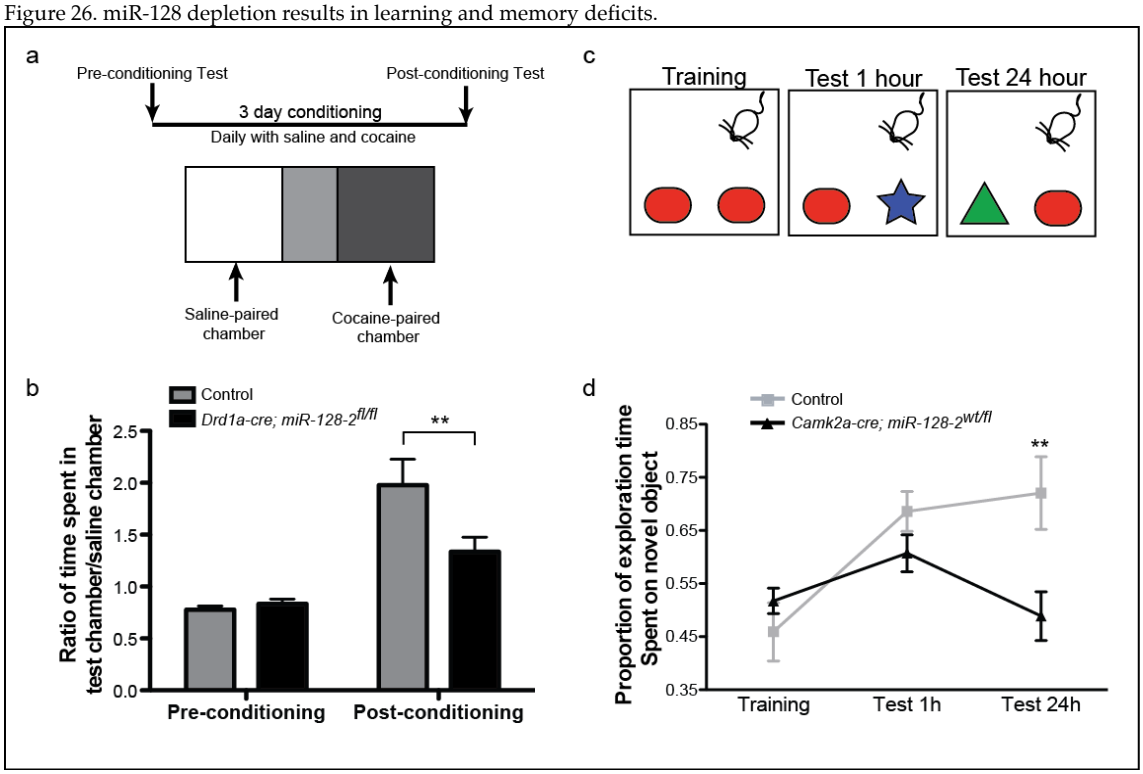

5.6 Summary

In summary, miR-128 loss induces basally elevated ERK2 signaling in D1-MSNs and the inhibition of ERK2 was sufficient to rescue basal hyperactivity, probably via ERK-dependent increases in neuronal excitability. In the absence of miR-128, D1-MSNs exhibit behavioral and ERK signaling supersensitivity similar to that which develops after dopamine depletion. This is also accompanied by a similar supersensitive transcriptional response. Furthermore, miR-128 overexpression was able to suppress behavioral supersensitivity. Lastly, we examined the performance of miR-128 mutants in learning and memory tasks and showed that their performances were strongly impaired, suggesting that ERK signaling hyperactivation does not necessarily enhance learning and memory.

Chapter 6 Discussion

6.1 Summary of findings

In this section, I will first summarize the key findings of the work presented here and subsequently expand on a few specific topics in separate sections.

We have demonstrated that segregated miRNA expression across neuronal types in the adult brain has enormous functional consequence. Prior studies found strong enrichment of miR-128 in projection neurons relative to interneurons of the forebrain. We demonstrated that the deletion of miR-128 in the former alone was sufficient to recapitulate fully the fatal epilepsy and severe hyperactivity observed upon ubiquitous deletion. We further extended this finding by showing that miR-128 is enriched in D1-MSNs over D2-MSNs of the striatum and that deletion of miR-128 in the former but not the latter was sufficient to recapitulate fully the hyperactivity induced by striatal deletion of miR-128.

By employing a combination of tools to identify RISC-associated transcripts and translationally repressed transcripts, we were able to isolate primary targets of miR-128 repression in an unbiased manner. This strategy allowed us to identify a relevant pathway (ERK signaling), the specific dysregulation of which accounts for some aspects of the behavioral changes. Our results strongly suggest that such a strategy would be very useful in other studies of miRNA function.

Finally, we showed that endogenous miR-128 expression suppresses ERK pathway activity and limits the excitability of neurons. This in turn could explain the development of spontaneous, fatal seizures and severe hyperactivity upon

miR-128 deletion. miR-128 suppresses a ERK hypersensitive response to dopamine and represses the supersensitivity of D1-MSNs in the dopamine-depleted striatum. This effect suggests clinical use to miR-128 in the treatment of neurological disorders in which hyperexcitability plays a major role, for example epilepsy and L-dopa induced dyskinesia.

In the following sections, I will discuss our miRNA target search strategy and other methods that might offer an improvement over the one we have employed. I will discuss the implication of ERK regulation by miR-128 for plasticity and learning, as well as possible roles of this regulation in other cell types. Finally, I will suggest further studies that might clarify the role of miR-128 in human dyskinesias and epilepsy.

6.2 *In-vivo* tools for primary target identification

In our search of physiologically relevant targets of miR-128, we have made use of two complementary tools: Ago2 CLIP-seq to profile RISC-associated mRNAs and TRAP-ribosomal profiling to profile transcript derepression in the absence of miR-128. This approach is a considerable improvement over methodologies used in previous studies undertaken to identify miRNA targets, mostly involving mRNA quantification.

MiRNA-dependent repression of target expression involves translational inhibition (reduced ribosomal association) and mRNA degradation (reduced mRNA quantity). These two processes are largely correlated but not necessarily linked, as such, quantification of ribosomal association is less restrictive and would include translationally-repressed transcripts for which no reduction in mRNA levels occur.

Ribosomal profiling experiments have previously been used in the study of miR-223-mediated repression in culture-differentiated neutrophils (*79*). The use of tagged ribosomes in TRAP technique allows cell-type specific expression profiling on rapidly dissected brain tissue and improves experimental resolution by excluding non-cell autonomous expression changes.

Other alternatives to ribosomal profiling include protein quantification using metabolic labeling experiments (*163*). However, such experiments are as yet difficult to implement in living animals (*164*), are also just beginning to be implemented in a cell-type specific manner (*165*) and is likely to offer only marginal improvements over ribosomal profiling.

Expression changes upon miRNA loss reflect not just the primary derepression of primary targets, but also the extensive secondary changes that invariably accompany chronic miRNA loss. To sieve out primary targets from secondary changes, in-silico predicted targets are often used. This approach depends greatly on the presence or absence of conserved complementary seed sequences in the altered transcripts, without evidence for whether such sites do indeed confer RISC association. Our method uses physiological RISC binding to identify primary targets.

All binary classification methodologies necessarily involve a trade-off between false positive rate and false negative rate. Because most if not all targets are repressed by miRNAs, and derepression of single targets are highly similar, changes in mean derepression can be used as a proxy of false positive rate. High mean derepression of a candidate target upon miRNA loss correlates with low false positive rate. By this measure, the use of CLIP-seq positive 6mer-containing targets as we have done produces a lower false positive rate than the use of all 6mer-containing targets in the genome. The use of conserved Targetscan predictions appears to produce an even lower false positive rate. However, previous studies have shown that non-conserved sites are also highly responsive to miRNAs, suggesting that limiting by conservation scores is too restrictive.

False negatives are more difficult to estimate from our data, but could arise in a number of situations. In some cases, full seed complementarity is not an absolute requirement for miRNA binding if non-canonical interactions exist along the rest of the miRNA. Future iterations of CLIP-seq might include such possibilities. However, the sequence determinants of such of "extra-seed" interactions are less well-defined and previous estimates suggest such pairings

are relatively rare. A more important source of false negatives is the detection limit imposed by RNA-sequencing. This group of false negatives would include target transcripts that are expressed at very low quantities, and transcripts of which only a small proportion are bound to the RISC-complex. Repeating the protocol using higher sequencing depth would address this issue to some extent.

In summary, we have used more physiological measures of derepression and RISC association, which allows us to reduce false positives without arbitrary sacrifices in sensitivity. New techniques in protein level quantification and the incorporation of known cis-determinants of targeting are likely to improve this process. New insights about miRNA-RISC biology might be gleaned from a quantitative and global view of miRNA targeting and repression.

6.3 Tuning and buffering of targets and ERK signaling

We have shown that primary target genes, in aggregate, respond in a bidirectional fashion to depleted and excess miR-128 levels. Most of these genes show a very mild repression by miR-128 in line with the fold changes observed by other groups. As transcription is an inherently noisy process, it is difficult to see how such mild changes could persist in single cells in the presence of stochastic fluctuations. In this and previous studies, the measured repression is a population mean of large cell populations, what remains unclear is if miR-128 repression has an effect on population variance. This could be determined by quantifying mRNA levels in single neurons or estimated using bins of small fixed numbers of neurons. If the mild repression level is a result of miR-128 buffering of stochastic transcriptional noise, one would expect the population variance of target expression to be increased substantially in the absence of miR-128. Conversely a strict tuning effect would preserve temporal variability in each neuron and preserve variability across the population of neurons.

We have also shown that miR-128 levels exert a specific and bidirectional regulation of ERK2 phosphorylation, although it is similarly unclear how the profile of the response is altered.

ERK signaling response is highly cooperative in Xenopus oocytes and in in-vitro systems (*166*, *167*), converting graded signals into an all-or-none response. In mammalian cells, a switch-like response is found in thymic selection and neuronal differentiation (*168*, *169*), while a more graded response is observed in other conditions (*170*). Increased steady-state phosphorylation levels in D1-MSNs might occur through a number of ways: decreased cooperativity,

reduced threshold for activation, or increased background by independent processes, or a mixture of the above.

Additional experiments to address this question could be performed in striatal slice cultures. Steady state phospho-ERK levels in striatal slices exposed to different levels of glutamate or KCl can be quantified for control and D1-mutant slices. These experiments could clarify which subsets of primary targets exert the greatest contribution to elevated steady state ERK signaling.

In conclusion, examination of population variance of miR-128 targets and examination of the population variance and input-dependence profile of ERK signaling are both interesting avenues to examine in detail the key primary effects of miR-128 regulation.

6.4 ERK signaling in neurons and the regulation of excitability

Among the electrophysiological consequences of miR-128 loss in D1-MSNs, we found a substantial increase in dendritic membrane excitability. Intrinsic dendritic or neuronal excitability is increasingly thought to be a vital mechanism of metaplasticity - processes which alter the ability to generate synapse-specific plasticity (LTP or LTD) (*171*, *172*). Kv4.2 regulation of dendritic branch excitability itself could be a form of persistent information-encoding change that allows specific input-patterns to promote persistence of LTP at synapses on the branch (*173*, *174*). A similar process appears to occur in D1-MSNs. Coordinate excitatory inputs induce an "up-state" characterized by depolarized distal dendritic potential, during which LTP induction is enhanced. D1 receptor activation enhances distal excitability and increases the duration of these "up-states".

A change in excitability is sufficient to account for the altered behaviors observed in *Drd1a-cre; miR128-2*$^{fl/fl}$ mutants. 1. Endogenous inputs would produce a higher firing probability that is sufficient to trigger locomotor activity, thus accounting for basal hyperlocomotion. 2. Longer "up-state" durations could enhance NMDA receptor activation that is required of ERK activation. This could account for the apparent ERK hypersensitivity upon D1 agonist stimulus.

Our results studying the effects of miR-128 on learning and memory provide important clues as to the role of miR-128 in ERK regulation. While the general dis-inhibition of ERK signaling potentiates intrinsic excitability and transcriptional responses, pairing of cocaine-induced dopamine signaling with contextual information is impaired. In light of the role of ERK in coincident input

detection I would venture to speculate that miR-128 loss produces a fundamental dysfunction of ERK signaling such that these signals no longer adequately represent and transduce external information. For example, "up-states" in D1-MSNs might be dissociated from cortical inputs that carry information about the context. In this model, ERK supersensitivity and enhanced transcriptional response enhances the induction of plasticity mechanisms. However, ERK activation could be "noisy" and become engaged even in the absence of physiological inputs, resulting in the strengthening of "inappropriate" synaptic associations.

6.5 miR-128 in other contexts

Given that miRNA targets are highly dependent on cellular context, it is unclear if miR-128 has a similar role in regulating ERK in other cell and tissue types. That being said, the known miR-128 expression in some specific cell types suggests that ERK regulation might be a significant component of miR-128 function in these specific contexts as well. I will highlight some of these examples below and speculate on the possible roles play by miR-128.

Thymocyte development is the process of producing of mature T lymphocytes that are able to respond to foreign antigens and are tolerant of self antigens. Within the thymus, immature thymocytes pass through a number of specific stages identifiable by surface markers, which correlate with a number of important processes such as gene rearrangement and positive and negative selection.

Both miR-128 and its host gene TARPP are strongly upregulated beginning at the DN3 stage, reaching a maximum during the DN4 stage (*175*, *176*). At the DN3 stage (CD4-CD8-CD44-CD25+), thymocytes initiate rearrangement of the TCRβ loci. Productive rearrangement leads to its expression in a complex with the alpha-T cell receptor (pre-TCR). This developmental stage coincides with beta-selection and αβ/γδ lineage divergence, both of which depends on pre-TCR signals which are transduced primarily by ERK signaling. It has been shown that the strength of ERK signaling downstream of pre-TCR provides an instructive signal for the commitment to the αβ or γδ lineage (*177*, *178*). A strong ERK signal favors γδ lineage differentiation while the opposite favors αβ lineage commitment.

In light of this model, the expression of miR-128 suppresses the signaling response to favor αβ lineage commitment. In agreement with this, our preliminary data suggests that constitutive deletion of miR-128 results in a small increase in the population of γδ positive T cells in the thymus.

Conversely, miR-128 expression begins to decrease in the DP stage (CD4+CD8+). Among the vital thymic selection processes that occur in this stage is positive selection, in which functional αβ TCR-MHC (major histocompatability complex) interaction results in an instructive signal that permits further maturation. Intracellular signaling during positive selection is transduced by the ERK pathway. Transition of DP thymocytes into a ERK hypersensitive condition is required for the amplification of weak TCR-MHC signals and for positive selection (*179*). Indeed, loss of the transcriptional program required to induce this ERK hypersensitivity results in failure of positive selection. In this model, miR-128 reduction might coincide with and contribute to the induction of ERK hypersensitivity.

Leukemia is a form of cancer characterized by uncontrolled increase in circulating white blood cells. Among acute forms of leukemia, acute lymphoblastic leukemia (ALL) is derived from lymphocytic precursors, which also give rise to thymocytes, while acute myeloid leukemia (AML) is derived from precursors of red blood cells and platelets.

miRNA profiling of ALL and AML samples and cell lines show that miR-128 is among the most differentially expressed among the 2 groups (*180*). High miR-128 DN4 stage is also highly proliferative, so at minimum miR-128 might not be tumor suppressing in the lymphoblast lineage, as is the case in other cancers. It might be interesting to speculate that commitment to the

lymphoblastic lineage confers changes that permit oncogenic property of miR-128 in ALL or reduce the tumor suppressing effects in ALL.

The tumor suppression properties of miR-128 is better characterized in other cancers, and has been studied as a potential therapeutic tool. For example, low miR-128 levels correlate with aggressive gliomas. miR-128 is shown to suppress stem-cell renewal factor Bmi-1 and reduce glioma proliferation (*181*). In another study, miR-128 suppresses oncogenic receptor tyrosine kinases to suppress proliferation and enhance differentiation (*182*). As ERK and MAP kinase signaling are key transduction events downstream of receptor tyrosine kinases, it might be possible that a broader examination of miR-128 targets in gliomas might identify further nodes of regulation.

In summary, our finding that miR-128 exerts a sensitive control of ERK signaling might be informative about the role of miR-128 in other contexts in which ERK signaling is an important transducer of external signals.

6.6 miR-128 in Parkinson's disease and human epilepsy

We have shown that substantial similarities exist between the D1-MSN hyperexcitability in miR-128 mutants and that induced upon dopamine depletion. D1-MSN hyperexcitability develops soon after dopamine depletion and persists even after dopamine replacement for example upon chronic L-DOPA treatment. However, the primary cause of this phenomenon is not well understood. Further experiments could address if miR-128 depletion occurs upon dopamine depletion and if this might be a primary cause of ERK hypersensitivity in this pathological condition. As post-depletion D1-MSN hyperexcitability is thought to share mechanisms that lead to the development of L-DOPA induced dyskinesias, this has clear clinical implications for the treatment of Parkinson's disease.

The fact that reduced miR-128 can lead to pronounced epilepsy in mice suggests that miR-128 and its target genes might contribute to genetic predisposition in human epilepsies. Human idiopathic epilepsies have a substantial genetic component, with an estimated heritability of over 80% from twin studies (*183*). While rare cases of genetic epilepsy have monogenic determinants (*184*), mostly involving mutations in voltage- or ligand-gated ion channels, the vast majority of idiopathic epilepsies are presumed to have complex polygenic causes and significant genetic-environmental interactions.

A common method for the identification of major susceptibility genes is the use of linkage mapping and positional candidate gene analysis but most studies have focused on protein coding genes included within the linkage region.

To see if miR-128 could be a susceptibility gene, I looked for studies that found linkage regions overlapping with one or both of the human miR-128 loci. In one analysis of childhood absence epilepsy involving over 300 individuals from 63 families, the authors found a large linkage region spanning 3p23-3p14, which overlaps with human miR-128-2 (*185*). In a separate study, the authors analyzed members of a multi-generation family presenting with autosomal dominant generalized epilepsy. This study found significant linkage in a much narrower region that also overlaps with human miR-128-2 (*186*). Interestingly, the epileptic condition in this family is accompanied by mental retardation, in agreement with the learning and memory deficits we observed in our miR-128 mutants. These studies suggest that genetic mutations resulting in aberrant miR-128 sequence or miR-128 expression might be a primary determinant in these cases.

Follow-up studies might be complicated by the small size of miRNAs, and by the fact that mutations in the hairpin are likely to be strongly deleterious. Instead, mutations are much more likely to cause expression changes. Besides mutations in the host gene promoter, mutations that alter the tertiary and secondary structure of the hairpin region and mutations that affect Drosha processing could also result in reductions in mature miR-128 levels. This makes the demonstration of a causative allele involving miR-128 particularly challenging, especially in the absence of a strong candidate allele.

Whether miR-128 is a naturally occurring epilepsy determinant or a cause of D1-MSN hyperexcitability, our data suggests that miR-128 expression might have therapeutic value. Such a treatment might require a mechanism to increase specificity to projection neurons to avoid potentially deleterious overexpression

in interneuron populations. Further experiments overexpressing miR-128 in local interneuron populations would help to identify these adverse effects if they do exist.

In conclusion, our findings presented here could have substantial implications for future clinical and therapeutic research.

Material and Methods

Mice

All procedures involving animals were performed in accordance with the National Institutes of Health Guide for the Care and Use of Laboratory Animals and were approved by the Rockefeller University Institutional Animal Care and Use Committee. All mice were generated and maintained in C57BL6/J background.

Generation of mice with neuron-specific tagged-Ago2 expression.

Transgenic mice expressing a Cre-inducible FLAG-HA2-tagged Ago2 under the control of the Rosa26 promoter were generated as previously described (Schaefer et al., 2010; Sasaki et al., 2006; the STOP-eGFP-ROSA26TV vector was a gift from K. Rajewsky, Harvard Medical School, Boston, MA). Rosa-Stop fl/fl-Flag-Ago2 mice were bred to Camk2a-Cre (provided by G. Schuetz, German Cancer Research Center, Heidelberg, Germany;) (*126*) , *Drd1-Cre* (EY262) and *A2a-Cre* (KG139) transgenic mice obtained from Gensat (*187*) to generate Camk2a-Cre; Rosa26-Ago2-Flag , Drd1-Cre; Rosa26-Ago2-Flag, and Drd2-Cre; Rosa26-Ago2-Flag mice.

Generation of mice with a conditional deletion of *miR128-1* and *miR128-2*.

Subcloning of targeting vectors

A region of the *miR-128-1* or *miR-128-2* genomic locus containing the arms of homology was recombinogenically subcloned from a BAC clone (*miR-128-1*: RP24-574G14, *miR-128-2*: RP24-242F13, C57Bl/6J, CHORI, Oakland CA, USA) into pBlueScriptIIKS+ as described (*188*), using amplicons that insert an AscI site and a XhoI site to flank the subcloned region.

PCR primers used for subcloning:

mir-128-1

5' ccttcatgttatgccctcatccctttatcacacaaatctgtgtagttttcggcgcgccattcgccctatagtgagtcg

5' aatcttctaaatttccatttgagcacctagttcatatgtaatttagattcctcgaggcttggcgtaatcatggtc

mir-128-2

5' cgaaaaatattttcatttattcttcgaaactttcatacattcatacaatgtggcgcgccattcgccctatagtgagtcg

5' tcaggcctgccagccttctgtctactgtttaatgactgacagccagtgaactcgaggcttggcgtaatcatggtc

Modification of targeting vector for miR128-1

pZeroloxP-FRT-neoR-FRT(-) plasmid was modified to replaced unique EcoRI site with unique SmaI site. Modified plasmid was digested with NsiI and fragment containing single loxP site and FRT-flanked *neo* gene was inserted into unique NsiI site in targeting vector and screened to proper orientation. For insertion of second loxP site, oligonucleotide fragments containing loxP sequences were annealed and inserted into the unique SpeI site:

Modification of targeting vector for miR128-2

pZeroloxP-FRT-neoR-FRT(-) plasmid was modified to introduce SmaI sites by insertion of oligonucleotide fragments at the SacI/ApaI site and at the Acc65I site. Modified plasmid was digested with SmaI and fragment containing single loxP site and FRT-flanked *neo* gene was inserted into unique SmaI site in targeting vector and screened to proper orientation. For insertion of second loxP site, oligonucleotides containing loxP sequences were annealed and inserted into a unique HindIII site.

Homologous recombination

For both targeting vectors, modified regions of homology were excised from pBluescript with XhoI and AscI digests and inserted into similarly digested pDTA-TK to produce final targeting constructs. Targeting constructs were linearized with NotI and E14 CY2.4 embryonic stem cells (homozygous C57Black/6JTyr-C-2J background with natural mutation in tyrosinase gene) were transfected and screened for successful recombination using southern probe. Positive clones were confirmed using an alternative Southern probe and by PCR sequencing of modified region. Positive clones were used to produce chimeric mice as described. Chimeras were crossed to C57BL6/J mice and germline transmission was assessed by coat color, PCR and southern blot analysis. Germline deletion of the FRT-flanked *neo* gene was accomplished by crossing mice carrying the targeted alleles with FLPe- transgenic mice (*3*). Germline deletion of *miR-128-1* and *miR-128-2* was achieved by crossing mice carrying floxed alleles to transgenic mice that express Cre-recombinase under the ubiquitously expressed *CMV* promoter (*CMV-Cre* mice, Jackson Laboratory).

Postnatal, neuron-specific deletion in the mouse forebrain was achieved by breeding mice carrying floxed alleles to *Camk2a- Cre* mice (*126*). *Drd1-Cre* (EY262) and *A2a-Cre* (KG139) transgenic mice were obtained from Gensat (*187*) and *Drd1*-Cre; *miR128-2fl/fl* mice and *A2a*-Cre; *miR128-2* mice were generated by breeding to *miR128-2fl/fl* mice.

PCR Genotyping

Routine genotyping of *miR-128-1* mice was performed using following primers:

5' tctggaccaaatgaaccaaag

5' ccgcaatgctgcctatattc

5' gcctgaagaacgagatcagc

5' gcagtcatgcaagcagctat

Wild type allele: 194bp

Null allele: 282bp

Floxed allele: 336bp

Routine genotyping of *miR128-2* mice was performed using following primers:

5' cgccttttagtttcccacag

5' gaccacacagcaagcaggta

5' aaagacgggaccattcacat

5' tctctcgtgggatcattgttt

Wild-type allele: 185bp

Null allele: 531bp

Floxed allele: 306bp

Generation of mice with a neuron-specific overexpression of miR-128

Targeting vector for homologous recombination at the ROSA26 locus was generously provided by K. Rajewsky. A 1kb region including miR128-2 hairpin was amplified from genomic DNA with the following primers and cloned into unique xhoI site in the targeting vector:

5′ aaaggcgcgccacgtgactaaaaggcgcgaggagat

5′ aaaggcgcgcctacgcattcctgtacggttg

Modified targeting vector was linearized by NotI and used to generate chimeras as above. Successful germ line transmission was assessed by coat color and confirmed by PCR and southern analysis. Postnatal, neuron-specific miR-128-2 overexpression in the mouse forebrain was achieved by breeding mice to *Camk2a- Cre* mice (*126*).

CLIP-seq analysis

In vivo Cross-Linking and ImmunoPrecipitation (CLIP) procedure.

Mice were sacrificed at 8 to 14 weeks; forebrains were excised and triturated to disrupt tissue. Immunoprecipitation on the UV-crosslinked triturated tissues was performed as described (*61*) with the following modifications to the protocol: After UV cross-linking the frozen lysates are sonicated to improve tissue homogenization. RNase digestion with RNase A is done twice during out protocol once before IP (using one fourth the concentration of RNAse A used by Chi et al) and once after IP (using one twentieth the concentration of RNAse A used by Chi et al). 30µl magnetic beads pre-coupled to the M2 FLAG antibody (M8823, Sigma) have been used for each IP on half a forebrain in 1.2 ml after pre-

blocking the beads with 2% BSA, 1% t-RNAs and 1% salmon sperm for 1.5 hrs at 4° C. Unlike Chi et al. we did not transfer RNA-protein conjugates to a membrane during RNA purification and we did not use hot labeled adapters in the preparation, instead RNA was directly decrosslinked from protein after extensive washing.

Illumina Sample Preparation and Sequencing.

The small RNA sample preparation kit, version 1.5 (Illumina) was used for library preparation with subtle modifications. Since low concentrations of RNA was purified from the CLIP procedure, as measured by Quant-iT RiboGreen RNA Assay (Invitrogen), the following modifications were made to the small RNA sample preparation kit (Illumina) to allow for extremely low RNA input: Both the v1.5 sRNA 3′ Adapter and the SRA 5′ Adapter were diluted 10 times in nuclease-free water compared to standard protocol before adapter ligation. The RT reaction was doubled (resulting in a final RT volume of 20 μl instead of the standard 10 μl), all of which was used for the downstream PCR reaction. To allow for the larger volume of RT product 10 μl less water was used in the PCR step, resulting in a final PCR volume of 50 μl. Instead of the 12 cycles of PCR directed in the standard protocol 15 cycles were performed to increase output.

Preparation of RNA for sequencing was performed in two sets: First, four Ago2-Flag and two control CLIP samples were prepared using RNA from one CLIP procedure each; from half a mouse forebrain each. At the end of the Illumina small RNA protocol a size range of 90 bp to 150 bp of final PCR product was purified; this size range contains both Ago2 associated miRNA and mRNA target sites. The second set of samples consisted of four Ago2-Flag and two control

samples, which each was prepared from a pool of RNA from four CLIP procedures; amounting to CLIP RNA from two mouse forebrains per sample. At the end of the Illumina small RNA protocol for this set of samples the products were purified in a band from 110 to 150 bp containing Ago2 associated mRNA target sites. All mRNA target site containing samples were Solexa sequenced Prepared samples were amplified onto flowcells using the Illumina cluster station per manufacturer protocol and sequenced on the Illumina GAIIx platform 76 cycles. Raw sequencing data was processed using the onboard SCS/RTA software yielding 76 bp reads.

Data pre-processing and miRNA detection

Sequence reads were filtered to remove low quality reads, using a minimum average cutoff quality score of 25 over 75% of the read. Sequence reads were trimmed of any identifiable adapter sequence using several variations on the adapter sequence supplied by Illumina. Reads not containing adapters were aligned to the mm9 genome build using bowtie, allowing for 3 mismatches for 76 bp reads. The last 8 bases were not used during the alignment to allow for incomplete adapter trimming. For those reads that did not align initially were 3′ trimmed and re-aligned at 36 bp allowing 2 mismatches to account for lower quality sequence at the 3′ end of the read. Adapter-trimmed reads from long libraries were aligned allowing for 2 mismatches.

Detection of mRNA target sites clusters:

For the downstream analysis of mRNA targets, clusters of Ago2-Flag reads were detected using a filtering approach described here. To reduce contributions of nonspecifically binding RNA species from cluster detection any Ago2-Flag read within 30 bp of overlapping reads from the grouped control samples were discarded. Then only reads occurring in at least two filtered Ago2-Flag samples were kept and 30 nucleotides of genomic sequence was added to each end of the filtered reads. These reads were filtered to only retain clusters composed of minimum of 10 overlapping reads. Genomic distribution of clusters was examined by use of Cis-regulatory Element Annotation System (CEAS). Filtered clusters that strand-specifically intersect RefSeq 3'UTR plus 1 kb additional downstream genomic sequence (3'UTR) were used for 6mer analysis and genome-wide target site analysis .

6mer enrichment analysis

The abundance of all possible 6mer sequences was found using the perl script countkmer.pl (by Marco Blanchette) in moderately filtered clusters that strand specifically intersect 3'UTR regions. The same was done for all refSeq 3'UTR genomic sequences for use as background (normalized to contain the same total number of 6mers as detected in clusters). The z-score and chi-square p-value were calculated for all 6mer sequences enriched in clusters over refSeq 3'UTR genomic sequences. The z-score was calculated for each 6mer by subtracting the abundance in refSeq (background) from the abundance in clusters and subsequently dividing by the standard deviation of the background subtracted abundance of all 6mers. The value of the z-score conveys how far away from the

mean a given 6mer is in units of standard deviation of the entire collection of 6mers.

Genome-wide target site analysis:

Bowtie was used to map all sequences complementary to miR-128 6mer seed to mouse genome mm9, allowing no mismatches. Intersection was done with the moderately filtered clusters in 3'UTR, generating genome browser tracks with predicted miRNA targeted sites. All genome browser tracks were converted into tables listing all genes detected with their predicted miRNA targeted sites

RNA Preparation

Mice were anaesthesized under CO2 and the cortex, hippocampus and striatum were rapidly dissected and frozen in liquid nitrogen until further processing. RNA extraction from frozen samples was performed using the TriZol/Chloroform technique according to manufacturer's instructions (Invitrogen Corporation, Carlsbad, CA). After extraction, RNA was precipitated overnight at -80C in isopropanol with 0.15M sodium acetate, washed once with 70% ethanol, air-dried and resuspended in RNase-free water. To address differences in miR-128 expression in D1-MSNs versus D2-MSNs, immunoprepitation of tagged Ago2 protein from the striatum of Drd1-Cre; Rosa26-Ago2-Flag (n=4) and Drd2-Cre; Rosa26-Ago2-Flag (n=4) mice was followed by isolation of associated RNA as described above.

Purification of mRNA for D1-TRAP-profiling

Drd1a-cre; miR128-2$^{fl/fl}$ mutants are crossed to mice carrying D1-MSN specific expression of eGFP tagged ribosome protein L10 (*135*). Procedure for striatal dissection and tissue processing for microarray analysis are as previously detailed (*135*).

Gene Expression Analysis by microarray.

Trizol-Chloroform extracted total RNA was further purified using an RNeasy Micro Kit (Qiagen, Valencia, CA) with in-column DNase digestion, and analysed using Nanodrop 1000 spectrophotometer (Thermo Scientific, Wilmington, DE) and a Bioanalyzer (Agilent Technologies, Santa Clara, CA) to assess RNA quantity and quality. Purified RNA was amplified and processed according to the Affymetrix cDNA synthesis kit. Affymetrix Mouse Genome 430 2.0 arrays were used in all experiments. Mouse Genome 430 2.0 arrays were scanned using the GeneChip Scanner 3000 (Affymetrix, Santa Clara, CA) and globally scaled to 150 using the Affymetrix GeneChip operating software (GCOS v1.4). GeneChip files (.cel) were imported into Genespring GX 11 (Agilent Technologies, Santa Clara, CA) processed with GC-RMA algorithm and expression values on each chip were normalized to median of all samples. Samples were compared to similarly processed littermate control samples (n=4 each). All probes with differential expression p-value<0.05, 2-way ANOVA (genotype) for TRAP-profiling were considered significantly changed in the absence of miR-128.

Absolute Quantification of mature miR-128 in the brain

Quantitative RT-PCR was used to estimate copy number of miR-128 in brain samples (Taqman, Life Technologies). Standard curve was generated using synthetic single stranded RNA oligonucleotides of the mature miR-128 sequence with 5'-phosphate and 3'-hydroxyl modification as synthetic miRNAs (IDT). RT-PCR and quantitative real-time PCR were performed on duplicate serial dilutions of the mimics according to manufacturer's protocol and cycle count was plotted against concentration of microRNA mimic. Mimic concentration was converted to copies per cell using the assumption of ~15pg of total extracted RNA per cell. All brain sample quantification used 15ng of total RNA input (~1000 cells) and mean cycle count values from miR-128 quantification of wild type striatum or cortex samples (n=16 and n=13 respectively) were used to estimate copy number per cell in each sample type.

Taqman Quantitative RT-PCR for miRNA and mRNA analysis

Relative expression levels of mature miRNAs and mRNAs were measured by Taqman assays using total extracted RNA from brain samples, according to manufacturer's protocol (Life Technologies, Carlsbad, CA). The purified RNA samples were assayed by qRT-PCR for relative gene expression using pre-designed Taqman gene expression assays from Applied Biosystems (ABI) as recommended by the manufacture. The following pre-designed Taqman gene expression assays from Applied Biosystems (ABI) were used: miR128 (Assay ID 002216), sno135 (Assay ID 001230), miR124a (Assay ID 001182). Cycle counts for miRNA quantification were normalized to snoRNA135 unless otherwise

indicated, cycle counts for mRNA quantification were normalized to GAPDH. Relative expression (ΔCt) and quantification ($RQ=2^{-\Delta\Delta C}$) for each mRNA were calculated using RQ Manager Software and the ΔΔCt method.

Luciferase Reporter Assay

Luciferase reporter assays were performed to measure repression of candidate target 3'UTR by miR-128 mimics. MicroRNA 3'UTR target reporter plasmids (Genecopoiea, MD) contained full length 3'UTR inserts cloned downstream of a Firefly Luciferase gene. Control plasmids containing no inserts were used for comparison. Reporter plasmids contained Renila Luciferase gene as reporter for transfection efficiency. All plasmids were verified by sequencing and restriction digests. Reporter or control plasmids were co-transfected into confluent Neuro2A cells grown in 24-well culture plates with either no mimics, control scrambled miR124 mimics or miR128 mimics at indicated concentrations (Dharmacon, Thermo Fisher Scientific, USA). Cells were harvested and lysed 24 hour after transfection and cell lysate was assayed for Firefly luciferase and Renilla Luciferase activity using Dual-Luciferase Reporter assay kit (Promega, Wisconsin, USA) according to manufacturer's instructions. Firefly Luciferase activity was normalized to Renilla Luciferase activity for each culture well and plotted as activity relative to control transfections with no mimics added. At least 3 biological replicates were performed consisting of 3 technical replicates each.

Protein Quantification

Mice were anaesthesized under CO2 and the cortex, hippocampus and striatum were rapidly dissected and frozen in liquid nitrogen until further processing. Samples were sonicated on ice in 1% SDS solution supplemented with protease inhibitor (Roche, Switzerland) and phosphatase inhibitor, and boiled for 10 minutes. Protein concentration was determined using BCA protein assay kit (ThermoFisherScientific, USA) according to the manufacturer's instructions. Protein samples were diluted in equal volume of 2X loading buffer (Invitrogen) and supplemented with DTT to a final concentration of 200mM (Sigma). 25ug of protein samples were separated on 4-12% Bis-tris precast denaturing gels (Invitrogen) and blotted onto PVDF membranes and blocked with 5% milk in TBS- 0.1% Tween (TBST) solution for 1 hour at room temperature. Membranes were probed with primary antibodies diluted in 5% milk-TBST solution overnight at 4C. Membranes were washed and probed with horseradish-peroxidase conjugated anti-mouse or anti-rabbit IgG secondary antibody for 1 hour at room temperature. Membranes were developed using enhanced chemiluminescence substrate (PerkinElmer, USA) and exposed on BioMax film (Kodak, USA). Exposed films were scanned and protein bands quantified using ImageJ Software (NIH, USA). Protein quantities were normalized using beta-Actin, phosphoprotein levels normalized to total non-phosphorylated protein levels and all values plotted as relative to its control littermate sample. Primary antibodies used: total ERK1/2 (137F5), phosphoERK1/2 (Thr202/Tyr204), DARPP32 (19A3), phosphoDARPP32 (Thr34) (Cell Signaling, MA). RCS (mouse monoclonal 6A, gift. A. Nairn), beta-Actin (Abcam), PEA15a (H80) (Santa Cruz), D4ertd22e (Atlas),

FACS analysis

Nuclei from mouse striatum were purified as previously described for cerebellar mouse nuclei (*189*) including minor changes. Briefly, brains from decapitated mice were frozen for 5 seconds in liquid nitrogen and the striata dissected on ice and homogenized with a glass dounce homogenizer using first a loose then tight pestle (Kimble Chase; 1984-10002). The cell homogenate was fixed with a final concentration of 1% paraformaldehyde for 12 minutes at room temperature and the reaction quenched with 0.125 M Glycine for 5 minutes at room temperature. To isolate the striatal nuclei, the fixed homogenate was spun through a 29% iodixanol cushion and the nuclei pellet resuspended in blocking buffer (0.25 M sucrose, 25 mM KCl, 5 mM MgCl2, 20 mM Tricine pH 7.8, 1% Donkey Serum and 0.01% Tween-20) supplemented with 0.15 mM spermine, 0.5 mM spermidine, EDTA-free protease inhibitor cocktail (Roche; 11836170001) and phosphatase inhibitor cocktail II (Calbiochem; 524625). For FACS analysis, nuclei were blocked overnight at 4ºC and stained for 1 hour at 4ºC using antibodies against Histone H3 phosphorylation of Serine 10 (H3S10) conjugated to an Alexa555 fluorophore (Cell Signaling Technology; 3475S). FACS analysis was carried out on a BD LSR instrument. Single nuclei were selected by gating on FSC and SSC singlets. For the analysis of activated D1 nuclei, gating by two dimensional criteria was used. First, the presence of a GFP signal above the background was used to determine D1 nuclei from other striatal nuclei. Second, activated D1 nuclei were determined by a higher Alexa555 signal than Saline-injected D1 nuclei. Percentages of various nuclei populations were analyzed using Prism software.

Brain slice preparation

Para-sagittal brain slices (275 μm) were obtained from 3-5 month old male and female wild type and mutant mice following procedures approved by the Northwestern University Animal Care and Use Committee. The mice were anesthetized with a mixture of ketamine (50 mg kg^{-1}) and xylazine (4.5 mg kg^{-1}) and perfused transcardially with 5–10 ml ice-cold artificial cerebrospinal fluid (ACSF) containing (in mM): 124 NaCl, 3 KCl, 1 $CaCl_2$, 1.5 $MgCl_2$, 26 $NaHCO_3$, 1 NaH_2PO_4, and 16.66 glucose, continuously bubbled with carbogen (95% O_2 and 5% CO_2). The slices were then transferred to a holding chamber where they were incubated in ACSF containing (in mM) 2 $CaCl_2$, 1 $MgCl_2$, at 35ºC for 60 min, after which they were stored at room temperature until recording.

Electrophysiology

Patch pipettes were pulled from thick-walled borosilicate glass on a Sutter P-97 puller. Pipette resistance was typically 3–5 MΩ when filled with recording solution. For studies involving bAP propagation the internal recording solution contained (in mM): 135 $KMeSO_4$, 5 KCl, 10 HEPES, 2 ATP-Mg^{2+}, 0.5 GTP-Na^+, 5 phosphocreatine-tris; 5 phosphocreatine-Na^+, 0.1 spermine; pH was adjusted to 7.25 with NaOH and osmolarity to 270–280 mOsm l^{-1}. For Ca^{2+} imaging experiments, the recording solution also contained 200 μM Fluo-4 pentapotassium salt and 50 μM Alexa Fluor 568 hydrazide Na^+ salt (Invitrogen). For voltage clamp studies the recording solution contained (in mM): 120 $CsMeSO_3$, 5 NaCl, 10 TEA-Cl (tetraethylammonium-Cl), 10 HEPES, 5 Qx-314, 4 ATP-Mg2, 0.3 GTP-Na, 0.2 Fluo 4 pentapotassium salt and 0.05 Alexa Fluor 568

hydrazide Na^+ salt (Invitrogen), pH 7.25, 270-280 $mOsm^{-1}$. Slices were transferred to a submersion-style recording chamber mounted on an Olympus BX51 upright, fixed-stage microscope and continuously perfused with carbogen-bubbled ACSF. Electrophysiological recordings were obtained with a Multiclamp 700B amplifier. Stimulation and display were obtained as previously described (*128*) using the custom-written shareware package WinFluor (John Dempster, Strathclyde University, Glasgow, Scotland, UK), which automates and synchronizes the two-photon imaging and electrophysiological protocols. The amplifier bridge circuit was adjusted to compensate for serial resistance and continuously monitored during recordings. Analysis of mEPSCs was performed in the presence of 1 μM TTX using MiniAnalysis software (Synaptosoft).

2-photon laser scanning microscopy (2PLSM) and Ca^{2+} imaging

2PLSM and Ca^{2+} imaging were performed as previously described (*128*). Striatonigral SPNs were identified by somatic eGFP two-photon excited fluorescence using an Ultima Laser Scanning Microscope system (Prairie Technologies). A DODT contrast detector system was used to provide a bright-field transmission image in registration with the fluorescent images. The green GFP signals (490–560 nm) were acquired using 810 nm excitation (Verdi/Mira laser). SPNs were patched using video microscopy with a Hitachi CCD camera and an Olympus 60X/0.9 NA lens. Alexa 568 fluorescence was used for visualization of cell bodies, dendrites, and spines. Following patch rupture, the internal solution was allowed to equilibrate for 15–20 minutes before imaging. Whole cell maximum projection images of the soma and dendrites were acquired with 0.36 μm^2 pixels with 10 μs pixel dwell time; ~80 images taken with 1 μm

focal steps. High magnification maximum projection images of dendrites were acquired with 0.072 μm^2 pixels with 10 μm pixel dwell time; ~20 images taken with 0.5 μm focal steps.

Spine density was calculated from maximum projection images of dendritic segments ~100-120 μm from the soma, as previously described (Chan et al., 2012). Spines were manually counted and normalized to the length of the corresponding dendrite.

Single bAPs were generated by injecting somatic current pulses (2 nA, 2 ms). Dendritic changes in Ca^{2+} were measured as $\Delta F/Fo$ via line scans, where Fo is the average green fluorescence before the bAP. Peak $\Delta F/Fo$ values were obtained from the average of 6 consecutive trials and calculated by a single exponential fit of the Ca^{2+} transient decay. Green fluorescent line scan signals were acquired at 6 ms per line and 512 pixels per line with 0.08 μm pixels and 10 μs pixel dwell time. The laser-scanned images were acquired with 810 nm light pulsed at 90 MHz (~250 fs pulse duration). Power attenuation was achieved with two Pockels cells electro-optic modulators (models 350–80 and 350–50, Con Optics, Danbury, CT). The two cells were aligned in series to provide an enhanced modulation range for fine control of the excitation dose (0.1% steps over four decades). The line scan was started 200 ms before the stimulation protocol and continued 4 s after the stimulation to obtain the background fluorescence and to record the decay of the optical signal after stimulation. To reduce photo-damage and photo-bleaching, the laser was fully attenuated using the second Pockels cell at all times during the scan except for the period directly flanking the bAP burst.

Dendritic line scans were acquired from proximal (~50 μm from soma) and distal (~100-120 μm from soma) dendritic regions for each cell. bAP attenuation was calculated by normalizing distal Ca^{2+} transient peaks to the maximum proximal Ca^{2+} transient per cell.

Drugs

Mice were injected intraperitoneally with volume of 10X body weight.

D1-receptor agonist SKF81297 (Taconic) is diluted from stock (10mg/ml in DMSO) with 0.9% saline to indicated concentration. MEK inhibitor SL327 (Taconic) is diluted from stock (diluted in DMSO) with 30% DMSO/Saline to indicated concentration.

Behavior Analyses

All behavior tests have been performed on 4- to 16-week-old mutants and their respective age and sex-matched littermate controls. All behavior tests were conducted between 7 AM and 7 PM.

Open-Field Analysis

Locomotion and exploratory behavior was measured using the open field analysis in novel environment (clear plexiglass chamber 40 X 40 X 30 cm). Activity was quantified by computer-operated Photobeam activity system (Accuscan Instruments, Columbia, OH). Mice were recorded for total distance moved in the whole arena, distance moved in center vs periphery of arena (thigmotaxis) and number of vertical episodes (rearing). Data was collected in 5 or 10 min intervals over 60-100 min test sessions.

Home Cage Seizure Monitoring

Animals were housed in clear plexiglass chambers with pre-installed cameras (Phenotyper, Noldus Information Technology), and provided with food and water ad libitum. Continuous 24-hour video recordings of mice were taken. Video recordings were manually scored for severity, duration and frequency of seizures. To constitute a recorded tonic-clonic seizures, mice must cease all normal activity such as walking, sniffing or grooming, adopt a rigid posture with arched back and progress to repeated rearing and falling. A large majority of tonic clonic seizure episodes progressed to a further stage with rapid running and bouncing behavior, although this was not required for inclusion as tonic-clonic seizure.

Chemically-induced seizures.

Mice were injected i.p. with kainic acid (30 mg/kg in saline) or picrotoxin (3 mg/kg in saline) and placed in chambers in isolation and observed for 60 min. All injected animals rapidly enter period of immobility (Stage 1). Animals were observed for the time of onset of tonic clonic seizures characterized by repeated rearing and falling followed by running and bouncing or constant limb movements if postural control is lost.

Survival Analysis

Date of sacrifice or death in the home cage is recorded for mutants and cage mate controls, and plotted as Kaplan-Meier survival curves and compared using log-rank tests.

6-OHDA lesion

Mice were anaesthesized with ketamine/xylazine. Stereotactic injection of 6-OHDA (3.5mg/ml in 0.02% ascorbic acid) 2X2ul in left striatum (ML=-2.1 AP=+1.0 DV=-3.4; ML=-2.3 AP=+0.3 DV=-3.4). and vehicle injection 2X2ul in right striatum (ML=+2.1 AP=+1.0 DV=-3.4; ML=+2.3 AP=+0.3 DV=-3.4). Mice were single housed for 3 weeks after surgery to allow for recovery before behavioral assays.

Rotational behavior

Rotational behavior in lesioned mice was assayed by an experimenter blind to the genotypes for 2X2min interval 5 min after injection of cocaine (10 mg/kg). Net contralateral rotations are average of 4 readings taken over 2 days. After 3 days, the same behavior was recorded in response to D1-agonist SKF81297 (5 mg/kg).

Cocaine-conditioned place preference

Mice were exposed to the 3-chamber experimental set-up (Med Associates) for 15 minutes, a day before the first test to allow mice to acclimatize to testing conditions. During testing phases, mice were placed in the center chamer and allowed free access to all chambers. Chamber entries and duration spent in each chamber was measured by the automated system. During daily conditioning, two pairings were performed. In the first pairing, mice were injected with either saline or cocaine (15mg/kg) and allowed to explore a pre-selected pairing chamber (left or right) for 15 minutes. 4 hours later, the second pairing is performed in which mice were injected with the other solution and placed in the

other chamber for 15 minutes. The duration of the time spent in each chamber during the test phases were recorded.

Novel object recognition task

Test was performed in a clear plexiglass chamber. Mice were allowed exposed to the empty chamber one day before tests to allow mice to acclimatize. During the training phase, the mice were first allowed to explore the empty chamber for 5 minutes.Then the mice are removed and 2 identical training objects were placed in opposite sides of the chamber before the mice were re-introduced into the chamber. Time spent in exploration of each object was manually assessed by an experimenter blinded to the genotypes of the mice. Exploration behavior was characterized by sniffing directed at the object or forelimb contact with the object. Mice were removed into a new cage for 1 hour until the first test phase. One training object and one novel object was placed in the same positions and mice was re-introduced and exploratory behavior was assessed as before. Object placements were randomized for each mouse to preclude position-dependent effects. Second test phase was performed 24 hour after the training phase using a new "novel" object and one training object.

Statistical analysis

Analyses were performed using either Microsoft Excel or Graphpad Prism software.

Bibliography

1. N. C. Lau *et al.*, Characterization of the piRNA complex from rat testes, *Science* **313**, 363–367 (2006).

2. O. H. Tam *et al.*, Pseudogene-derived small interfering RNAs regulate gene expression in mouse oocytes, *Nature* **453**, 534–538 (2008).

3. B. J. Reinhart *et al.*, The 21-nucleotide let-7 RNA regulates developmental timing in Caenorhabditis elegans, *Nature* **403**, 901–906 (2000).

4. R. C. Lee, R. L. Feinbaum, V. Ambros, The C. elegans heterochronic gene lin-4 encodes small RNAs with antisense complementarity to lin-14, *Cell* **75**, 843–854 (1993).

5. B. Wightman, I. Ha, G. Ruvkun, Posttranscriptional regulation of the heterochronic gene lin-14 by lin-4 mediates temporal pattern formation in C. elegans, *Cell* **75**, 855–862 (1993).

6. A. E. Pasquinelli *et al.*, Conservation of the sequence and temporal expression of let-7 heterochronic regulatory RNA, *Nature* **408**, 86–89 (2000).

7. R. C. Lee, V. Ambros, An extensive class of small RNAs in Caenorhabditis elegans, *Science* **294**, 862–864 (2001).

8. M. Lagos-Quintana, R. Rauhut, W. Lendeckel, T. Tuschl, Identification of novel genes coding for small expressed RNAs, *Science* **294**, 853–858 (2001).

9. N. C. Lau, L. P. Lim, E. G. Weinstein, D. P. Bartel, An abundant class of tiny RNAs with probable regulatory roles in Caenorhabditis elegans, *Science* **294**, 858–862 (2001).

10. B. J. Reinhart, E. G. Weinstein, M. W. Rhoades, B. Bartel, D. P. Bartel, MicroRNAs in plants, *Genes Dev.* **16**, 1616–1626 (2002).

11. S.-C. Li, C.-Y. Pan, W.-C. Lin, Bioinformatic discovery of microRNA precursors from human ESTs and introns, *BMC Genomics* **7**, 164 (2006).

12. S. Griffiths-Jones, The microRNA Registry, *Nucleic Acids Res.* **32**, D109–11 (2004).

13. J. Hertel *et al.*, The expansion of the metazoan microRNA repertoire, *BMC Genomics* **7**, 25 (2006).

14. A. Fire *et al.*, Potent and specific genetic interference by double-stranded RNA in Caenorhabditis elegans, *Nature* **391**, 806–811 (1998).

15. R. F. Ketting *et al.*, Dicer functions in RNA interference and in synthesis of small RNA involved in developmental timing in C. elegans, *Genes Dev.* **15**, 2654–2659 (2001).

16. A. Grishok *et al.*, Genes and mechanisms related to RNA interference regulate expression of the small temporal RNAs that control C. elegans developmental timing, *Cell* **106**, 23–34 (2001).

17. G. Hutvágner *et al.*, A cellular function for the RNA-interference enzyme Dicer in the maturation of the let-7 small temporal RNA, *Science* **293**, 834–838 (2001).

18. G. Hutvágner, P. D. Zamore, A microRNA in a multiple-turnover RNAi enzyme complex, *Science* **297**, 2056–2060 (2002).

19. F. Ozsolak *et al.*, Chromatin structure analyses identify miRNA promoters, *Genes Dev.* **22**, 3172–3183 (2008).

20. S. Baskerville, D. P. Bartel, Microarray profiling of microRNAs reveals frequent coexpression with neighboring miRNAs and host genes, *RNA* **11**, 241–247 (2005).

21. Y. Lee *et al.*, MicroRNA genes are transcribed by RNA polymerase II, *EMBO J.* **23**, 4051–4060 (2004).

22. X. Cai, C. H. Hagedorn, B. R. Cullen, Human microRNAs are processed from capped, polyadenylated transcripts that can also function as mRNAs, *RNA* **10**, 1957–1966 (2004).

23. A. M. Monteys *et al.*, Structure and activity of putative intronic miRNA promoters, *RNA* **16**, 495–505 (2010).

24. G. M. Borchert, W. Lanier, B. L. Davidson, RNA polymerase III transcribes human microRNAs, *Nat. Struct. Mol. Biol.* **13**, 1097–1101 (2006).

25. M. Ballarino *et al.*, Coupled RNA processing and transcription of intergenic primary microRNAs, *Mol. Cell. Biol.* **29**, 5632–5638 (2009).

26. R. I. Gregory *et al.*, The Microprocessor complex mediates the genesis of microRNAs, *Nature* **432**, 235–240 (2004).

27. A. M. Denli, B. B. J. Tops, R. H. A. Plasterk, R. F. Ketting, G. J. Hannon, Processing of primary microRNAs by the Microprocessor complex, *Nature* **432**, 231–235 (2004).

28. Y.-K. Kim, V. N. Kim, Processing of intronic microRNAs, *EMBO J.* **26**, 775–783 (2007).

29. I. J. MacRae, E. Ma, M. Zhou, C. V. Robinson, J. A. Doudna, In vitro reconstitution of the human RISC-loading complex, *Proc. Natl. Acad. Sci. U.S.A.* **105**, 512–517 (2008).

30. A. Khvorova, A. Reynolds, S. D. Jayasena, Functional siRNAs and miRNAs exhibit strand bias, *Cell* **115**, 209–216 (2003).

31. D. S. Schwarz *et al.*, Asymmetry in the assembly of the RNAi enzyme complex, *Cell* **115**, 199–208 (2003).

32. D. O'Carroll *et al.*, A Slicer-independent role for Argonaute 2 in hematopoiesis and the microRNA pathway, *Genes Dev.* **21**, 1999–2004 (2007).

33. S. Gu, L. Jin, Y. Huang, F. Zhang, M. A. Kay, Slicing-independent RISC activation requires the argonaute PAZ domain, *Curr. Biol.* **22**, 1536–1542 (2012).

34. P. B. Kwak, Y. Tomari, The N domain of Argonaute drives duplex unwinding during RISC assembly, *Nat. Struct. Mol. Biol.* **19**, 145–151 (2012).

35. E. Berezikov, W.-J. Chung, J. Willis, E. Cuppen, E. C. Lai, Mammalian mirtron genes, *Mol. Cell* **28**, 328–336 (2007).

36. C. R. Sibley *et al.*, The biogenesis and characterization of mammalian microRNAs of mirtron origin, *Nucleic Acids Res.* **40**, 438–448 (2012).

37. J.-S. Yang *et al.*, Conserved vertebrate mir-451 provides a platform for Dicer-independent, Ago2-mediated microRNA biogenesis, *Proc. Natl. Acad. Sci. U.S.A.* **107**, 15163–15168 (2010).

38. D. Cifuentes *et al.*, A novel miRNA processing pathway independent of Dicer requires Argonaute2 catalytic activity, *Science* **328**, 1694–1698 (2010).

39. S. Cheloufi, C. O. Dos Santos, M. M. W. Chong, G. J. Hannon, A dicer-independent miRNA biogenesis pathway that requires Ago catalysis, *Nature* **465**, 584–589 (2010).

40. A. Schaefer *et al.*, Cerebellar neurodegeneration in the absence of microRNAs, *J. Exp. Med.* **204**, 1553–1558 (2007).

41. M. P. Gantier *et al.*, Analysis of microRNA turnover in mammalian cells following Dicer1 ablation, *Nucleic Acids Res.* **39**, 5692–5703 (2011).

42. J. Krol *et al.*, Characterizing light-regulated retinal microRNAs reveals rapid turnover as a common property of neuronal microRNAs, *Cell* **141**, 618–631 (2010).

43. J. Brennecke, A. Stark, R. B. Russell, S. M. Cohen, Principles of microRNA-target recognition, *PLoS Biol.* **3**, e85 (2005).

44. J. G. Doench, P. A. Sharp, Specificity of microRNA target selection in translational repression, *Genes Dev.* **18**, 504–511 (2004).

45. W. P. Kloosterman, E. Wienholds, R. F. Ketting, R. H. A. Plasterk, Substrate requirements for let-7 function in the developing zebrafish embryo, *Nucleic Acids Res.* **32**, 6284–6291 (2004).

46. N. T. Schirle, I. J. MacRae, The crystal structure of human Argonaute2, *Science* **336**, 1037–1040 (2012).

47. E. Elkayam *et al.*, The structure of human argonaute-2 in complex with miR-20a, *Cell* **150**, 100–110 (2012).

48. Y. Wang *et al.*, Structure of an argonaute silencing complex with a seed-containing guide DNA and target RNA duplex, *Nature* **456**, 921–926 (2008).

49. Y. Wang *et al.*, Nucleation, propagation and cleavage of target RNAs in Ago silencing complexes, *Nature* **461**, 754–761 (2009).

50. S. Gu, L. Jin, F. Zhang, P. Sarnow, M. A. Kay, Biological basis for restriction of microRNA targets to the 3' untranslated region in mammalian mRNAs, *Nat. Struct. Mol. Biol.* **16**, 144–150 (2009).

51. H.-R. Lin, D. Ganem, Viral microRNA target allows insight into the role of translation in governing microRNA target accessibility, *Proc. Natl. Acad. Sci. U.S.A.* **108**, 5148–5153 (2011).

52. W. H. Majoros, U. Ohler, Spatial preferences of microRNA targets in 3' untranslated regions, *BMC Genomics* **8**, 152 (2007).

53. A. Grimson *et al.*, MicroRNA targeting specificity in mammals: determinants beyond seed pairing, *Mol. Cell* **27**, 91–105 (2007).

54. G. Sun, H. Li, J. J. Rossi, Sequence context outside the target region influences the effectiveness of miR-223 target sites in the RhoB 3'UTR, *Nucleic Acids Res.* **38**, 239–252 (2010).

55. C. B. Nielsen *et al.*, Determinants of targeting by endogenous and exogenous microRNAs and siRNAs, *RNA* **13**, 1894–1910 (2007).

56. P. Saetrom *et al.*, Distance constraints between microRNA target sites dictate efficacy and cooperativity, *Nucleic Acids Res.* **35**, 2333–2342 (2007).

57. L. S. Hon, Z. Zhang, The roles of binding site arrangement and combinatorial targeting in microRNA repression of gene expression, *Genome Biol.* **8**, R166 (2007).

58. D. Baek *et al.*, The impact of microRNAs on protein output, *Nature* **455**, 64–71 (2008).

59. G. Easow, A. A. Teleman, S. M. Cohen, Isolation of microRNA targets by miRNP immunopurification, *RNA* **13**, 1198–1204 (2007).

60. M. Beitzinger, L. Peters, J. Y. Zhu, E. Kremmer, G. Meister, Identification of human microRNA targets from isolated argonaute protein complexes, *RNA Biol* **4**, 76–84 (2007).

61. S. W. Chi, J. B. Zang, A. Mele, R. B. Darnell, Argonaute HITS-CLIP decodes microRNA-mRNA interaction maps, *Nature* **460**, 479–486 (2009).

62. D. D. Licatalosi *et al.*, HITS-CLIP yields genome-wide insights into brain alternative RNA processing, *Nature* **456**, 464–469 (2008).

63. A. K. L. Leung *et al.*, Genome-wide identification of Ago2 binding sites from mouse embryonic stem cells with and without mature microRNAs, *Nat. Struct. Mol. Biol.* **18**, 237–244 (2011).

64. M. Hafner *et al.*, Transcriptome-wide identification of RNA-binding protein and microRNA target sites by PAR-CLIP, *Cell* **141**, 129–141 (2010).

65. J. Wen, B. J. Parker, A. Jacobsen, A. Krogh, MicroRNA transfection and AGO-bound CLIP-seq data sets reveal distinct determinants of miRNA action, *RNA* **17**, 820–834 (2011).

66. S. Yekta, I.-H. Shih, D. P. Bartel, MicroRNA-directed cleavage of HOXB8 mRNA, *Science* **304**, 594–596 (2004).

67. C. P. C. Petersen, M.-E. M. Bordeleau, J. J. Pelletier, P. A. P. Sharp, Short RNAs Repress Translation after Initiation in Mammalian Cells, *Mol. Cell* **21**, 10–10 (2006).

68. P. H. P. Olsen, V. V. Ambros, The lin-4 Regulatory RNA Controls Developmental Timing in Caenorhabditis elegans by Blocking LIN-14 Protein Synthesis after the Initiation of Translation, *Dev Biol* **216**, 10–10 (1999).

69. S. N. Bhattacharyya, R. Habermacher, U. Martine, E. I. Closs, W. Filipowicz, Relief of microRNA-mediated translational repression in human cells subjected to stress, *Cell* **125**, 1111–1124 (2006).

70. X. C. Ding, H. Grosshans, Repression of C. elegans microRNA targets at the initiation level of translation requires GW182 proteins, *EMBO J.* **28**, 213–222 (2009).

71. R. S. Pillai *et al.*, Inhibition of translational initiation by Let-7 MicroRNA in human cells, *Science* **309**, 1573–1576 (2005).

72. M. Wakiyama, K. Takimoto, O. Ohara, S. Yokoyama, Let-7 microRNA-mediated mRNA deadenylation and translational repression in a mammalian cell-free system, *Genes Dev.* **21**, 1857–1862 (2007).

73. G. Mathonnet *et al.*, MicroRNA inhibition of translation initiation in vitro by targeting the cap-binding complex eIF4F, *Science* **317**, 1764–1767 (2007).

74. A. Zdanowicz *et al.*, Drosophila miR2 primarily targets the m7GpppN cap structure for translational repression, *Mol. Cell* **35**, 881–888 (2009).

75. S. Djuranovic *et al.*, Allosteric regulation of Argonaute proteins by miRNAs, *Nat. Struct. Mol. Biol.* **17**, 144–150 (2010).

76. L. Zekri, E. Huntzinger, S. Heimstädt, E. Izaurralde, The silencing domain of GW182 interacts with PABPC1 to promote translational repression and degradation of microRNA targets and is required for target release, *Mol. Cell. Biol.* **29**, 6220–6231 (2009).

77. I. Behm-Ansmant, J. Rehwinkel, T. Doerks, mRNA degradation by miRNAs and GW182 requires both CCR4: NOT deadenylase and DCP1: DCP2 decapping complexes, *Genes & …* (2006).

78. M. Selbach *et al.*, Widespread changes in protein synthesis induced by microRNAs, *Nature* **455**, 58–63 (2008).

79. H. Guo, N. T. Ingolia, J. S. Weissman, D. P. Bartel, Mammalian microRNAs predominantly act to decrease target mRNA levels, *Nature* **466**, 835–840 (2010).

80. D. G. Hendrickson *et al.*, Concordant regulation of translation and mRNA abundance for hundreds of targets of a human microRNA, *PLoS Biol.* **7**, e1000238 (2009).

81. R. Yi, M. N. Poy, M. Stoffel, E. Fuchs, A skin microRNA promotes differentiation by repressing 'stemness', *Nature* **452**, 225–229 (2008).

82. K. R. Cordes *et al.*, miR-145 and miR-143 regulate smooth muscle cell fate and plasticity, *Nature* **460**, 705–710 (2009).

83. A. S. Yoo *et al.*, MicroRNA-mediated conversion of human fibroblasts to neurons, *Nature* **476**, 228–231 (2011).

84. A. S. Yoo, B. T. Staahl, L. Chen, G. R. Crabtree, MicroRNA-mediated switching of chromatin-remodelling complexes in neural development, *Nature* **460**, 642–646 (2009).

85. N. Xu, T. Papagiannakopoulos, G. Pan, J. A. Thomson, K. S. Kosik, MicroRNA-145 regulates OCT4, SOX2, and KLF4 and represses pluripotency in human embryonic stem cells, *Cell* **137**, 647–658 (2009).

86. K. K.-H. Farh *et al.*, The widespread impact of mammalian MicroRNAs on mRNA repression and evolution, *Science* **310**, 1817–1821 (2005).

87. A. Stark, J. Brennecke, N. Bushati, R. B. Russell, S. M. Cohen, Animal MicroRNAs confer robustness to gene expression and have a significant impact on 3'UTR evolution, *Cell* **123**, 1133–1146 (2005).

88. Y. Li, F. Wang, J.-A. Lee, F.-B. Gao, MicroRNA-9a ensures the precise specification of sensory organ precursors in Drosophila, *Genes Dev.* **20**, 2793–2805 (2006).

89. E. Hornstein, N. Shomron, Canalization of development by microRNAs, *Nat. Genet.* **38 Suppl**, S20–4 (2006).

90. J. R. Chubb, T. B. Liverpool, Bursts and pulses: insights from single cell studies into transcriptional mechanisms, *Curr. Opin. Genet. Dev.* **20**, 478–484 (2010).

91. T. Subkhankulova, M. J. Gilchrist, F. J. Livesey, Modelling and measuring single cell RNA expression levels find considerable transcriptional differences among phenotypically identical cells, *BMC Genomics* **9**, 268 (2008).

92. A. Raj, S. A. Rifkin, E. Andersen, A. van Oudenaarden, Variability in gene expression underlies incomplete penetrance, *Nature* **463**, 913–918 (2010).

93. X. Li, J. J. Cassidy, C. A. Reinke, S. Fischboeck, R. W. Carthew, A microRNA imparts robustness against environmental fluctuation during development, *Cell* **137**, 273–282 (2009).

94. J. S. Karres, V. Hilgers, I. Carrera, J. Treisman, S. M. Cohen, The conserved microRNA miR-8 tunes atrophin levels to prevent neurodegeneration in Drosophila, *Cell* **131**, 136–145 (2007).

95. M. Osella, C. Bosia, D. Corá, M. Caselle, The role of incoherent microRNA-mediated feedforward loops in noise buffering, *PLoS Comput. Biol.* **7**, e1001101 (2011).

96. S. Mukherji *et al.*, MicroRNAs can generate thresholds in target gene expression, *Nat. Genet.* **43**, 854–859 (2011).

97. E. Bernstein *et al.*, Dicer is essential for mouse development, *Nat. Genet.* **35**, 215–217 (2003).

98. D. Damiani *et al.*, Dicer inactivation leads to progressive functional and structural degeneration of the mouse retina, *J. Neurosci.* **28**, 4878–4887 (2008).

99. J. Kim *et al.*, A MicroRNA feedback circuit in midbrain dopamine neurons, *Science* **317**, 1220–1224 (2007).

100. T. H. Davis *et al.*, Conditional loss of Dicer disrupts cellular and tissue morphogenesis in the cortex and hippocampus, *J. Neurosci.* **28**, 4322–4330 (2008).

101. K. L. Stark *et al.*, Altered brain microRNA biogenesis contributes to phenotypic deficits in a 22q11-deletion mouse model, *Nat. Genet.* **40**, 751–760 (2008).

102. A. Schaefer *et al.*, Argonaute 2 in dopamine 2 receptor-expressing neurons regulates cocaine addiction, *J. Exp. Med.* **207**, 1843–1851 (2010).

103. N. F. M. Olde Loohuis *et al.*, MicroRNA networks direct neuronal development and plasticity, *Cell. Mol. Life Sci.* **69**, 89–102 (2012).

104. D. Edbauer *et al.*, Regulation of synaptic structure and function by FMRP-associated microRNAs miR-125b and miR-132, *Neuron* **65**, 373–384 (2010).

105. G. Siegel *et al.*, A functional screen implicates microRNA-138-dependent regulation of the depalmitoylation enzyme APT1 in dendritic spine morphogenesis, *Nat. Cell Biol.* **11**, 705–716 (2009).

106. R. D. Smrt *et al.*, MicroRNA miR-137 regulates neuronal maturation by targeting ubiquitin ligase mind bomb-1, *Stem Cells* **28**, 1060–1070 (2010).

107. G. M. Schratt *et al.*, A brain-specific microRNA regulates dendritic spine development, *Nature* **439**, 283–289 (2006).

108. J. Gao *et al.*, A novel pathway regulates memory and plasticity via SIRT1 and miR-134, *Nature* **466**, 1105–1109 (2010).

109. J. A. Hollander *et al.*, Striatal microRNA controls cocaine intake through CREB signalling, *Nature* **466**, 197–202 (2010).

110. S. T. Magill *et al.*, microRNA-132 regulates dendritic growth and arborization of newborn neurons in the adult hippocampus, *Proc. Natl. Acad. Sci. U.S.A.* **107**, 20382–20387 (2010).

111. R. Johnson *et al.*, A microRNA-based gene dysregulation pathway in Huntington's disease, *Neurobiol. Dis.* **29**, 438–445 (2008).

112. A. N. Packer, Y. Xing, S. Q. Harper, L. Jones, B. L. Davidson, The bifunctional microRNA miR-9/miR-9* regulates REST and CoREST and is downregulated in Huntington's disease, *J. Neurosci.* **28**, 14341–14346 (2008).

113. J. P. Cogswell *et al.*, Identification of miRNA changes in Alzheimer's disease brain and CSF yields putative biomarkers and insights into disease pathways, *J. Alzheimers Dis.* **14**, 27–41 (2008).

114. N. J. Beveridge *et al.*, Dysregulation of miRNA 181b in the temporal cortex in schizophrenia, *Hum. Mol. Genet.* **17**, 1156–1168 (2008).

115. D. O. Perkins *et al.*, microRNA expression in the prefrontal cortex of individuals with schizophrenia and schizoaffective disorder, *Genome Biol.* **8**, R27 (2007).

116. R. Sanuki *et al.*, miR-124a is required for hippocampal axogenesis and retinal cone survival through Lhx2 suppression, *Nat. Neurosci.* **14**, 1125–1134 (2011).

117. H. Xia *et al.*, Loss of brain-enriched miR-124 microRNA enhances stem-like traits and invasiveness of glioma cells, *J. Biol. Chem.* **287**, 9962–9971 (2012).

118. L. F. Sempere *et al.*, Expression profiling of mammalian microRNAs uncovers a subset of brain-expressed microRNAs with possible roles in murine and human neuronal differentiation, *Genome Biol.* **5**, R13 (2004).

119. E. A. Miska *et al.*, Microarray analysis of microRNA expression in the developing mammalian brain, *Genome Biol.* **5**, R68 (2004).

120. P. Landgraf *et al.*, A mammalian microRNA expression atlas based on small RNA library sequencing, *Cell* **129**, 1401–1414 (2007).

121. C. Chen *et al.*, Real-time quantification of microRNAs by stem-loop RT-PCR, *Nucleic Acids Res.* **33**, e179 (2005).

122. E. Wienholds *et al.*, MicroRNA expression in zebrafish embryonic development, *Science* **309**, 310–311 (2005).

123. M. Kapsimali *et al.*, MicroRNAs show a wide diversity of expression profiles in the developing and mature central nervous system, *Genome Biol.* **8**, R173 (2007).

124. M. He *et al.*, Cell-type-based analysis of microRNA profiles in the mouse brain, *Neuron* **73**, 35–48 (2012).

125. R. C. Friedman, K. K.-H. Farh, C. B. Burge, D. P. Bartel, Most mammalian mRNAs are conserved targets of microRNAs, *Genome Res.* **19**, 92–105 (2009).

126. E. Casanova *et al.*, A CamKIIalpha iCre BAC allows brain-specific gene inactivation, *Genesis* **31**, 37–42 (2001).

127. G. E. Alexander, M. R. DeLong, P. L. Strick, Parallel organization of functionally segregated circuits linking basal ganglia and cortex, *Annu. Rev. Neurosci.* **9**, 357–381 (1986).

128. M. Day, D. Wokosin, J. L. Plotkin, X. Tian, D. J. Surmeier, Differential excitability and modulation of striatal medium spiny neuron dendrites, *J. Neurosci.* **28**, 11603–11614 (2008).

129. H. S. Bateup *et al.*, Cell type-specific regulation of DARPP-32 phosphorylation by psychostimulant and antipsychotic drugs, *Nat. Neurosci.* **11**, 932–939 (2008).

130. J. Bertran-Gonzalez *et al.*, Opposing patterns of signaling activation in dopamine D1 and D2 receptor-expressing striatal neurons in response to cocaine and haloperidol, *J. Neurosci.* **28**, 5671–5685 (2008).

131. W. Shen, M. Flajolet, P. Greengard, D. J. Surmeier, Dichotomous dopaminergic control of striatal synaptic plasticity, *Science* **321**, 848–851 (2008).

132. H. S. Bateup *et al.*, Distinct subclasses of medium spiny neurons differentially regulate striatal motor behaviors, *Proc. Natl. Acad. Sci. U.S.A.* **107**, 14845–14850 (2010).

133. A. V. Kravitz, L. D. Tye, A. C. Kreitzer, Distinct roles for direct and indirect pathway striatal neurons in reinforcement, *Nat. Neurosci.* **15**, 816–818 (2012).

134. A. V. Kravitz *et al.*, Regulation of parkinsonian motor behaviours by optogenetic control of basal ganglia circuitry, *Nature* **466**, 622–626 (2010).

135. M. Heiman *et al.*, A translational profiling approach for the molecular characterization of CNS cell types, *Cell* **135**, 738–748 (2008).

136. G. Pearson *et al.*, Mitogen-activated protein (MAP) kinase pathways: regulation and physiological functions, *Endocr. Rev.* **22**, 153–183 (2001).

137. G. Pagès *et al.*, Defective thymocyte maturation in p44 MAP kinase (Erk 1) knockout mice, *Science* **286**, 1374–1377 (1999).

138. M. Aouadi, B. Binetruy, L. Caron, Y. Le Marchand-Brustel, F. Bost, Role of MAPKs in development and differentiation: lessons from knockout mice, *Biochimie* **88**, 1091–1098 (2006).

139. C. Mazzucchelli *et al.*, Knockout of ERK1 MAP kinase enhances synaptic plasticity in the striatum and facilitates striatal-mediated learning and memory, *Neuron* **34**, 807–820 (2002).

140. J. C. Selcher, T. Nekrasova, R. Paylor, G. E. Landreth, J. D. Sweatt, Mice lacking the ERK1 isoform of MAP kinase are unimpaired in emotional learning, *Learn. Mem.* **8**, 11–19 (2001).

141. Y. Satoh *et al.*, Extracellular signal-regulated kinase 2 (ERK2) knockdown mice show deficits in long-term memory; ERK2 has a specific function in learning and memory, *J. Neurosci.* **27**, 10765–10776 (2007).

142. A. S. Nateri *et al.*, ERK activation causes epilepsy by stimulating NMDA receptor activity, *EMBO J.* **26**, 4891–4901 (2007).

143. E. Valjent *et al.*, Regulation of a protein phosphatase cascade allows convergent dopamine and glutamate signals to activate ERK in the striatum, *Proc. Natl. Acad. Sci. U.S.A.* **102**, 491–496 (2005).

144. S. Fasano *et al.*, Ras-guanine nucleotide-releasing factor 1 (Ras-GRF1) controls activation of extracellular signal-regulated kinase (ERK) signaling in the striatum and long-term behavioral responses to cocaine, *Biol. Psychiatry* **66**, 758–768 (2009).

145. M. A. Schwarzschild, R. L. Cole, M. A. Meyers, S. E. Hyman, Contrasting calcium dependencies of SAPK and ERK activations by glutamate in cultured striatal neurons, *J. Neurochem.* **72**, 2248–2255 (1999).

146. E. Valjent *et al.*, Involvement of the extracellular signal-regulated kinase cascade for cocaine-rewarding properties, *J. Neurosci.* **20**, 8701–8709 (2000).

147. E. Valjent, J.-C. Corvol, J. M. Trzaskos, J.-A. Girault, D. Hervé, Role of the ERK pathway in psychostimulant-induced locomotor sensitization, *BMC Neurosci* **7**, 20 (2006).

148. V. Pascoli, M. Turiault, C. Lüscher, Reversal of cocaine-evoked synaptic potentiation resets drug-induced adaptive behaviour, *Nature* **481**, 71–75 (2012).

149. L.-L. Yuan, J. P. Adams, M. Swank, J. D. Sweatt, D. Johnston, Protein kinase modulation of dendritic K+ channels in hippocampus involves a mitogen-activated protein kinase pathway, *J. Neurosci.* **22**, 4860–4868 (2002).

150. J. J. Zhu, Y. Qin, M. Zhao, L. Van Aelst, R. Malinow, Ras and Rap control AMPA receptor trafficking during synaptic plasticity, *Cell* **110**, 443–455 (2002).

151. A. C. Boudreau, J. M. Reimers, M. Milovanovic, M. E. Wolf, Cell surface AMPA receptors in the rat nucleus accumbens increase during cocaine withdrawal but internalize after cocaine challenge in association with altered activation of mitogen-activated protein kinases, *J. Neurosci.* **27**, 10621–10635 (2007).

152. Z. Ren *et al.*, Dopamine D1 and N-methyl-D-aspartate receptors and extracellular signal-regulated kinase mediate neuronal morphological changes induced by repeated cocaine administration, *Neuroscience* **168**, 48–60 (2010).

153. K. Brami-Cherrier *et al.*, Parsing molecular and behavioral effects of cocaine in mitogen- and stress-activated protein kinase-1-deficient mice, *J. Neurosci.* **25**, 11444–11454 (2005).

154. J. M. Shulman, P. L. De Jager, M. B. Feany, Parkinson's disease: genetics and pathogenesis, *Annu Rev Pathol* **6**, 193–222 (2011).

155. G. Mercanti, G. Bazzu, P. Giusti, A 6-hydroxydopamine in vivo model of Parkinson's disease, *Methods Mol. Biol.* **846**, 355–364 (2012).

156. R. M. Kostrzewa, J. P. Kostrzewa, R. W. Brown, P. Nowak, R. Brus, Dopamine receptor supersensitivity: development, mechanisms, presentation, and clinical applicability, *Neurotox Res* **14**, 121–128 (2008).

157. C. R. Gerfen, S. Miyachi, R. Paletzki, P. Brown, D1 dopamine receptor supersensitivity in the dopamine-depleted striatum results from a switch in the regulation of ERK1/2/MAP kinase, *J. Neurosci.* **22**, 5042–5054 (2002).

158. E. Santini *et al.*, Critical involvement of cAMP/DARPP-32 and extracellular signal-regulated protein kinase signaling in L-DOPA-induced dyskinesia, *J. Neurosci.* **27**, 6995–7005 (2007).

159. A. Barbeau, L-dopa therapy in Parkinson"s disease: a critical review of nine years" experience, *Can Med Assoc J* **101**, 59–68 (1969).

160. E. Santini *et al.*, L-DOPA activates ERK signaling and phosphorylates histone H3 in the striatonigral medium spiny neurons of hemiparkinsonian mice, *J. Neurochem.* **108**, 621–633 (2009).

161. S. M. Ferguson, S. Fasano, P. Yang, R. Brambilla, T. E. Robinson, Knockout of ERK1 enhances cocaine-evoked immediate early gene expression and behavioral plasticity, *Neuropsychopharmacology* **31**, 2660–2668 (2006).

162. A. Kelly, S. Laroche, S. Davis, Activation of mitogen-activated protein kinase/extracellular signal-regulated kinase in hippocampal circuitry is required for consolidation and reconsolidation of recognition memory, *J. Neurosci.* **23**, 5354–5360 (2003).

163. M. Mann, Functional and quantitative proteomics using SILAC, *Nat. Rev. Mol. Cell Biol.* **7**, 952–958 (2006).

164. M. Krüger *et al.*, SILAC mouse for quantitative proteomics uncovers kindlin-3 as an essential factor for red blood cell function, *Cell* **134**, 353–364 (2008).

165. J. T. Ngo *et al.*, Cell-selective metabolic labeling of proteins, *Nat. Chem. Biol.* **5**, 715–717 (2009).

166. J. E. Ferrell, E. M. Machleder, The biochemical basis of an all-or-none cell fate switch in Xenopus oocytes, *Science* **280**, 895–898 (1998).

167. K. Aoki, M. Yamada, K. Kunida, S. Yasuda, M. Matsuda, Processive phosphorylation of ERK MAP kinase in mammalian cells, *Proc. Natl. Acad. Sci. U.S.A.* **108**, 12675–12680 (2011).

168. M. A. Daniels *et al.*, Thymic selection threshold defined by compartmentalization of Ras/MAPK signalling, *Nature* **444**, 724–729 (2006).

169. S. D. M. Santos, P. J. Verveer, P. I. H. Bastiaens, Growth factor-induced MAPK network topology shapes Erk response determining PC-12 cell fate, *Nat. Cell Biol.* **9**, 324–330 (2007).

170. J. P. Mackeigan, L. O. Murphy, C. A. Dimitri, J. Blenis, Graded mitogen-activated protein kinase activity precedes switch-like c-Fos induction in mammalian cells, *Mol. Cell. Biol.* **25**, 4676–4682 (2005).

171. W. C. Abraham, Metaplasticity: tuning synapses and networks for plasticity, *Nat. Rev. Neurosci.* **9**, 387 (2008).

172. V. Sourdet, D. Debanne, The role of dendritic filtering in associative long-term synaptic plasticity, *Learn. Mem.* **6**, 422–447 (1999).

173. A. Losonczy, J. K. Makara, J. C. Magee, Compartmentalized dendritic plasticity and input feature storage in neurons, *Nature* **452**, 436–441 (2008).

174. J. K. Makara, A. Losonczy, Q. Wen, J. C. Magee, Experience-dependent compartmentalized dendritic plasticity in rat hippocampal CA1 pyramidal neurons, *Nat. Neurosci.* **12**, 1485–1487 (2009).

175. J. R. Neilson, G. X. Y. Zheng, C. B. Burge, P. A. Sharp, Dynamic regulation of miRNA expression in ordered stages of cellular development, *Genes Dev.* **21**, 578–589 (2007).

176. J. Kisielow, A. C. Nairn, K. Karjalainen, TARPP, a novel protein that accompanies TCR gene rearrangement and thymocyte education, *Eur. J. Immunol.* **31**, 1141–1149 (2001).

177. S. M. Hayes, L. Li, P. E. Love, TCR signal strength influences alphabeta/gammadelta lineage fate, *Immunity* **22**, 583–593 (2005).

178. M. C. Haks *et al.*, Attenuation of gammadeltaTCR signaling efficiently diverts thymocytes to the alphabeta lineage, *Immunity* **22**, 595–606 (2005).

179. E. M. Gallo *et al.*, Calcineurin sets the bandwidth for discrimination of signals during thymocyte development, *Nature* **450**, 731–735 (2007).

180. S. Mi *et al.*, MicroRNA expression signatures accurately discriminate acute lymphoblastic leukemia from acute myeloid leukemia, *Proc. Natl. Acad. Sci. U.S.A.* **104**, 19971–19976 (2007).

181. J. J. Godlewski *et al.*, Targeting of the Bmi-1 oncogene/stem cell renewal factor by microRNA-128 inhibits glioma proliferation and self-renewal, *Cancer Res* **68**, 9125–9130 (2008).

182. T. Papagiannakopoulos *et al.*, Pro-neural miR-128 is a glioma tumor suppressor that targets mitogenic kinases, *Oncogene* **31**, 1884–1895 (2012).

183. S. F. Berkovic, R. A. Howell, D. A. Hay, J. L. Hopper, Epilepsies in twins: genetics of the major epilepsy syndromes, *Ann. Neurol.* **43**, 435–445 (1998).

184. A. Poduri, D. Lowenstein, Epilepsy genetics--past, present, and future, *Curr. Opin. Genet. Dev.* **21**, 325–332 (2011).

185. B. A. Chioza *et al.*, Genome wide high density SNP-based linkage analysis of childhood absence epilepsy identifies a susceptibility locus on chromosome 3p23-p14, *Epilepsy Res.* **87**, 247–255 (2009).

186. M. A. Blair, B. Abou-Khalil, A. Crunk, J. L. Haines, P. Hedera, A new locus for autosomal dominant generalized epilepsy associated with mild mental retardation on chromosome 3p, *Epilepsia* **52**, 993–999 (2011).

187. S. Gong *et al.*, A gene expression atlas of the central nervous system based on bacterial artificial chromosomes, *Nature* **425**, 917–925 (2003).

188. E. C. Lee *et al.*, A highly efficient Escherichia coli-based chromosome engineering system adapted for recombinogenic targeting and subcloning of BAC DNA, *Genomics* **73**, 56–65 (2001).

189. S. Kriaucionis, N. Heintz, The nuclear DNA base 5-hydroxymethylcytosine is present in Purkinje neurons and the brain, *Science* **324**, 929–930 (2009).